A HEART ARTIFICIAL: BUILDING THE FOUNDATION FOR THE DEVELOPMENT AND MAINTENANCE OF *IN VITRO* TISSUE MIMETIC CARDIOVASCULAR MODELS.

A Dissertation

Presented to

the Faculty of the Department of Biomedical Engineering

University of Houston

In Partial Fulfillment

of the Requirements for the Degree

Doctor of Philosophy

in Biomedical Engineering

by

Matthew Kevin Hogan

May 2015

A HEART ARTIFICIAL: BUILDING THE FOUNDATION FOR THE DEVELOPMENT AND MAINTENANCE OF *IN VITRO* TISSUE MIMETIC CARDIOVASCULAR MODELS.

Matthew K. Hogan

Approved:

Chair of the Committee
Dr. Ravi K. Birla, Associate Professor,
Department of Biomedical Engineering

Committee Members:

Dr. Yingchun Zhang, Assistant Professor,
Department of Biomedical Engineering

Dr. Tianfu Wu, Assistant Professor,
Department of Biomedical Engineering

Dr. Chandra Mohan, Professor,
Department of Biomedical Engineering

Dr. Glauco Souza, President and CSO,
Nano3D Biosciences Inc.

Dr. Suresh K. Khator,
Associate Dean,
Cullen College of Engineering

Dr. Metin Akay, Professor and Chair,
Department of Biomedical Engineering

Acknowledgements

I would like to thank my advisor, Dr. Birla, for giving me this opportunity to succeed. Your encouragement and guidance have helped me to accomplish the work presented herein. Without your assistance, without your belief in me, I'm not sure that I would have achieved a Doctorate at all. Thanks to my lab mates Betsy, Mohamed, Niki and Zewei. I am lucky to have landed in such a competent, fun, and insightful group. I admire you all, and I hope you achieve everything you deserve.

I am grateful to my loving girlfriend, Molly. You are my ship in storm; you are my safe place when all is else is chaos. Your constant love and encouragement are steadying forces, without which I'd be lost. Thank you, Toby. You truly are man's best friend. I am sure those late nights writing and researching would have been far less comfortable and companionable without your services as a lap warmer. You are a good boy.

I don't know what I would do without my family. They are always there for me. Yvonne…mom, you always believe in me, always sees the best in me, even when I struggle to. Steve, my stepfather, you make sure everything is running, be it my car or some other such thing; I'm grateful to have such a friend. My brother and sister, Kirsten and Robert, thank you for helping me laugh. I would also like to thank my grandmother, Margaret, and my Aunt and Uncle, Aileen and Morgan, across the pond in Scotland. Though the distance is not kind, I still feel close to you all.

Thanks to the many others who, for some reason or other, have seen fit to be my friends. I'm sure it is not always easy. Thanks for being there.

Thank you, all of you.

-M

A HEART ARTIFICIAL: BUILDING THE FOUNDATION FOR THE DEVELOPMENT AND MAINTENANCE OF *IN VITRO* TISSUE MIMETIC CARDIOVASCULAR MODELS.

An Abstract

of a

Dissertation

Presented to

the Faculty of the Department of Biomedical Engineering

University of Houston

In Partial Fulfillment

of the Requirements for the Degree

Doctor of Philosophy

in Biomedical Engineering

by

Matthew Kevin Hogan

May 2015

Abstract

Given the prevalence of cardiovascular disorders and the distinct lack of significant repair mechanisms within cardiovascular systems, effective therapy for long-term treatment of cardiovascular degeneration remains a significant challenge. Further, the fundamental importance of such systems to all mammalian life begs the development of realistic component structures for *in vitro* assessment.

Significant effort was expended to create *in vitro* models, which mimicked a subset of structure and function of coordinate native components within cardiovascular systems. Towards this end, we developed a 3D-Artificial Heart Muscle (AHM) model utilizing fibrin gel and neonatal cardiac myocytes. We extracted functional metrics in order to probe the optimal protocol for generation of the tissue model. Building on the outcome of this experiment, we applied the optimal 3D-AHM model to a decellularized adult rat heart in order to re-append function to a complex acellular scaffold. The resultant bioartifical heart (BAH) model was assessed to identify the efficacy of 3D-AHM as a functional delivery mechanism and to lay a framework for heart model development. An alternative strategy for the generation of 3D heart muscle was explored through magnetic levitation of cardiovascular cells. Magnetic sensitivity was appended to cells through incubation with ferromagnetic nanoparticles. The cells were then levitated and cultured within a magnetic field to form 3D multicellular aggregates. (MCAs) We utilized a magnetized fibrin gel scaffold in order to apply non-contact, magnetic stretch conditioning to our AHM model through a novel bioreactor system.

We were able to develop a highly functional 3D-AHM and extracted 4M cells as the optimal concentration for the generation of our artificial heart muscle. Application of a layer of 3D-AHM to an acellular rat heart proved the 3D-AHM an effective mechanism for delivery of a subset of function to a structure. Magnetic levitation generated hundreds of cell-dense, functional and phenotypically relevant heart muscle analogs. We have developed a completely novel system for

the application of mechanical stretch conditioning to artificial heart muscle models and are working to implement more complex conditioning systems. The work presented herein surveys the generation of 3 unique cardiovascular model systems and a novel method for model conditioning.

Table of Contents

Acknowledgements ..... **v**

Abstract ..... **vii**

Table of Contents ..... **ix**

List of Figures ..... **xiv**

List of Tables ..... **xv**

Nomenclature ..... **xvi**

Chapter 1: Introduction **1**

Cardiovascular Disease and Tissue Engineering *1*

1.1 Background 1

1.2 Tissue Engineering 2

1.3 Key Challenges 5

1.3.1 Cell Sourcing 5

1.3.2 Natural vs. Synthetic Scaffolds 6

1.3.3 Microenvironment and cellular distribution 6

Section 1: Engineering Cardiovascular Tissue Models **8**

Chapter 2: Artificial Heart Muscle Model **9**

Optimizing a spontaneously contracting heart tissue patch with rat neonatal cardiac cells on fibrin gel *9*

2.1 Introduction 10

2.2 Materials and Methods 11

2.2.1 Isolation of primary cardiac cells 12

2.2.2 Fabrication of artificial cardiac patch 12

2.2.3 Pacemaker cells, patch formation and contraction rate 13
2.2.4 Contractile twitch force and electrocardiogram (ECG) 14
2.2.5 Morphology 15
2.2.6 Immunofluorescence 16
2.2.7 Statistics 17
2.3 Results 17
2.3.1 Patch formation 17
2.3.2 Pacemaker cells and contraction rate 17
2.3.3 Contractile twitch force and ECG 18
2.3.4 Effect of culture time on contractile twitch force 20
2.3.5. Morphology 21
2.4 Discussion and Conclusion 24
Chapter 3: Bioartificial Heart 30
Establishing the Framework to Support Bioartificial Heart Fabrication Using Fibrin-Based 3D Artificial Heart Muscle 30
3.1 Introduction 30
3.2 Materials and Methods 33
3.2.1 Decellularization of scaffolds 34
3.2.2 Isolation of primary cardiac cells 34
3.2.3 Fabrication of AHM 35
3.2.4 Contractile twitch force of AHM 36
3.2.5 BAH formation 37
3.2.6 Contraction 37
3.2.7 Biopotential measurement 38
3.2.8 Histology 38
3.2.9 Immunohistochemistry 39
3.3 Results 39

3.3.1 Patch formation 39
3.3.2 Decellularization 39
3.3.3 BAH formation 40
3.3.4 Contraction of BAH 41
3.3.5 Morphology 42
3.3.6 Immunohistochemistry 42
3.3.7 Biopotential measurements 43
3.4 Discussion and Conclusion 44
Chapter 4: Magnets and 3D Cultures 48
Magnetic Cell Labeling and Levitation to Support the Rapid Assembly of Three-Dimensional Cardiac Cultures 48
4.1 Introduction 48
4.2 Materials and methods: 51
4.2.1 Ethics Statement 51
4.2.2 Isolation of primary cardiac cells 51
4.2.3 Magnetic Levitation 52
4.2.4 3D Culture Formation and Activity 53
4.2.5 Histology and Immunohistochemistry 54
4.3 Results 55
4.3.1 Formation 55
4.3.2 Activity 56
4.3.3 Histology and immunohistochemistry 56
4.4 Discussion 57
4.5 Summary 61
Section 2: Bioreactors for Conditioning of Cardiovascular Tissue Models 62
Chapter 5: Magnetic Stretch Conditioning 63

Field Manipulation for Non-Contact Magnetic Stretch Conditioning of Cardiovascular Tissue Models *63*

5.1 Introduction 63

5.1.1 Motivation 63

5.1.2 Viable Tissue Engineered Heart Muscle 64

5.1.3 Current Models 64

5.1.4 Effects of Stretch Conditioning 65

5.1.5 Bioreactors: Current State of the Art 67

5.1.6 Novel Stretch Bioreactors 67

5.2 Materials and Methods 68

5.2.1 Isolation of primary cardiac cells 69

5.2.2 Fabrication of artificial cardiac patch 69

5.2.3 Magnetized fibrin gel 70

5.2.4 Patch formation and contraction rate 70

5.2.5 Contractile twitch force and electrocardiogram (ECG) 71

5.2.6 Morphology 71

5.2.7 Immunofluorescence 72

5.2.8 Statistics 73

5.2.9 Magnetic conditioning 73

5.2.10 Synthesis of Fe_3O_4 Magnetic Nanoparticles (MNPs) 73

5.2.11 Characterization of MNPs 74

5.2.12 SEM Sample Preparation for MNPs in Fibrin Gel 74

5.3 Results 75

5.3.1 Concept 75

5.3.2 Bioreactor Design 75

5.4 Discussion 83

5.5 Summary 85

References: **86**

List of Figures

***Figure 1**: Tissue Engineering Process,* 4

***Figure 2**: Schematic methods for artificial cardiac tissue patch fabrication.* 13

***Figure 3**: Pacemaker cells and spontaneous contraction rates* 18

***Figure 4:** Contractile force and ECG* 19

***Figure 5**: Effects of culture time and electrical stimulation on contractile pacing* 21

***Figure 6**: Patch morphology* 23

***Figure 7**: Cardiac thicknesses and gap junctions* 24

***Figure 8:** Protocol for the generation of a BAH using AHM.* 33

***Figure 9**: Decellularization process of a rat heart* 34

***Figure 10**: Photographs of Stages of the Artificial Heart Formation Process* 36

***Figure 11**: Histology of the Bioartificial Hearts (H&Es)* 40

***Figure 12**: Histology of a cross section of the Bioartificial Heart (Masson's trichrome)* 41

***Figure 13**: Histology of the BAH* 42

***Figure 14**: Biopotential measurements of a beating BAH* 43

***Figure 15**: Schematic of magnetic levitation in a 24-well plate* 53

***Figure 16**: MCA aggregate formations over time* 55

***Figure 17:** IHC images of whole-mount MCAs* 56

***Figure 18**: Z-stack 3D reconstruction of IHC images from whole-mount MCA* 57

***Figure 19**: Cell dense structures* 59

***Figure 20**: Structural Preservation* 60

***Figure 22:** Design concept of magnetic stretch bioreactor* 78

***Figure 23**: Prototype of a magnetic stretch bioreactor* 79

***Figure 24**: Magnetic stretch forces* 80

***Figure 25**: Toxicity effects of Iron Oxide (Fe_2O_3)* 81

***Figure 26**: SEM of characterized Fe_3O_4 particles and fibrin gel.* 82

List of Tables

Table 1: *Decellularization protocol.....34*

Nomenclature

AHM	Artificial Heart Muscle (in vitro muscle model)
BAH	Bioartificial Heart (in vitro total heart model)
MCA	Multicellular Aggregate (levitated 3D heart muscle model)
ACE	Angiotensin-converting enzyme inhibitor
CPD	Counterpulsation device
IABP	Intra-aortic balloon pump
LVAD	Left ventricular assist device
TAH	Total artificial heart (mechanical heart replacement)
vWF	von Willebrand Factor
Cx43	Connexin 43
BEHM	Bio-engineered heart muscle (early heart muscle model)
ECM	Extracellular matrix
H&E	Hemotoxylin and Eosin (staining technique)
NanoShuttle	Nano3D ferromagnetic nanoparticle assembly
cTnI	Cardiac Troponin I
CD31	Cluster of differentiaition 31 (Endothelial marker)
ki67	Discovered in **Ki**el, Germany on a 24 well plate with the number **67** (antibody associated with proliferation)
DS	Dissociation solution
CM	Culture medium
IHC	Immunohistochemistry
NBF	Neutral buffered formalin
TGF-β	Transforming growth factor beta

PDGF	Platelet-derived growth factor
b-FGF	basic Fibroblast growth Factor
IGF-1	Insulin-like growth factor I
AngII	Angiotensin II
ET-1	Endothelin I

Chapter 1: Introduction

Cardiovascular Disease and Tissue Engineering

1.1 Background

The heart is a fairly ubiquitous organ within the animal kingdom. Though the structure may vary, the base action remains unchanged. While it is difficult and perhaps arbitrary to rank importance of common organ systems, it can be said with some degree of certainty that cardiovascular disorders are the most prevalent source of fatality when compared with diseases of other common systems such as neural, digestive, immune, etc. Humans are no exception to this observation as heart disease is the leading cause of death in the western world and accounts for roughly ¼ of the deaths in the United States annually (Go et al., 2013). More than this, treatment is a prolonged and expensive ordeal with a $108.9 billion annual cost in the United States alone. The prevalence, cost and severity of cardiovascular disorders prompts several basic questions.

Why are cardiovascular disorders, in particular, so pervasive and deadly? The heart, unlike many other common structures, lacks a significant capacity for repair. In humans, a typical myocardial infarction accounts for cell death on the order of a *billion* cells. There is no mechanism to replace these lost cells to anywhere near the previous numbers. By its very nature, heart disease is progressive. Once functional cells in the cardiovascular system are lost, the system can stabilize and compensate but cannot return to a fully functional state. Deleterious effects compound leading to further damage and destabilization of the system (Maton and Prentice-Hall 1994; Kelly et al., 2010; Mendis et al., 2011; Finegold, Asaria, and Francis 2013).

What are the current treatments options? Angiotensin-converting enzyme (ACE) inhibitors, angiotensin II receptor blockers, digoxin, statins, aspirin and beta blockers are a few of the medications used to treat cardiovascular disease (Hennekens, Dyken, and Fuster 1997; Gutierrez et al., 2012; Singh, Shishehbor, and Ansell 2007). Pharmacological treatments for heart

disease certainly have benefit, but cannot address a fundamental lack of sufficient healthy tissue. Small molecules are limited in their activity by the lack of an innate repair mechanism. Primary methods of action typically encourage peripheral compensation, or mitigate side effects of overcompensation by the heart itself. Counterpulsation devices (CPDs), intra-aortic balloon pumps (IABPs), left ventricular assist devices (LVADs) and total artificial hearts (TAHs) are a few examples of medical devices designed to combat heart disease (J. Wei et al., 1998; Kantrowitz et al., 1968; Scheidt et al., 1982; McCarthy et al., 1995). Immunogenic and thrombogenic responses of the host to such devices limit the scope of their application. Such devices are typically seen only as a bridge to transplant and not as a final solution. The only true long term therapy for end-stage heart failure is heart transplant. Only 3,000 heart transplants are performed in the U.S. every year leaving some 30,000-70,000 Americans without proper treatment. A lack of compatible organs severely limits the only long-term therapy for the most deadly condition known to man (Go et al. 2014).

What is the way forward? While the current state of therapy for heart disease remains insufficient, there is promising research that indicates two new treatment paths are evolving. One such path centers on stemming the progression of heart disease. By attempting to address the lack of a repair mechanism, researchers hope to replace damaged cells with new and healthy tissue. It is hoped that protocols for either guided injection of healthy cells, or application of tissue engineered heart muscle to damaged areas of the heart, may sufficiently compensate for the functional loss experienced during cardiac trauma. Another far more ambitious goal is to find a new source for organ transplant. There have been many promising advances which indicate that it may one day be possible to grow a patient specific heart replacement outside of the body.

1.2 Tissue Engineering

Tissue engineering strategies are focused on the fabrication of artificial tissue constructs in a controlled laboratory environment (Atala 2004; Fisher and Mauck 2013; Hecker and Birla 2007;

Luda Khait et al., 2008; Nerem 2006; Rustad et al., 2010; Sipe 2002). The definition of tissue engineering was provided by Dr. Robert Langer in one of his seminal papers, where he states that "*Tissue engineering is an interdisciplinary field that applies the principles of engineering and the life sciences toward the development of biological substitutes that restore, maintain, or improve tissue function"* (Langer and Joseph 1993). This seminal publication has been influential in the field and has resulted in an exponential increase in research participation. Advances in tissue and organ fabrication technology have led to clinical implantation of bioengineered tracheas and bladders and organ model have been developed for artificial hearts, lungs and kidneys.

Tissue Engineering represents a relatively new approach to address existing medical conditions. Translation of cardiovascular tissue engineering strategies into the clinic may allow therapy to stem the progression of cardiovascular disorders and eventually provide a source for new donor organs. Along these lines, researchers have attempted to recreate many functional components of the cardiovascular system, including heart muscle, valves, SA and AV nodes, blood vessels, ventricles, atriums and indeed entire hearts.

The field of cardiovascular tissue engineering has rapidly expanded since the first publication in 1997 (Chiu et al., 2011; Williams et al., 2014; Tallawi et al., 2014; Bhaarathy et al., 2014; Baheiraei et al., 2014; Shevach et al., 2014; Dhingra, Weisel, and Li 2014; Ehler and Jayasinghe 2014; Cui et al. 2014; Qazi et al., 2014; Yu et al., 2014; Matsuura, Masuda, and Shimizu 2014; Srinivasa Reddy et al., 2014; Annabi et al., 2013; Fleischer et al., 2013; Ravichandran et al., 2013; Gálvez-Montón et al., 2013; Prabhakaran et al., 2012; Ye, Sullivan, and Black 2011; Prabhakaran et al., 2011; Curtis and Russell 2009; Blan and Birla 2008; H.-J. Wei et al., 2006; Dar et al., 2002; Shimizu, Yamato, Isoi, et al., 2002; Shimizu, Yamato, Akutsu, et al., 2002; Shimizu et al., 2001; Papadaki et al., 2001; Li et al., 2000; Leor et al., 2000; W. H. Zimmermann et al., 2000; Li et al., 1999; Akins et al., 1999; Eschenhagen et al., 1997). The most common strategy to fabricate 3D-AHM has been to culture neonatal cardiac myocytes within a suitable 3D scaffold, resulting in artificial tissue that replicates a partial subset of mammalian heart muscle function (Y. Huang,

Khait, and Birla 2007; Baar et al., 2005; Bursac et al., 1999; Curtis and Russell 2009; Blan and Birla 2008; Dar et al., 2002; Li et al., 1999; W. H. Zimmermann et al., 2000; Akins et al., 1999; Papadaki et al., 2001; Li et al., 2000). Three pillars of heart muscle tissue engineering have evolved: cells, biomaterials and bioreactors.

- *Cells* – cells provide the functional component of 3D artificial tissue and most models of artificial heart muscle have been developed using neonatal cardiac myocytes. While artificial tissue fabricated using neonatal cells cannot be used clinically, these models provide valuable insight into 3D organization and development.
- *Biomaterials* – many biomaterials have been tested to support artificial heart muscle, including fibrin, collagen, alginate, chitosan and polyglycolic acid. These materials have demonstrated varying degrees of success and replicated partial functionality of artificial heart muscle.
- *Bioreactors* – bioreactors are used to replicate *in vivo* conditions during controlled *in vitro* culture; specific signals include mechanical stretch, electrical stimulation and fluid stress. These signals are important in guiding the formation and function.

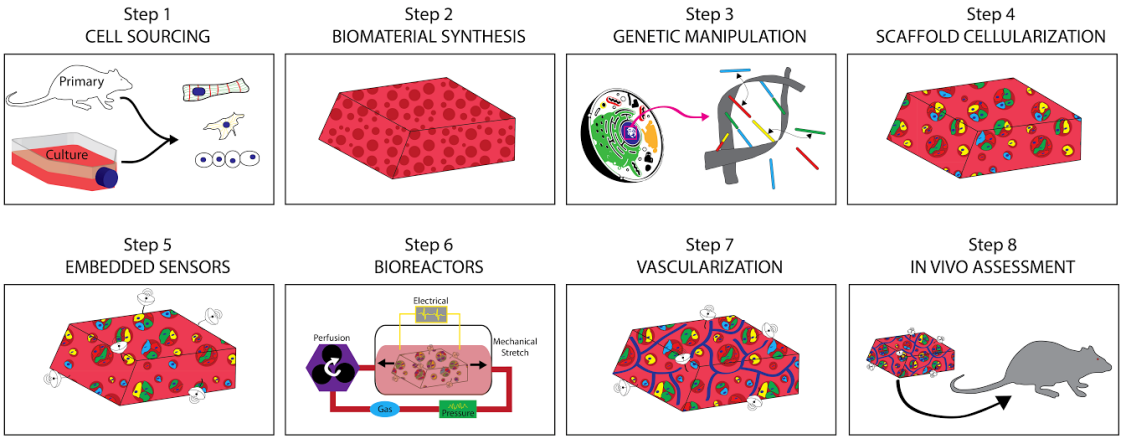

Figure 1: Tissue Engineering Process, A general outline of the process for developing a bioengineered tissue model through tissue engineering.

1.3 Key Challenges

The vast potential of the field of tissue engineering presents clear and astounding goals to those researchers who endeavor to bioengineer tissues. It is clear much benefit could be provided through a successful development of nearly any engineered organ system. While there have been promising advances and even intermediate developments with clinical applications, many issues separate the immediate future of tissue engineering from the stuff of science fiction.

1.3.1 Cell Sourcing

A primary concern when attempting to replicate an organ, system or tissue, is *where do you get your cells?* There are a multitude of issues surrounding the selection of an appropriate cell source. This question transcends concerns of science into the murky realm of morality. Embryonic stem cells were long considered the future of a multitude of therapeutic scientific endeavors, and tissue engineering was no exception. The ability of embryonic stem cells to mature into nearly any phenotype, given the proper conditioning, made them the center of study in many countries for several years. Moral concerns extended from the source of these cells. It is perhaps not hard to envision a dystopian future where embryos are cultured in vats and harvested for their cells. In 2006, Yamanaka's group uncovered a Nobel Prize winning method to induce mature adult cells to a pluripotent state (Takahashi and Yamanaka 2006). Adult cells can now be reprogrammed to return to a state where they are roughly as phenotypically plastic as embryonic stem cells, alleviating much societal pressure on the field. There is little inherent moral dilemma when cells can be harvested from consenting adults. Still, there are many issues with this method as well. The genes which were inserted into the cells to induce pluripotency are inherently oncogenic. While biological techniques have evolved to completely remove these oncogenic sequences post cellular transformation, the yield of such techniques is still fairly low. Further, successful differentiation of iPS cells to specific cell types remains a significant challenge. While protocols have been developed, the efficiency of directed differentiation of iPS cells leaves much to be desired. Given

the vast numbers of cells expected to be required in even the simplest tissue engineered models, a more efficient means of transformation and differentiation is necessary.

As such, many models rely heavily on neonatal, mesenchymal, stromal and other readily available and well understood cell types in order to generate tissue models. Clinically, a well understood, readily available and patient specific cell source is ideal. Autologous cell sourcing can eliminate any immune response, and functional integration of created constructs into host tissue will eliminate thrombogenic and external control considerations (Foy 2007).

1.3.2 Natural vs. Synthetic Scaffolds

A debate regarding the future of biomaterials within and outside the field of tissue engineering has arisen due to arguments over the proper choice for scaffold material. Natural scaffolds offer much in the way of mimicking properties which may be found in the microenvironments of cells in natural tissue. Cellular binding sites, microarchitecture and composition of natural scaffolds are generally considered to be more sophisticated than those of synthetic scaffold mimics. Synthetic scaffolds however, can be controlled via their manufacturing process. Favorable results will be more readily reproducible using synthetic scaffolds as the synthesis process will be the same every time. Further, synthetic scaffolds offer an off the shelf option. Finally, FDA approval of synthetic materials is a far less complex and time consuming process. While natural scaffolds currently offer the best properties for replication of bodily tissue features, I believe that advancements within the field of synthetics will inevitably lead to a shift towards controlled synthesis biomaterials.

1.3.3 Microenvironment and cellular distribution

Throughout the history of cellular biology, it has become clear that cellular function and activity rely heavily on signals from the environment around the cell. Cell-cell communication, ECM protein signal cascades and small molecule uptake are just a few ways with which the cell can communicate with its environment. The context in which a cell is placed plays a pivotal role in

the cell's action. As such, it is important to mimic the cellular composition and organization of native tissues at the most granular level of detail in order to achieve the optimal cellular phenotype. Further, tissues are often aligned in complex fashion with distinct layers of differing cell types. Replicating these patterns is not straightforward and guided cellularization of biomaterials has become a popular area of study.

Section 1: Engineering Cardiovascular Tissue Models

Chapter 2: Artificial Heart Muscle Model

Optimizing a spontaneously contracting heart tissue patch with rat neonatal cardiac cells on fibrin gel

Over the years, engineered cardiac tissues have been constructed with primary or stem cell-derived cardiac cells on natural or synthetic scaffolds. They represent a tremendous potential for treatment of injured areas or repair of congenital heart defects through addition of tensional support and delivery of sufficient cells. In this study 1 to 6 million (M) neonatal cardiac cells were seeded on fibrin gels to fabricate cardiac tissue patches. We analyzed the effects of culture time and cell density on spontaneous contraction rates, twitch forces, electrocardiograms and expression of connexin 43. The patches were also electrically paced at various frequencies to determine the response in contraction rate. Patches of all cell densities exhibited maximum contraction rates between 305-410 bpm within the first 4 days after plating. When measuring contractile twitch forces, low cell density (1-3M) patches sustained a longer rhythmic contraction whereas high cell density patches just an arrhythmic contraction. 1-6M patches generated 2245-8514 kN/m^3 of the high rate mean and 3959-14065 kN/m^3 of the low rate mean contractile forces on days 4-6. After patch formation, both high and low rate contractile forces and electrical pacing response frequency dramatically decreased with culture period. The difference in maximum contraction rates with 1-6M resulted from the density-related variation of pacemaker cells which competitively paced within the tissue; the greater twitch forces generated by higher cell density relied on a thicker real cardiac layer which also summed greater R wave amplitude. Overpopulation of myoblasts and the aging and apoptosis of cardiomyocytes might be responsible for the decreases of twitch force and pacing response frequency along with culture time. However, 2M patches with a greater signal volume index of connexin 43 when comparing with 4 and 6M patches gave the evidence to longer

spontaneous rhythmic contraction with 1-3M patches in contrast to just an arrhythmic contraction with 4-6M patches. In addition, all the patches manifested endothelia cell growth and a robust nuclear division. The present study demonstrates a spontaneously contracting cardiac patch fabricated by seeding neonatal cardiac cells on fibrin gel scaffold and its specific characteristics.

2.1 Introduction

Tissue engineering combines cellular and molecular biology with material and mechanical sciences to provide an alternative to organ and tissue transplants which are limited by the supply of donor organs. Engineered cardiac tissues, constructed with primary or stem cell-derived cardiac cells on a natural or synthetic scaffold, have tremendous potential to offer alternative treatment modalities in the healing process of large injured areas and in repairing congenital defects in hearts. By embedding a sufficient number of cells in the tissue and by providing additional tension support to the damaged area, they circumvent low rates of cell engraftment and poor cell survival which have occurred in present cell therapies (Sekine et al., 2011; H.-J. Wei et al., 2008; Wollert and Drexler 2010).

Cardiac tissue constructs have been fabricated by embedding neonatal cardiac cells (Fujimoto et al., 2010; Kensah et al., 2011; W.-H. Zimmermann et al., 2006) with collagen type I supplemented with Matrigel, and by embedding pluripotent stem cell-derived cardiomyocytes with collagen type I gel, (Guo et al., 2006; Tulloch et al., 2011) poly-L-lactic acid and polylactic-glycolic acid gel, (Caspi et al., 2007) momentum flap (Kawamura et al., 2013) and hydrogel (Liau et al., 2011).

Some *in vivo* studies showed that these cardiac constructs improved cell survival, (Sekine et al., 2011; Kawamura et al., 2013) vascular network formation (Zhou and Graham 2009) and cardiac function (Zimmermann et al., 2006) though their twitch force and physical properties varied with scaffold materials, embedded cell densities, and culture conditions.

Neonatal cardiac cells possess a tremendous differentiation potential and regenerative capacity. The hearts of 1-day-old neonatal mice can regenerate after a partial surgical resection (Porrello et al., 2011). Fibrin is a natural, self-assembling peptide found in the body that is used to form clots along damaged endothelium. Fibrin gels possess high seeding efficiency, uniform cell distribution, and adhesion capabilities (Guyette et al., 2013; Swartz, Russell, and Andreadis 2005). It is formed by the reaction of thrombin and fibrinogen, which can be produced from the patient's own blood, thus reducing the potential risk of rejection when used as a component in clinical application. We previously described a model for the self-organization of primary cardiac cells on laminin substrate to form a cardioid, (Baar et al., 2005) which exhibited physiological performance metrics comparable to normal mammalian cardiac tissue. We then developed an engineered heart muscle by seeding or embedding 2-3 day old neonatal rat cardiac cells on the surface of, and within, a fibrin gel. Histological evaluation showed the presence of uniformly distributed cardiac cells throughout the engineered heart muscle tissue. The stimulated active force of this tissue by the seeding approach was 835.5 ± 57.2 μN and by embedding 145.3 ± 44.9 μN (Y. Huang, Khait, and Birla 2007). The present study fabricated a cardiac tissue patch by seeding the neonatal rat heart cells on fibrin gel with the intent to optimize natural spontaneous contraction by evaluating cell densities and length of culture. Optimized patches will be used for *in vivo* grafting in future studies.

2.2 Materials and Methods

All animal protocols were approved by the Institutional Animal Care and Use Committee (IACUC) at University of Houston, in accordance with the "Guide for the Care and Use of Laboratory Animals" (NIH publication 86-23, 1996). All materials were purchased from Sigma-Aldrich (St. Louis, MO) unless otherwise specified.

2.2.1 Isolation of primary cardiac cells

Cardiac cells were isolated from the hearts of 2-3 day old neonatal Sprague-Dawley rat pups using an established method (Y. Huang, Khait, and Birla 2007). Each heart was cut into 3-4 pieces in an ice-cold phosphate buffer consisting of 116 mM NaCl, 20 mM HEPES, 1 mM Na_2HPO_4, 5.5 mM glucose, 5.4 mM KCl and 0.8 mM $MgSO_4$. After blood cells were rinsed out, heart pieces were transferred to a dissociation solution (Porrello et al., 2011) consisting of 0.32 mg/ml collagenase type 2-filtered (Worthington Biochemical Corporation, Lakewood, NJ) and 0.6 mg/ml pancreatin in phosphate buffer. The hearts were cut into 1 mm^3 pieces and then transferred to an orbital shaker and maintained at 37^{O}C for 30 minutes at 60 rpm. At the end of the digestion process, the supernatant was collected in 3 ml of horse serum to neutralize the enzyme and centrifuged at 1000 rpm for 5 minutes at 4^{O}C. The cell pellet was re-suspended in 5 ml horse serum and kept in an incubator at 37^{O}C supplied with 5% CO_2. Fresh DS was added to the partially digested tissue and the digestion process was repeated an additional 2-3 times. Cells from all the digests were pooled, centrifuged and suspended in culture medium (CM) consisting of M199 (Life Technologies, Grand Island, NY), with 20% F12k (Life Technologies, Grand Island, NY), 10% fetal bovine serum, 5% horse serum, 1% antibiotic-antimycotic, 40 ng/ml hydrocortisone and 100 ng/ml insulin. Cell viability was analyzed by Trypan blue (4%) staining according to the manufacturer's protocol.

2.2.2 Fabrication of artificial cardiac patch

The method to fabricate the cardiac patch is shown in Figure 2A-H. A 35 mm tissue culture plate was coated with 2 ml of SYLGARD (PDMS, type 184 silicone elastomer) (Dow Chemical Corporation, Midland, MI). The plate was air dried for 2 weeks and sterilized with 80% ethanol before use. Four minutien pins (Fine Science Tools, Foster City, CA), 0.1 mm diameter, were placed in the culture plate to form a 2 × 2 cm square. The fibrin gel was made by plating 1 ml of CM containing 10 U/ml thrombin and adding 500 µl of saline containing 20

mg/ml fibrinogen, and mixed well to promote gel formation within 10 minutes. Primary cardiac cells were diluted in CM at a pre-set density, and 2 ml of the cell suspension CM was transferred to the culture plate. Aminocaproic acid (2 mg/ml) was added to the culture plate to inhibit the fibrinolysis by endogenous proteases. The cells were cultured in an incubator at $37^{O}C$ and 5% CO_2 with CM changes every other day.

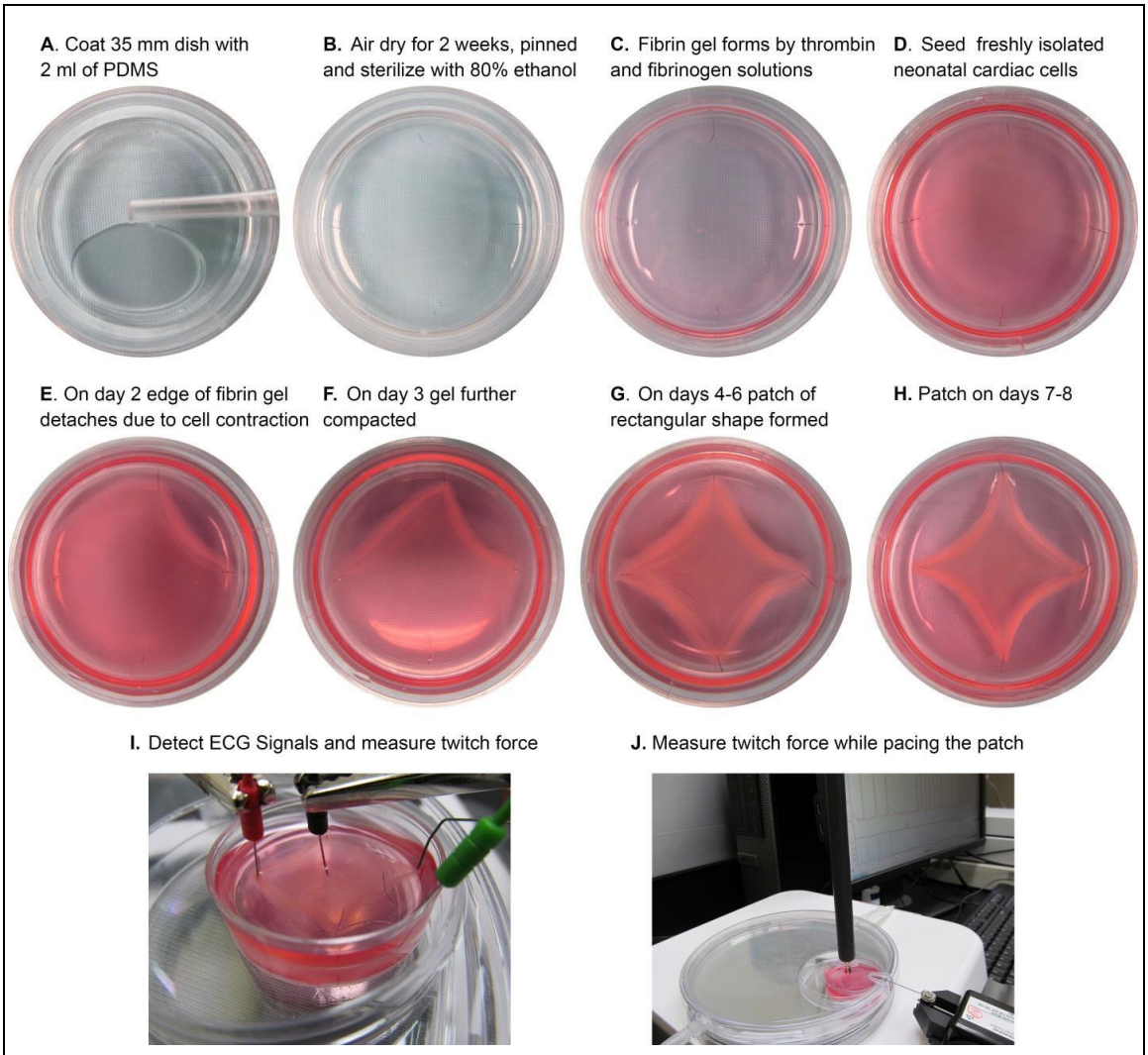

Figure 2: Schematic methods for artificial cardiac tissue patch fabrication.

2.2.3 Pacemaker cells, patch formation and contraction rate

Sixteen hours after cell plating, pacemaker cells were counted manually from five 200× fields (center and top, right, left, and bottom most from the center of the patch) under an

inverted phase-contrast microscope (Olympus, Center Valley, PA). The total pacemaker cells of one patch from one density were averaged. The contraction of cultured cardiac constructs and fibrin gel detachment from culture plates were observed from day 1 to day 6, the patch growth progress was captured in still photographs and videos using a camera (Lumenera, Ottawa, ON) mounted on an inverted phase-contrast microscope. The videos were slowly replayed and the contraction rates manually counted.

2.2.4 Contractile twitch force and electrocardiogram (ECG)

From the first day of patch formation, spontaneous twitch force and the twitch force by electrical pacing (10V, 0.1s) were measured using a high sensitivity isometric force transducer (MLT0202, ADInstruments, Colorado Springs, CO) connected to a quad bridge amplifier (FE224, ADInstrument, Colorado Springs, CO). ECG signal was measured using Octal Bio Amp (ML138, ADInstrument, Colorado Springs, CO) within a thermostatic water bath. Data was acquired through a 16 channel PowerLab system (PL3516/P, ADInstruments, Colorado Springs, CO). As shown in Figure 2I and 2J, the contractile twitch force was measured by attaching the force transducer arm to one free-corner of the square patch, while the other three ends of the square patch were held fixed by pins. In order to obtain the Frank-Starling relationship for the measured twitch force, pretension was adjusted using a micro-manipulator (Radnoti LLC, Monrovia, CA) and measurements of spontaneous contraction were recorded. We defined that a spontaneous contraction rate of more than 120 bpm is high rate contraction, and that a spontaneous contraction rate of less than 20 bpm is low rate contraction. ECG of the patch was measured, as shown in Figure 2I, by inserting a needle cathode (MLA1213, ADInstruments, Colorado Springs, CO) into the center of the patch and a needle anode in one of the four patch corners. The media immersing the patch was used as ground. LabChart (ADInstruments, Colorado Springs, CO) was used for data analysis. The peak analysis module was used to calculate the maximal twitch force and baseline force (pretension). The ECG analysis module was used to calculate the R wave amplitude. Electrical

pacing was performed by attaching the stimulating electrodes (MLA0320, ADInstruments, Colorado Springs, CO) on the edge of patch tissue at frequencies of 0.25, 0.5, and 1-8 (in 1 unit increments) Hz at 2, 4, and 6 days after patch formation. An effective electrical pacing frequency was determined by the initiation of a contraction.

2.2.5 Morphology

Seven days after plating, formed patches were cut diagonally. The diagonal edge of the triangular block was aligned with the edge of a slide. The cross section and the surface of the triangle block were photographed and the images were trace by ImageJ 1.47d (Wayne Rashand, National Institute of Health, USA) to get the area of the cross section, the thickness and the height of the triangular block, and then this triangle block was weighed. From the central part of the patch two 0.5 × 0.5 cm blocks were taken, placed in a peel-a-way disposable embedding mold (VWR International, Radnor, PA), frozen in liquid N_2, and then immediately immerged in Tissue Tek OCT compound (VWR International, Radnor, PA) and placed in a –80°C freezer. Once the OCT compound solidified, each sample was sliced using a cryostat (Thermo Fisher Scientific, Waltham, MA). Tissue cross- and planar-sections were cut at a thickness of 10 μm or 6 μm. The sections were placed on VWR® Microslides for preparation of morphological and immunofluorescence examinations. Images from cross-sections of 6 μm thickness were taken directly under a phase contrast light microscope (Olympus, Center Valley, PA). For measurement of the "real cardiac layer" (a layer of cells and naturally produced extracellular matrix forming on top of the fibrin gel scaffold) thickness, 10 μm cross-sections were stained with Masson's trichrome reagents, according to manufacturer's protocol, and images were taken under a light microscope. The distinct tissue layers were traced and thicknesses calculated with ImageJ.

2.2.6 Immunofluorescence

For observation of endothelial cell growth, nuclear division and collagen type I distribution in the patch, fresh tissue patches were directly fixed in ice cold acetone for 10 minutes. 1.0 ×1.0 cm tissue patch blocks from the center were trimmed and nonspecific epitope antigens were blocked and cell membranes permeated with 10% goat serum / 0.5% Trition X-100 at room temperature for 45 minutes. Tissue patch blocks were then incubated in mouse anti- α-actinin antibody (Sigma, A7811) 1:200, rabbit anti-collagen type I (Abcam, ab34710) 1:100, rabbit anti- von Willebrand factor (vWF) (Abcam, ab6994) 1:750, rabbit anti-ki 67 (Abcam, ab66155) 1:100, or rabbit anti-connexin 43 (Cx43) 1:100 at room temperature for 2 hours. Subsequently, tissue blocks were treated with goat anti-mouse and goat anti-rabbit secondary antibodies (Alexa Fluor 488, Alexa Fluor 546 and Alexa Fluor 633, Life Technologies, Grand Island, NY) 1:400 at room temperature for 1 hour. Nuclei were counterstained with 4,6-diamidino-2-phenylindole (DAPI) (2.5 μg/ml) for 5 min at room temperature. Fluorescent images were obtained with a Nikon $C2^{+}$ confocal laser scanning microscope (Nikon Instruments Inc., Melville, NY). For measurement of the volume indexes of gap junctions, collagens and myofibrils, signal volumes of Cx43, collagen type I and α-actinin expressions were examined within 6 μm cross-sections. Two Z-stack scans from each sample were acquired with a signal depth of 8 μm over 33 frames. After determining specific thresholds for Cx43, collagen type I, and α-actinin, signal volumes for each sample were measured. The signal volume indexes of Cx43 (or collagen type I) for different cell densities were expressed as

$$Cx43\ signal\ volume\ index = Cx43\ signal\ volume\ /\ (\alpha\ actin\ signal\ volume\ +\ Cx43\ signal\ volume) \quad (1)$$

and averaged for each sample.

2.2.7 Statistics

Results are presented as mean ± standard deviation. Chi-Square analysis was used to test frequency variables. Comparisons among groups were made with a one-way analysis of variance (ANOVA) followed by the Bonferroni post hoc comparison test. In all tests, differences were considered statistically significant at a value of $p<0.05$.

2.3 Results

2.3.1 Patch formation

By the present established isolation method, cell viability was 81.0 ± 2.2% (n=16). The time required for patch formation was a function of the initial plating density. On day 4, formation was complete for 28.0% (n=7/25), 56.3% (9/16), and 40.0% (6/15) of patches with 1, 3 and 5M densities, respectively; Pearson Chi-Square analysis indicated $p = 0.195$. On day 6, formation was complete for 68.0% (17/25), 87.5% (14/16), and 60.0% (9/15) of patches with 1, 3 and 5M densities, respectively; Fisher's Exact test demonstrated $p = 0.232$.

2.3.2 Pacemaker cells and contraction rate

After cell plating, live cardiac cells (Figure 3A, green arrow heads) scatter and attach to fibrin gels with a spindle-shaped morphology; however, dead cardiac cells (Figure 3A, red arrow heads) congregate with a sphere-shaped morphology. Each pacemaker cell (Figure 3A-C, white arrows) contracts at its own rate. At 16 hours after plating, pacemaker cells in 1M density is less (9.4 ± 3.6, n=7) than that in 3M (16.9 ± 2.8, n=7, $p<0.01$) and 5M (23.1 ± 2.5, n=8, $p<0.01$) densities; compared with 5M density, pacemaker cells in 3M density is less too ($p<0.01$) (Figure 3D).

Arrythmic contraction in separate areas of patches were observed and occurred due to uneven pacing from different pacemaker cells which compete with each other. Upon day 2 after plating, spontaneous tissue contractions were observable under a microscope for 1-3M densities. The highest contraction rates appeared on days 4, 3 and 3 and they are 305 ± 54

(n=7), 330 ± 49 (n=8) and 374 ± 69 (n=9) bpm for 1, 2 and 3M densities, respectively. For the 4-6M densities, spontaneous contractions were observable 1 day after plating. Their highest contraction rates were attained on day 2; the highest contraction rates for 4, 5 and 6M densities are 365 ± 52 (n=11), 405 ± 34 (n=11) and 410 ± 33 (n=12) bpm, respectively. The highest contraction rates for 1, 3 and 5M patches are illustrated in Figure 3E. Compared with 1M density, the highest contraction rates in 3 and 5M densities are significantly greater ($p<0.05$ or $p<0.01$). However, on day 6, the contraction rate in 1M (243 ± 71 bpm, n=7) is significantly greater than that in 3M (32 ± 23, n=9) ($p<0.01$) and 5M (43 ± 78, n=11) ($p<0.01$) densities.

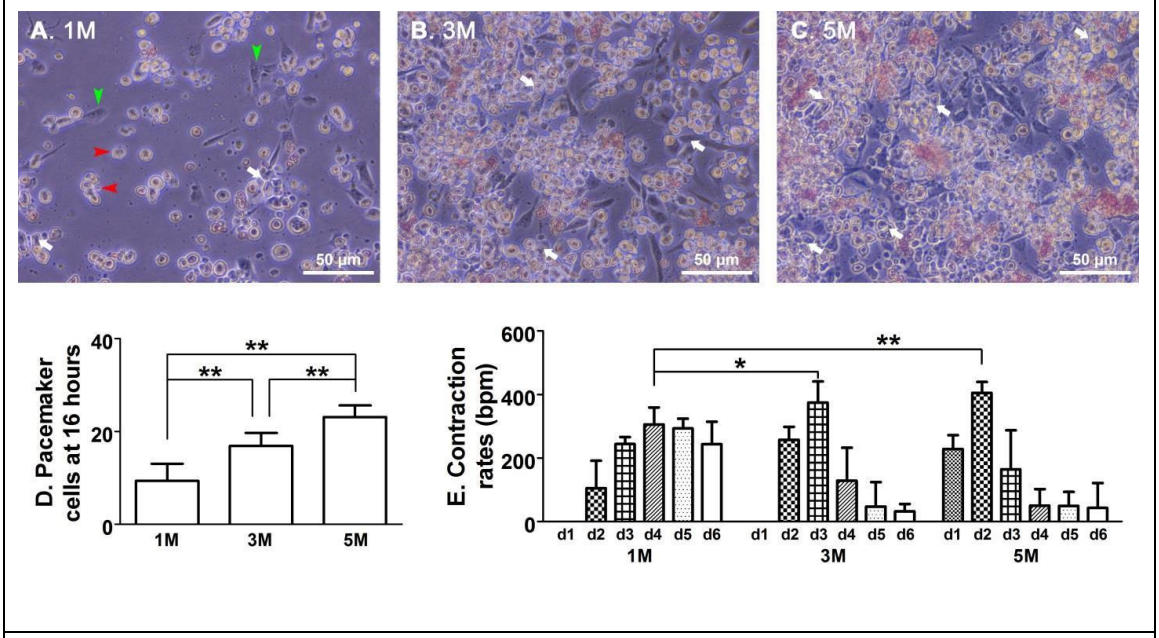

Figure 3: Pacemaker cells and spontaneous contraction rates, **A**, 1M density at 16 hours, **B**, 3M, **C**, 5M densities at 16 hours after plating, **D**, number of pacemaker cells, **E**, spontaneous contraction rates at 1-6 days, Values are mean ± SD; *p<0.05, **p<0.01

2.3.3 Contractile twitch force and ECG

High rate (>120 bpm) and low rate (<20 bpm) twitch forces were recorded from formed patches from day 4 to day 6. For 1, 2 and 3M patches, high rate rhythmic contractions were detected throughout the entire recording period (starting at the onset of pretension). Figure 4A shows rhythmic contraction from a 3M patch and Figure 4B demonstrates its synchronous ECG. The largest twitch force was recorded when the pretension was set between 1000 to

3000 μN. However, for 4, 5 and 6M patches, high rate arrhythmic contractions were detected for a few seconds after pretension loads were applied, after which low rate contractions were observed. Figure 5C, D show the arrhythmic contraction and its synchronous ECG from a 5M patch.

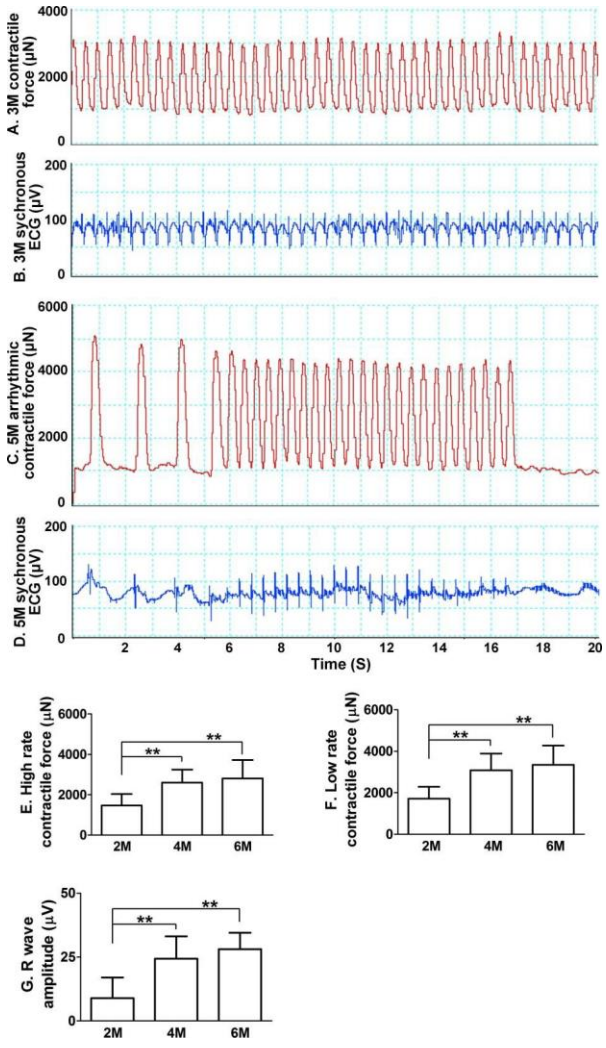

Figure 4: Contractile force and ECG, **A**, Contraction from a 3M patch, **B**, ECG of **A**, **C**, Arrhythmic contraction from a 5M patch, **D**, ECG of **C**, **E**, **F**, average contractile forces, **G**, average R wave amplitude of high rate.

The high rate contractile force recorded with a pretension range of 1000 to 3000 μN for 1 to 6M densities are 550 ± 120 μN (n=11) to 2806 ± 916 μN (n=10); the greatest high rate contractile force is 4443 μN from a 6M patch. The low rate contractile force recorded with a pretension range of 1000 to 3000 μN for 1 to 6M patches are 970 ± 132 μN (n=11) to 3346 ±

932 μN (n=10); the greatest low rate contractile force is 4917 μN from a 6M patch. When compared with 2M density patch (1463 ± 576 μN, n=11), the high rate contractile force of 4M (2602 ± 638 μN, n=9) and 6M (3346 ± 932 μN, n=10) patches are significantly greater (p<0.01) (Figure 5G). Likewise, the low rate contractile force of 2M patch (1710 ± 575 μN, n=10) is also significantly lower than that of 4M (3086 ± 804 μN, n=11) and 6M (3346 ± 932 μN, n=10) patches (p<0.01) (Figure 5H). Electrocardiograms of the patches exhibited natural QRS complex patterns, as evidenced by the representative 3 and 5M patches in Figure 4B and D. Figure 4G demonstrates the R wave amplitudes of high rate patches from 4M (24.4 ± 8.7 μV, n=10) and 6M (28.1 ± 6.4 μV, n=5) patches were greater than that from 2M (8.9 ± 8.1 μV, n=8) patch (p<0.01).

2.3.4 Effect of culture time on contractile twitch force

The effects of culture time on patch twitch force were examined for 4M density patch at 0, 2, 4 and 6 days after patch formation. High and low rate twitch force decreased during culture (Figure 6A, B). High rate twitch force on days 0, 2 and 4 are 2602 ± 638 (n=9), 1912 ± 898 (n=7) and 1530 ± 463 (n=5) μN, respectively. On day 6 high rate twitch forces were not detectable. Low rate twitch forces on days 0, 2, 4 and 6 are 3068 ± 804 (n=11), 1879 ± 822 (n=11), 1509 ± 538 (n=8) and 1318 ± 279 (n=6) μN, respectively. A significant difference in high rate twitch force (p<0.05) was obtained between day 0 and day 4 (Figure 5C), A significant difference in low rate twitch force (p<0.01) was obtained between day 0 and days 2, 4, and 6 (Figure 5D). Contractile response frequencies with 1-6M patches are synchronous with electrical pacing which can reach to the 1-6M patches' maximal spontaneous contraction rate. Figure 5A shows a representative synchronous response frequency is 8 Hz obtained from a 4M patch at its formation. The mean synchronous response frequency for 4M patches on days 0, 2, 4 and 6 are 5.9 ± 0.8 (n=9), 5.6 ± 0.9 (n=9), 5.0 ± 0.8 (n=8) and 3.2 ± 1.0 (n=7) Hz, respectively. Synchronous response frequency decreases during culture (Figure 5B), and it is significantly smaller on day 6 relative to the other days (Figure 5E, p<0.01). The contractile

forces by 0.25 and 2 Hz electrical pacing for 4M patch, which correspond to the spontaneous low and high rate contractions, also decrease during culture (Figure 5F, G). However, no significant difference in the contractile force by 0.25 or 2 Hz pacing was observed when compared with low or high rate spontaneous contractile force on the same day points.

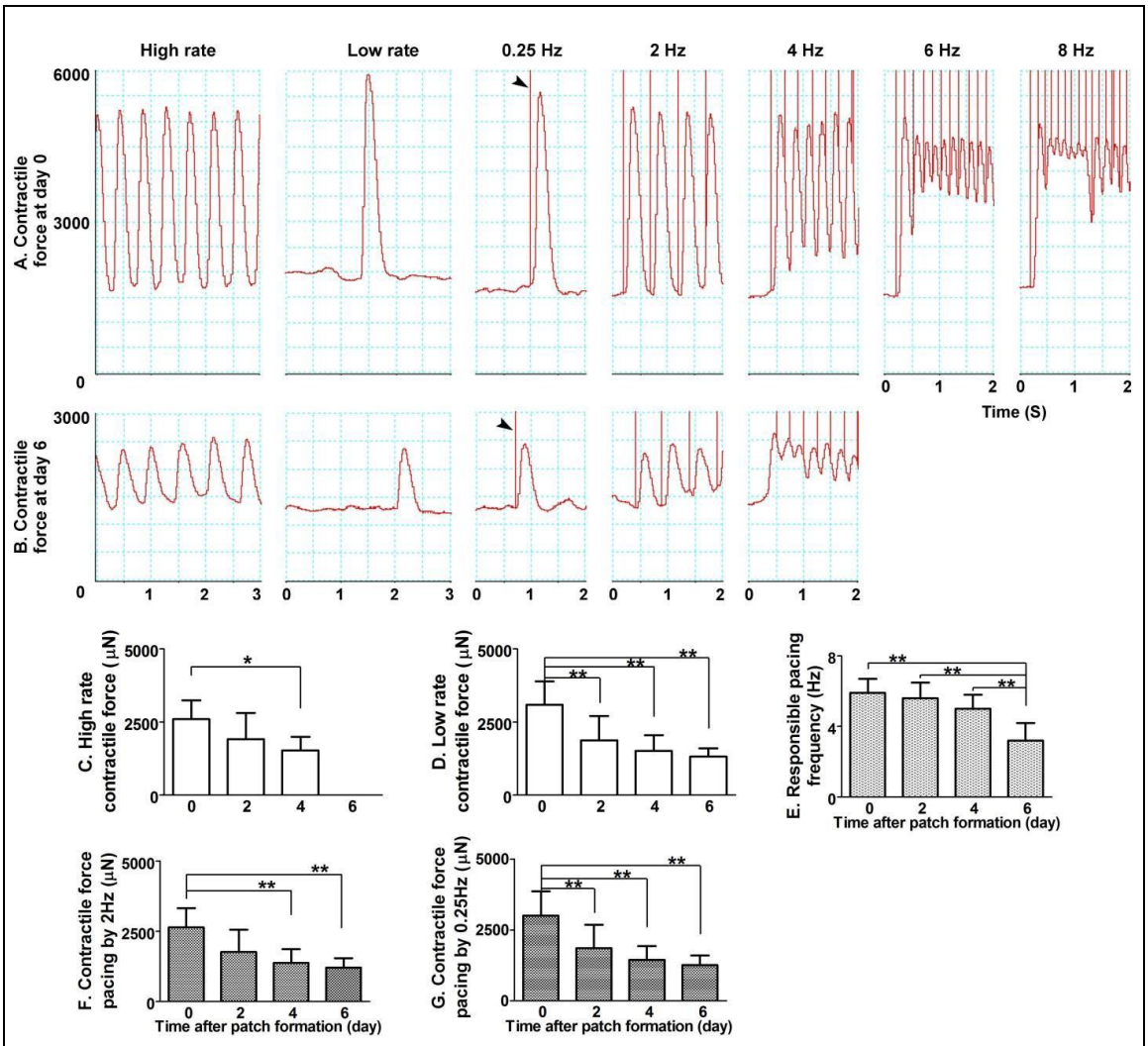

Figure 5: Effects of culture time and electrical stimulation on contractile pacing, **A**, twitch forces at time of formation, **B**, at 6 days, **C** and **D**, high and low rate contractile forces with culture time, **E**, electrical response, **F** and **G**, force with 0.25 and 2.0 Hz pacing.

2.3.5. Morphology

The physical properties of fibrin gel scaffolds of formed patches were examined on day 7. The cross-section area of the triangular patch tissue with 1-6M densities was 32.5 ± 2.8

mm^2 (n=10), its thickness was 0.94 ± 0.13 mm (n=10), its height was 15.1 ± 2.1 mm (n=10), and its weight was 494 ± 43 mg (n=10), there are no significant differences in the cross-sectional areas, patch thicknesses, heights and weights of the triangle blocks with 1-6M densities (p>0.05). The high and low rate contractile twitch forces are generated by one corner of patch tissue (half of the patch, a triangular block), therefore, for 6M density patch the high rate mean contractile force per m^3 volume or per gram wet weight was calculated as 2086μN ÷ (0.5 × 32.5mm^2 × 15.1mm) = 8514 kN/m^3 or as 2086μN ÷ 494mg = 4.22 N/g. By the same formula, the low rate mean contractile force for the 6M density is 14065 kN/m^3 or 6.77 N/g; the high rate mean contractile force for 1M is 2245 kN/m^3 or 1.11 N/g, and its low rate mean contractile force 3959 kN/m^3 or 1.96 N/g.

A layer of cardiac cells and self-produced extracellular matrix proteins, which we call the real cardiac layer, formed on top of the fibrin gel scaffold network (arrow heads, Figure 6A) and the planar networks of fibrin gel scaffold are shown in Figure 6B. The thickness (arrow heads, Figure 6C) of the real cardiac tissue layer was further revealed by Masson trichrome staining though they were physically altered by fixing process. The positive staining for vWF (red) (Figures 6D) suggests that endothelial cells were growing and some endothelial cell grow together to be a congregation (Figure 6D, arrow), the positive staining for the ki67 (white) (Figures 6E) suggests the presence of robust nuclear division, and the positive staining for the collagen type I (purple, Figure 6F) indirectly demonstrates the distribution of myoblasts within the cardiac tissue. A larger endothelial cell congregation within the patch is shown in Figure 6G and a dividing cardiac nucleus in karyokinesis is shown in Figure 5H (arrow). The positive staining for connexin 43 (yellow) (Figure 6I) indicates the intercellular coupling via gap junctions between cardiomyocytes.

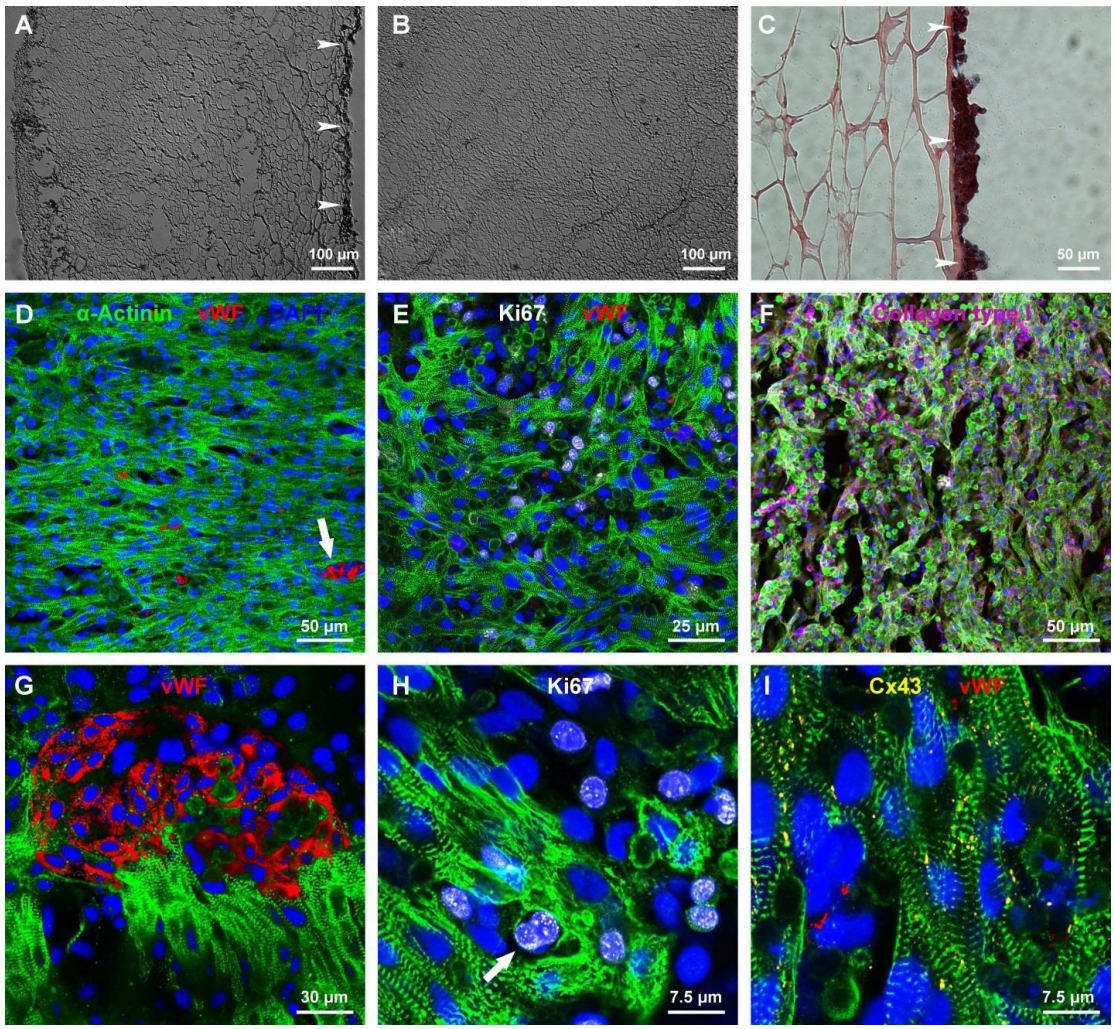

Figure 6: Patch morphology. **A**, cross-section, **B**, planar, **C**, cross-section Masson's, **D**, IHC at 20x **E**, nuclear division (Ki67), **F**, collagen type I within the constructs, **G**, congregation of endothelial cells (vWF), **H** a nucleus in karyokinesis.

The real cardiac layer and part of the support fibrin scaffold stained with Masson's trichrome from 2, 4 and 6M patches are shown in Figures 7A-C. The representative expressions of myofibrils by α-actinin staining and gap junctions by Cx43 staining for 2, 4 and 6M patches are shown in Figures 7D-O. The average thicknesses of real cardiac layers for 2, 4 and 6M were 18.2 ± 2.4 (n=13), 21.4 ± 1.4 (n=14) and 20.6 ± 2.4 (n=12) µm, respectively; there were significant differences when compared 4 and 6M (p<0.05 or p<0.01) with 2M (Figure 7P). The signal volume index of Cx43 was greater for 2M (0.182 ± 0.051, n=13), than

for 4M (0.132 ± 0.039, n=13) and 6M (0.126 ± 0.038, n=16) (p<0.05 or p<0.01) (Figure 7Q). The signal volume index of collagen type I was also calculated to be (0.221 ± 0.065, n=9), (0.209 ± 0.070, n=8) and (0.196 ± 0.050, n=15) for 2, 4 and 6M, respectively; however, there were no significant statistical differences (p>0.05).

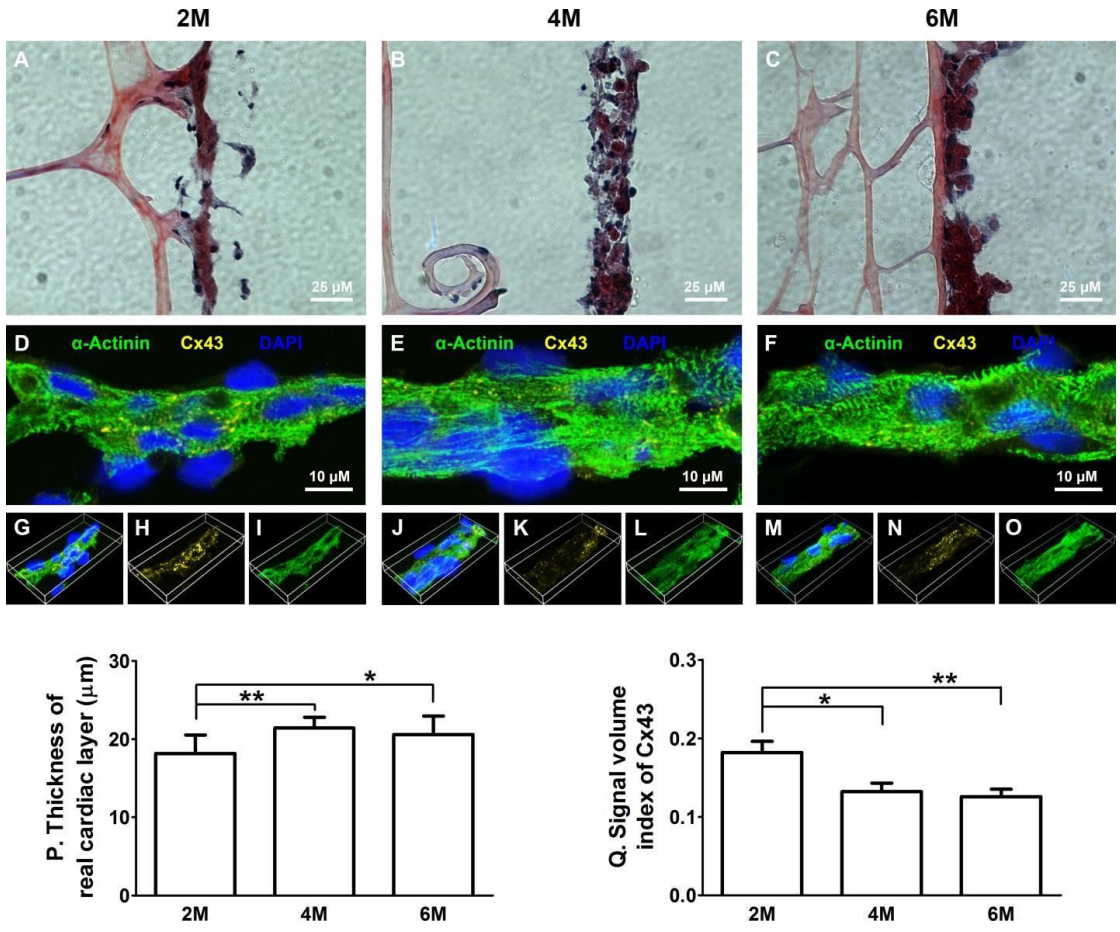

Figure 7: Cardiac thicknesses and gap junctions. **A**, **B**, and **C** cross-section Masson's trichrome stains, **D**, **E** and **F** cross-sections IHC stains, **G**, **J, M** total signal volumes, **H**, **K, N** Cx43, **I**, **K, O** α-actinin, **P**, cardiac layer thickness, **Q**, signal volume index of Cx43.

2.4 Discussion and Conclusion

Fibrin is a natural biopolymer with many interesting properties, such as biocompatibility, bioresorbability, ease of processing, ability to be tailored to modify the conditions of polymerization, and potential incorporation of both cells and cell mediators

(Barsotti et al., 2011). Cardiac cell sheet transplantation improves damaged heart function via superior cell survival in comparison with dissociated cell injection. Native, fully-hydrated fibrin gels can form at different fibrinogen and thrombin concentrations and at different ionic strengths (Blombäck et al., 1989). Fibrin alone, or in combination with other materials, has been used as a biological scaffold for stem and primary cells to regenerate adipose tissue, bone, cardiac tissue, cartilage, liver, nervous tissue, ocular tissue, skin, tendons, and ligaments (Ahmed, Dare, and Hincke 2008). The fibrin support scaffold in the present study was developed with human fibrinogen and thrombin. Under a light microscope, a thin layer of real cardiac tissue (Figure 7A, C) was seen on the top of fibrin gel network, the thickness of the real cardiac layer varied with the plated cell density, with the 4 and 6M patches having a significantly thicker layer than the 2M patches (Figure 7P). The reason for this difference might result from the different initial cell densities and/or the growth rate of each cell type within the patch.

Freshly isolated neonatal cardiac cells consist of myoblasts, cardiomyocytes, smooth muscle cells, endothelial cells and cardiac stem cells. The proliferation rate of cardiac cells is higher in the fetal stage than in the neonatal stage, and greatly diminishes in adulthood (Anversa et al., 2013; Fujimoto et al., 2010). We used 2 to 3-day-old rat heart cells to construct our patch. As shown in Figures 7D, E, and I, specifically in G, endothelial cells and endothelial cell congregation, positively stained by vWF which is secreted by the endothelial cells lining blood vessels, (Ruggeri 1999) were growing in the cultured cardiac patches. A positive staining for vWF demonstrated that there were potential angiogenesis buds, which would be suitable to grow and connect to host micro blood vessels and bring nutrients into the patch during in vivo applications. There were signs of robust cell proliferation in this patch, which were revealed by nuclear division and marked by ki67 positive staining (Figures 6E, H). Ki67 is a nuclear protein which is tightly associated with somatic cell proliferation (Endl and Gerdes 2000).

The Cx43 positive staining indicates that cardiomyocytes in the present cardiac tissue patch exhibit electromechanical coupling (Figure 6I, 7D-F). The detected ECG signal and the natural, adult-heart-like QRS complex revealed that these patches can sustain electrical propagation with speeds that would be close to native tissues. The R wave amplitudes increased with thickness of real cardiac tissue; as shown in Figure 4B, D and G, 4 and 6M patches exhibit greater R wave amplitude than 2M patch because they possess more cardiomyocytes, which can generate a higher depolarization current.

Dishes with higher cell densities (4 to 6M) began localized spontaneous contractions earlier, after only 1 day of incubation. The average contraction rate for 6M density was 410 ± 33 bpm (n=12) on day 2, which falls within the range of a normal adult rat heartbeat. For 1, 2 and 3M densities, the highest mean contraction occurred on days 4, 3 and 3, respectively, and then steadily decreased from day 5 to 6. For 4 to 6M densities, the highest contraction rates occurred much earlier, on day 2 but it decreased sharply from day 3 to 6. As shown in Figure 3A-C, the number of viable cardiac cells (Figure 3A, green arrow heads) that attached to the fibrin gel was dependent on the initial plating densities. Sixteen hours after plating, the pacemaker cells for five 200× fields with 1M density is less than 3 and 5M densities (Figure 3D, $p<0.01$), and that with 3M density is less than 5M too (Figure 3D, $p<0.01$). Supplemental movie 1 was taken 36 hours after cell plating from a 3M density, which shows the pacemaker cells are pacing at different frequencies and so they will compete with each other. After a few more days of incubation, the various frequencies coalesce into a single contraction frequency for the majority of the patch, this results adheres to a synchronization phenomenon that is dependent on the number of initial pacemaker cells and the conduction of their action potentials. The surrounding cardiac tissue comes from the proliferation of the initial seeding myoblasts and the limit dividing of initial seeding myocardiocytes. When it is ready, the dominate fast-speed pacemaker cells can propagate their action potential and initiate the whole tissue contraction. High density cardiac cell plating supplies more high-rate pacemaker cells,

cardiomyocytes and myoblasts. Figure 3E shows that it took 4 days for the pacemaker cells with 1M density to reach maximal contraction rate at 305 ± 54 (n=7) bpm and then plateaued at (average of last day 5 and 6); however, it took only 2 days for the pacemaker cells with 5M density to reach maximal contraction rate of 405 ± 34 (n=11) bpm and plateaued at a significantly lower frequency of (average of day 4, 5, and 6). 3M density dishes may have possessed an ideal proportion of cardiomyocytes to myoblasts, thus allowing them to reach their maximal contraction rate early. This may be the explanation for 3M density dishes having completely formed 56.3% of patches on day 4 and 87.5% patches on day 6, which were quicker than 1M and 5M dishes.

A synchronized contraction relies on the appropriate proportion of cardiomyocytes to myoblasts as well as smooth muscle cells and endothelial cells. In the present study, patches with 1 to 3M densities presumably maintained the appropriate cell-type proportion that enhanced the synchronization and increased the contraction rate. Because the myoblasts proliferate faster than cardiomyocytes, after day 3 or 4 the appropriate proportion no longer existed. The aging and apoptosis of the pacemaker cells and the myoblast overpopulation and the mismatch of contraction cells with extracellular matrix are the main causes for a decrease in contraction rate by affecting the initiation of pacemaker cells, the efficiency of gap junctions and delaying the propagation of action potential. The varying rates of proliferation between myoblasts and cardiomyocytes could also partially explain why steady contractions were detected from 1 to 3M patches, while more arrhythmic contractions were detected from 4 to 6M patches.

The strength of a muscle's contraction is influenced by the number of fibers within the muscle that have interactions of myosin cross bridges with actin, the rate of contraction, and the relaxed length of the muscle fibers. We treated the present cardiac tissue patch as a whole functional unit and analyzed the contractile forces generated by the 1-6M patches. The real cardiac tissue layers of 4 and 6M patches were thicker than 2M (Figure 7P); however, the

signal volume indexes of collagen type I within the 3 densities were not significantly different. This suggests that the myofibril content in 4 to 6M patches may be higher than that in 2M patches. As such, the difference in myofibril content may explain the greater twitch forces generated from the 4 to 6M patches than the 2M one. Based on the results for percentage of complete formation of patches on days 4-6, contractile force, and thickness of the real cardiac layer, a 3 or 4M patch is the optimal choice for future in vivo study.

The reasons for the decreases of response frequency due to electrical pacing and twitch force presumably resulted from the aging and apoptosis of cardiomyocytes, and inappropriate proportion of cardiomyocytes to surrounding matrix caused by the overpopulation of myoblasts. To determine the underlying mechanisms for arrhythmic contractions exhibited in 4-6M patches, we examined the signal volume index of the gap junction protein Cx43. Our results revealed a statistical difference of Cx43 signal volume indexes in 4 and 6M patches when compared with 2M one ($p<0.05$ or $p<0.01$) (Figure 7Q). Cx43 is the major protein of cardiac ventricular gap junctions and is crucial to cell-cell communication and cardiac function (Boengler, Schulz, and Heusch 2006).

Recent works reported that changed expression of Cx43 might contribute to a higher level of arrhythmogenicity (A Salameh et al., 2009; Severs et al., 2008). Criteria for cardiac tissue constructs have been proposed by Zimmermann's group (W.-H. Zimmermann, Melnychenko, and Eschenhagen 2004). These constructs should display functional and morphological properties similar to native heart muscle and remain viable after implantation. The present 3-4M density cardiac constructs possess adult-heart-like spontaneous contraction. Endothelial cell growth, robust cellular division, and electromechanical coupling proteins were all observed. This will allow for invagination of host vasculature and electrical propagation. When it is applied to *in vivo* transplantation, this artificial graft may not only supply enough tension support but also conduct action potential and synchronously contract with the host muscle. Furthermore, it is possible to use host origin fibrinogen and thrombin

to produce non-immunogenic fibrin scaffolds before *in vivo* application. However, the thickness, longevity, and synchronicity of the present patch model are limited due to low levels of nutrient supply within the scaffold network. Future enhanced nutrient delivery will result in a stronger and more energetic artificial cardiac constructs.

Chapter 3: Bioartificial Heart

Establishing the Framework to Support Bioartificial Heart Fabrication Using Fibrin-Based 3D Artificial Heart Muscle

Only 3,000 heart transplants are performed in the U.S. every year leaving some 30,000-70,000 Americans without proper treatment. Current treatment modalities for heart failure have saved many lives yet still do not correct the underlying problems of congestive heart failure. Tissue engineering represents a potential field of study wherein a combination of cells, scaffolds and/or bioreactors can be utilized to create constructs to mimic, replace and/or repair defective tissue. The focus of this study was to generate a basic framework for a bioartificial heart (BAH) using artificial heart muscle (AHM), composed of fibrin gel and neonatal rat cardiac myocytes, and a decellularized scaffold, formed by subjecting an adult rat heart to a series of decellulurization solutions. By suturing the AHM around the outside of the decellularized heart and culturing suspended in media, we were able to generate a construct with the primary rudiments of form and function in a native heart. Visible contractility was correlated with biopotential measurements to confirm basic functionality of the constructs. Cross-sections of the hearts show successful decellularization of the scaffold and contiguous cell-containing AHM around the perimeter of the heart. The study outlines the methods for the successful generation of a novel framework for a BAH construct.

3.1 Introduction

Heart disease is one of the most important medical concerns in this country and is the leading cause of death in the United States. Around 5.7 million people live with heart disease in the United States (Members et al., 2012). Managing these patients accrues costs of nearly 34 billion per year. Coronary heart disease causes about 1 in every 9 deaths in this country. It has been estimated that 30,000 to 70,000 Americans each year would benefit from a heart transplant that

they could not get (Copeland et al., 2004). Conversely, only about 3,000 heart transplants are performed in the U.S. every year.

A variety of heart disease treatment modalities have been explored and are clinically available. Mechanical assist devices have been used in order to bypass or replace failing hearts. Left ventricular assist devices (LVAD) are mechanical pumps designed to increase cardiac output (Bond et al., 2003). Similarly, total artificial hearts (TAH) are mechanical pumps designed to bypass the function of the entire heart, effectively serving as a bridge to heart transplant (Platis and Larson 2009). LVAD and TAH treatments are limited by bio-incompatibility, device failure and absence of bio-integration. Pharmaceutical agents have been developed to combat some of the symptoms of heart disease. ACE inhibitors, diuretics, vasodilators, digitalis preparations, blood thinners and calcium channel blockers are all cardiovascular medications used for the treatment of heart disease. Unfortunately, these medications typically treat the symptoms of heart disease and do little to combat the underlying problem of damaged cardiac tissue.

Presently, the only long-term solution to heart failure is organ transplantation. Unfortunately, there are far too few donor hearts to meet this need. Due to the rapid deterioration of excised tissue, donor hearts must be used within several hours of explantation. This can make planned procedures very difficult and reduces the efficacy of treatment for end stage heart failure. Furthermore, donor and recipient must be matched for blood type and body size in order to reduce risk of rejection. The lack of donor hearts, along with the difficulty of scheduling and prohibitive costs of heart transplants contribute to the inadequacy of heart transplant procedures as effective means of cardiovascular disease treatment.

In the field of regenerative medicine, researchers attempt to develop methods to circumvent current clinical limitations. Archundia *et al.* and Amado *et al.* experimented with direct injection of cells for cardiovascular regeneration (Archundia et al., 2005; Amado et al., 2005). Another common regenerative medicine approach involves introduction of tissue inducing substances *in vivo*. Hayashi *et al.* developed scaffolds designed to promote endogenous bone growth (Hayashi et

al., 2009). Tissue engineering is an interdisciplinary field applying the principles of engineering to biological components. In the field of tissue engineering, a combination of cells, scaffolds and/or bioreactors are used in order to create a construct designed to emulate native tissues (Langer and Vacanti 1993). Complex biomimetic tissues can also be created *in vitro* using combinations of cells, scaffolds, and bioreactors, which mimic *in vivo* conditions (Shachar, Benishti, and Cohen 2012). The field provides many promising potential research avenues for treatment alternatives to conventional therapies.

Our lab has extensive experience with regards to the creation of AHM tissues and cardiovascular components (Evers, Khait, and Birla 2011; Birla, Hollister, and Migneco 2008; L Khait and Birla 2007; Baar et al., 2004; Blan and Birla 2008; Y.-C. Huang, Khait, and Birla 2007). Using laminin as a scaffold on PDMS coated dishes, Baar *et al.* created self-organized contractile 3D cardiac tissue using neonatal cardiac myocytes (Baar et al., 2004). Deemed cardiods, this work produced one of the first 3D cardiac muscle tissue constructs capable of generating a contractile force of roughly 140 μN (Baar et al., 2004). Using a porous chitosan scaffold and rat neonatal cardiac cells, Blan and Birla created a smart material integrated heart muscle (SMIHM) with a maximum contractile twitch force of 439.5 μN (Blan and Birla 2008). Using fibrin gel as a scaffold, Huang, Khait and Birla created bioengineered heart muscle (BEHM) with an active twitch force of ~835 μN (Y.-C. Huang, Khait, and Birla 2007). Most recently, our group developed a fibrin based AHM with structural similarity to native heart muscle tissue capable of generating an active twitch force upwards of 4 mN.

We plan on capitalizing on our expertise in AHM generation for the development of a framework for a bioartificial heart. BAHs are a potential alternative therapy for end stage heart failure using decellularized hearts as a scaffold for functional cardiac myocytes (Gilbert, Sellaro, and Badylak 2006; Ketchedjian et al. 2005). If properly seeded and conditioned, decellularized constructs can function as basic pumps providing a model for a total artificial heart (Black et al.,

2008). The focus of this study is the production of a BAH using fibrin gel based AHM sheets and decellularized heart scaffolds.

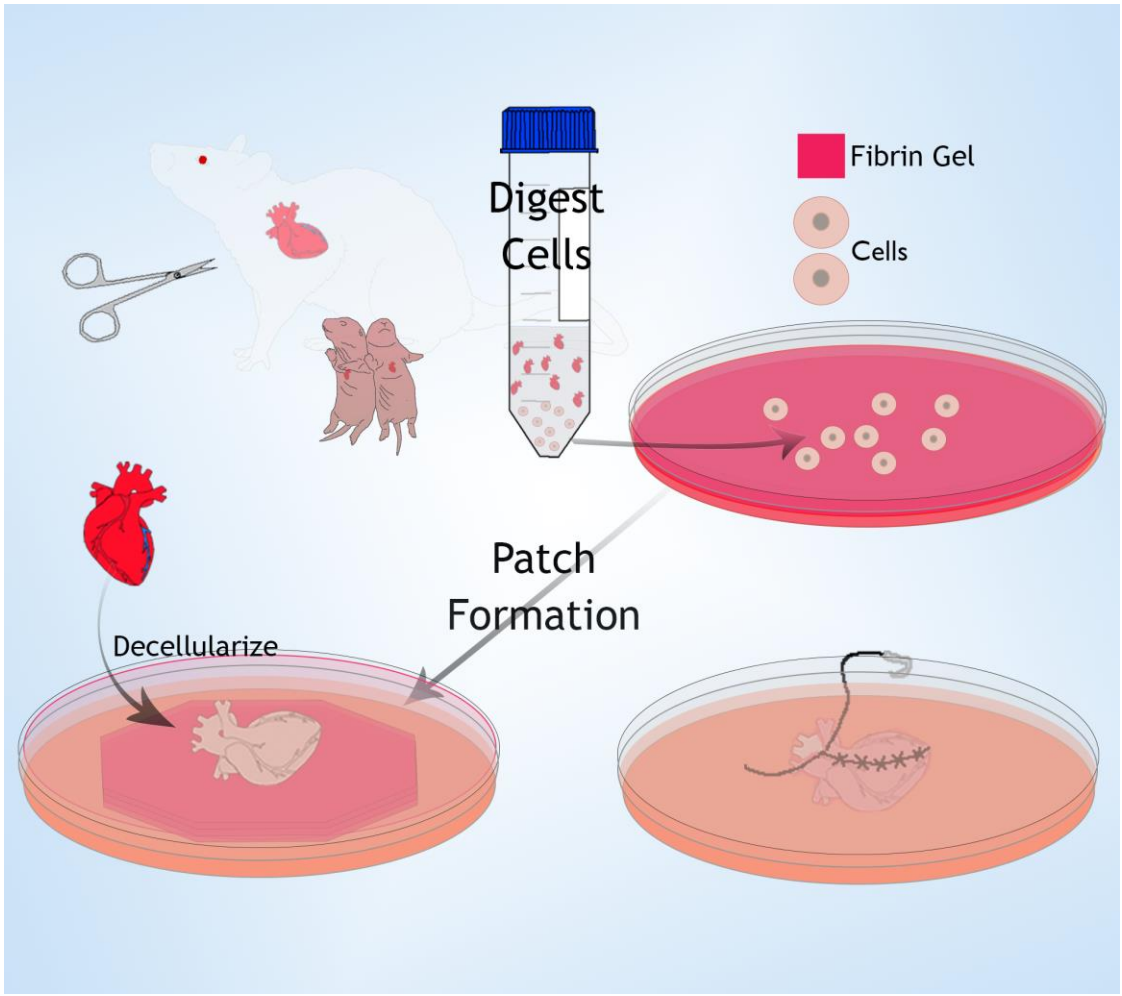

Figure 8: Protocol for the generation of a BAH using AHM.

3.2 Materials and Methods

All animal protocols were approved by the Institutional Animal Care and Use Committee (IACUC) at the University of Houston. All materials were purchased from Sigma-Aldrich (St. Louis, MO) unless otherwise specified.

3.2.1 Decellularization of scaffolds

Rat hearts were obtained from 3-6 month old Sprague-Dawley rats and immediately washed in a phosphate buffered saline solution to prevent blood coagulation. The hearts were then sequentially incubated in 15 mL of a series of decellularization solutions as indicated in Table 1 and shaken at 60 RPM in an orbital shaker at 25°C over the course of 14 days.

Table 1: Decellularization protocol

	Components	Schedule
Solution 1	80% Glycerol* 0.9% NaCl 0.05% NaN_3 25 mM EDTA	Day 0-2
Solution 2	4.2% sodium deoxycholate 0.05% NaN_3	Day 2-4
Solution 3	1% SDS 0.05% NaN_3	Day 4-6, Day 8-10
Solution 4	.05% NaN_3	Day 12-14
Solution 5	3% Triton X-100* 0.05% NaN_3	Day 6-8, Day 10-12

*By volume

3.2.2 Isolation of primary cardiac cells

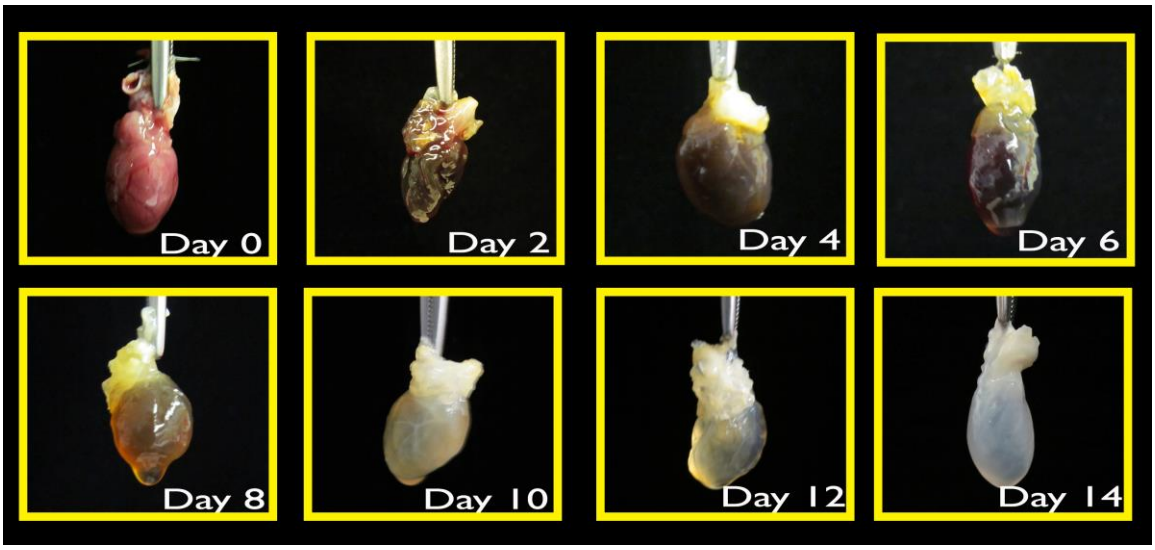

Figure 9: Decellularization process of a rat heart, Progress of decellularization of the rat hearts at 2-day increments over 14 days.

Cardiac cells were isolated from the hearts of 2-3 day old neonatal Sprague-Dawley rats using an established method. Each heart was cut into 3-4 pieces in an ice-cold phosphate buffer consisting of 116 mM NaCl, 20 mM HEPES, 1 mM Na_2HPO_4, 5.5 mM glucose, 5.4 mM KCl and 0.8 mM $MgSO_4$. The pieces were gently rinsed in order to remove blood and transferred to a

secondary phosphate buffer solution. Tissues were minced into 1 mm^3 pieces and transferred to a dissociation solution (DS) consisting of filtered 0.32 mg/ml collagenase type 2 (Worthington Biochemical Corporation, Lakewood, NJ) and 0.6 mg/ml pancreatin in phosphate buffer. A 50 mL conical tube containing 15 mL of DS and the minced tissues was placed in an orbital shaker and maintained at 37°C for 30 minutes at 60 rpm. At the end of the digestion process, the supernatant was collected in 3 ml of horse serum to neutralize the enzyme and centrifuged at 1,000 rpm for 5 minutes at 4°C. The cell pellet was re-suspended in 5 ml horse serum and kept in an incubator at 37°C supplied with 5% CO_2. Fresh DS was added to the partially digested tissue and the digestion process was repeated an additional 2-3 times. Cells from all the digests were pooled, centrifuged and suspended in culture medium (CM) consisting of M199 (Life Technologies, Grand Island, NY), with 20% F12k (Life Technologies), 10% fetal bovine serum, 5% horse serum, 1% antibiotic-antimycotic, 40 ng/ml hydrocortisone and 100 ng/ml insulin. Cell concentration and viability was assessed by Trypan blue (4%) staining according to the manufacturer's protocol.

3.2.3 Fabrication of AHM

The heart muscle was fabricated using a fibrin gel and neonatal cardiac myocytes (Figure 8 and Figure 10). A 35 mm tissue culture plate was coated with 2 ml of SYLGARD (PDMS, type 184 silicone elastomer) (Dow Chemical Corporation, Midland, MI). The plate was air dried for 2 weeks and sterilized with 80% ethanol before use. Eight minutien pins (Fine Science Tools, Foster City, CA), 0.1 mm diameter, were placed in the culture plate to form a regular octagon with a radius of 1.3 cm, a square with 2 cm and a square with 3 cm edges. Mixing 1 mL of CM containing 10 U thrombin/mL with 500 μL of saline containing 20 mg/mL fibrinogen in a PDMS coated petri dish allowed for the formation of a fibrin gel scaffold. The petri dishes were shaken well to promote mixing and placed in the incubator in order to promote gel formation within 15 minutes. Cells were seeded with a density of 4M per plate. Epsilon-aminocaproic acid (2 mg/mL) was added to the culture plate to inhibit the fibrinolysis by endogenous proteases. The cells were cultured in an incubator at 37°C and 5% CO_2 with CM changes every two days.

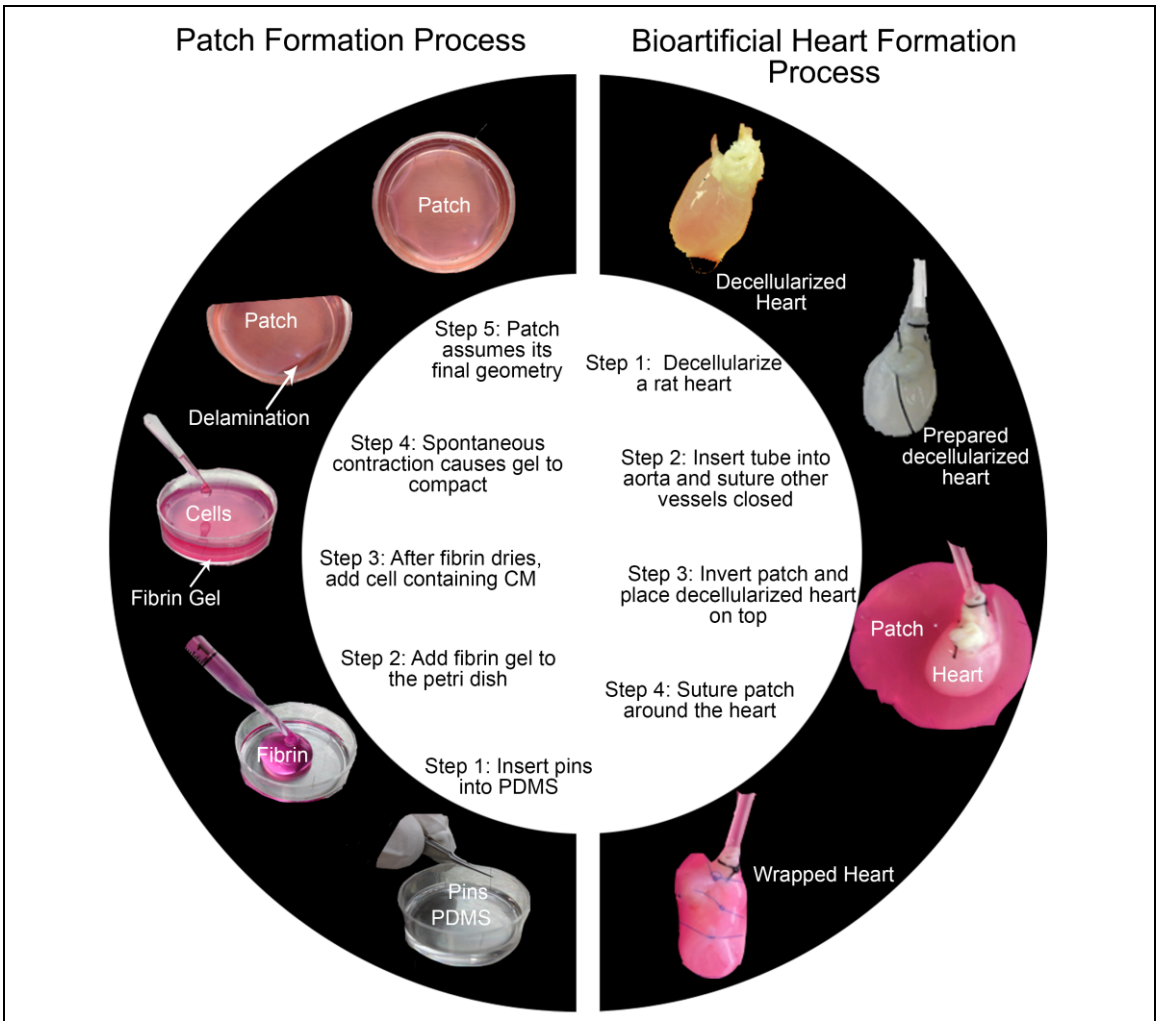

Figure 10: Photographs of Stages of the Artificial Heart Formation Process, The left side of the figure illustrates the stages in the AHM fabrication process and the right side shows the various steps when constructing the total bioartificial heart.

3.2.4 Contractile twitch force of AHM

From day 4, twitch force was measured using a high sensitivity isometric force transducer (MLT0202, ADinstruments, Colorado Springs, CO), connected to a quad bridge amplifier (FE224, ADinstrument, Colorado Springs, CO). Data acquisition was performed through a 16 channel PowerLab system (PL3516/P, ADInstruments, Colorado Springs, CO). The force transducer arm was attached to one free-corner of the patch, while the other ends were held fixed; spontaneous measurements were recorded for 30-60 seconds. Pretension was adjusted using a micro-manipulator (Radnoti LLC, Monrovia, CA) and measurements of spontaneous contraction were

recorded. A Stable-Temp hotplate (Cole-Parmer, Vernon Hills, IL) was used to maintain media temperatures at 37°C throughout the course of measurement. LabChart's (ADInstruments, Colorado Springs, CO) peak analysis module was used to calculate the maximum twitch force and baseline force (pretension).

3.2.5 BAH formation

Decellularized heart scaffolds were washed 3 times and placed in PBS 24 hours prior to construct formation to wash out decellularization solutions. At 4-6 days after plating, most AHM tissues were fully formed. The anchoring minutien pins were gently removed from the AHM. The artificial muscle was then lifted using two forceps and delicately inverted on the petri dish surface. Artificial heart tissues were re-pinned to the PDMS using minutien pins. The decellularized heart scaffolds were placed on the inverted tissues. The AHM was unpinned and gently sutured around the outside of the decellularized scaffolds using sterile 6-0 polypropylene sutures (AD Surgical, Sunnyvale, CA). The completely wrapped construct was suspended in a 50 mL conical tube by a 1/16" diameter tubule inserted through the aorta of the decellulularized construct. Subsequently, 15 mL of CM was added along with ε-aminocaproic acid (2 mg/ml), and the construct was placed in an incubator at 37°C and 5% CO_2 with CM changes every two days and observed periodically for contraction.

3.2.6 Contraction

Bioartificial hearts were examined daily for contractile action using an inverted phase-contrast microscope (Olympus, Center Valley, PA). Hearts were removed from culture and placed in a small amount of CM in a 60 mm petri dish coated with PDMS. Still photographs and videos were captured using a camera (Lumenera, Ottawa, ON) mounted on a light microscope. (Olympus, Center Valley, PA).

3.2.7 Biopotential measurement

Biopotential measurements were observed through the direct application of 8 electrodes to the construct after a period of culture. Constructs were placed in a PDMS coated petri dish with warmed media. A Stable-Temp hotplate (Cole-Parmer, Vernon Hills, IL) was used to maintain media temperatures at 37°C throughout the course of measurement. Eight electrodes were pierced into the construct in a 4x2 grid with 2.54 mm of space horizontally between each electrode column and 3.8 mm of space vertically between each row. A reference wire was secured in PDMS in direct contact with the media at the edge of the dish. Electrodes were connected to an Octal Bio Amp (ML138, ADInstruments, Colorado Springs, CO). Data acquisition was performed through a 16 channel PowerLab system (PL3516/P, ADInstruments, Colorado Springs, CO). LabChart (ADInstruments, Colorado Springs, CO) was used to output the 8 measured channels into a table with a sampling rate of 1000 Hz over 2 minute periods. Matlab (Mathworks, Natick, MA) was used to analyze and process the data. A moving average smoothing function with an 8% span was applied to the data for all 8 channels to reduce noise.

3.2.8 Histology

Histology was performed on natural and fully decellularized rat hearts, and BAHs after 6 days of culture. Samples were all washed in PBS and gently patted dry using VWR® light-duty tissue wipers. Samples were suspended upright in a peel-a-way disposable embedding mold (VWR International, Radnor, PA) and submerged in liquid nitrogen for several seconds. Samples were then covered with Tissue Tek OCT (VWR International Radnor, PA) and placed immediately into a -85°C freezer. Once samples were completely solid, each sample was cross-sectioned using a cryotome (Thermo Fisher Scientific, Waltham, MA). Tissue samples were cut at a thickness of 10-40 μm and placed on VWR® microslides. Cross-sections were stained with Masson's trichrome and H&E reagents according to manufacturer's protocol, and images were taken under the light microscope.

3.2.9 Immunohistochemistry

Samples were frozen in OCT compound and sectioned to 10-40 μm thicknesses and placed on VWR® microslides. Cross-sections were fixed in ice cold acetone for 10 minutes; nonspecific epitope antigens were blocked with 10% goat serum at room temperature for 1 hour. Sections were incubated with mouse anti-α-actinin monoclonal antibody (Sigma, Catalog No A7811) 1:200 and rabbit anti-collagen type I (Abcam, ab34710) 1:100 at room temperature for 1 hour. Subsequently, sections were treated with goat anti-mouse and goat anti-rabbit secondary antibodies (Alexa Fluor 488 and Alexa Fluor 546, Life Technologies, Grand Island, NY) 1:400 at room temperature for 1 hour. Nuclei were counterstained with 4,6-diamidino-2-phenylindole (DAPI) (2.5 μg/ml) for 5 min at room temperature. Fluorescent images were obtained with a Nikon C2+ confocal laser scanning microscope (Nikon Instruments Inc., Melville, NY). Z-stack images were taken in order to examine 3D structures of sample slices with more than 20 μm thicknesses.

3.3 Results

3.3.1 Patch formation

Established cell isolation methods were used to harvest cells with a viability of 81.0 ± 2.2% (n=16). Delamination typically began at day 3 with patch formation usually completing by day 4 or 5. Contractile forces of patches plated with 4M cells using this method measured up to ~3,000 μN. Patches exhibited macroscopic spontaneous contractions after 2 days of culture. The frequency of spontaneous contraction was in the range of 1-5 Hz. Patches were observed to contract continuously and actively for upwards of 3 weeks.

3.3.2 Decellularization

Hearts isolated from adult Sprague Dawley rats were subjected to a series of decellularization solutions as outlined in Table 1. The hearts became noticeably clearer and more translucent at each stage in the process (Figure 9). Hearts at day 0 and 14 of the decellarization process were sectioned and stained with H&E and Masson's trichrome staining (Figure 11 and

Figure 12). Sections of hearts at day 0 in the decellularization process exhibited typical H&E and Masson's trichrome patterns for untreated rat hearts. Masson's trichrome stains at day 14 contained only blue stains and revealed no nuclei. H&E stains at day 14 in the process showed only red stained networks with no nuclei.

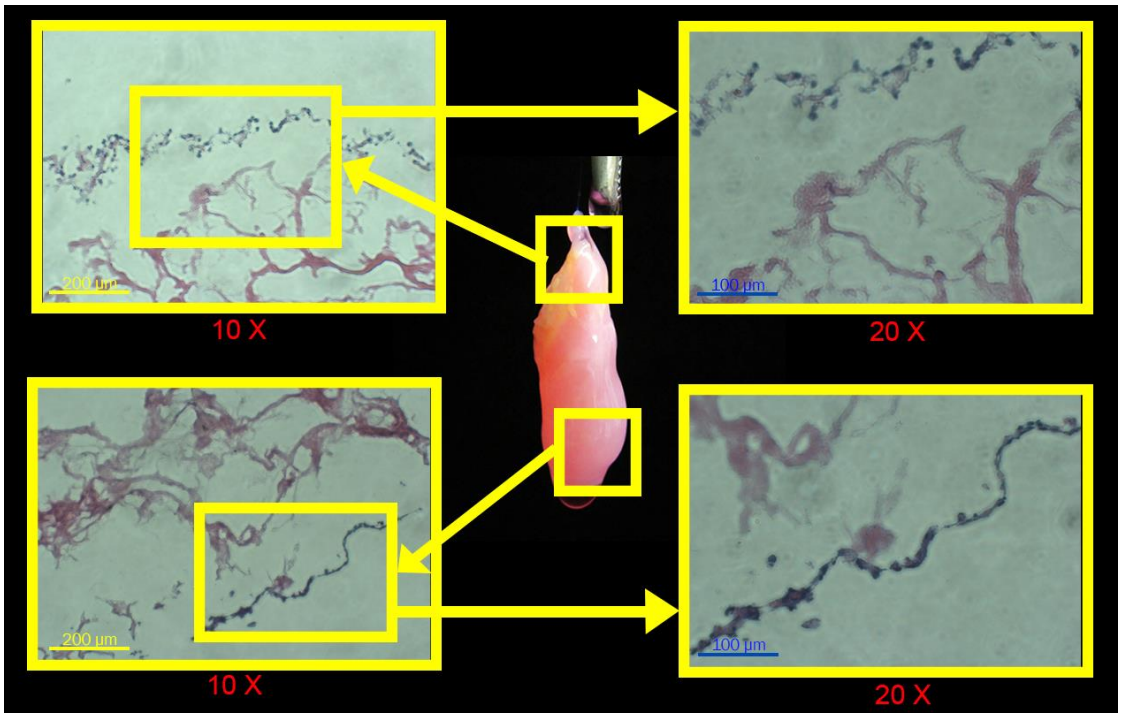

Figure 11: Histology of the Bioartificial Hearts (H&Es), H&E stains of a cross section of the total bioartificial heart. Cell nuclei are stained black and eosinophilic structures such as fibrin and collagen are stained pink.

3.3.3 BAH formation

Decellularized hearts were washed in PBS in order to remove sodium azide from the structures. Sodium azide typically lyses cells and if not washed, destroys viable cells from AHMs removing functionality of the construct. Patches were treated gently in order to avoid destroying fragile cardiac myocytes. Constructs were formed using both inverted and non-inverted heart muscle formation techniques. Cells tend to aggregate on the upper layers of the fibrin gel using normal AHM formation techniques. Inverting the heart muscle prior to wrapping exposed the majority of the functional cells to the outer surface. When heart muscle tissue was inverted, there

was a noticeable increase in frequency of contraction of the artificial heart constructs viewed under the light microscope when compared with non-inverted muscle tissues.

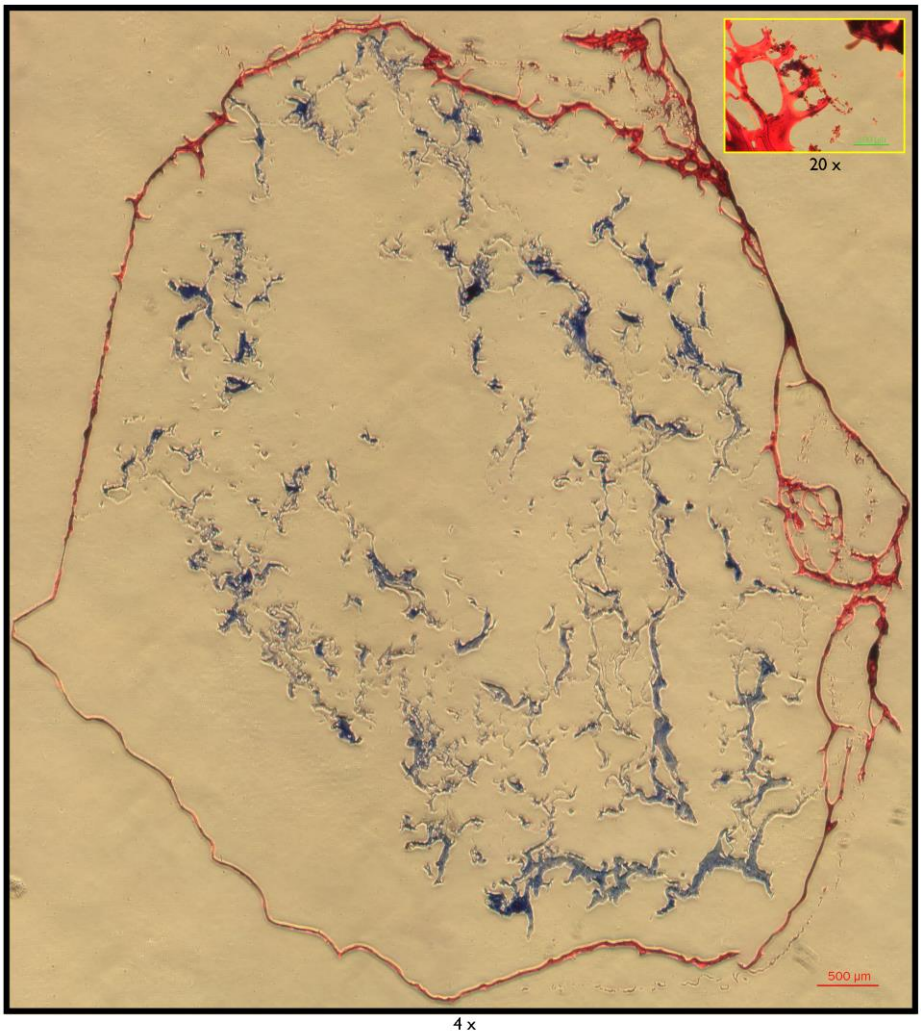

Figure 12: Histology of a cross section of the Bioartificial Heart (Masson's trichrome), A stitched image consisting of 28 4x images of a Masson's trichrome stained cross-section of a BAH.

3.3.4 Contraction of BAH

After wrapping the patches around the outside of the decellularized hearts and securing them with sutures, contraction frequency would diminish or temporarily halt. After culturing the constructs for 1-2 days, contraction would resume at or near pre-wrapping frequency. Noticeable contractility was observed around the entire area of the heart under an inverted microscope. Observed contractile frequencies of beating BAHs ranged from 0.3 to 5 Hz.

3.3.5 Morphology

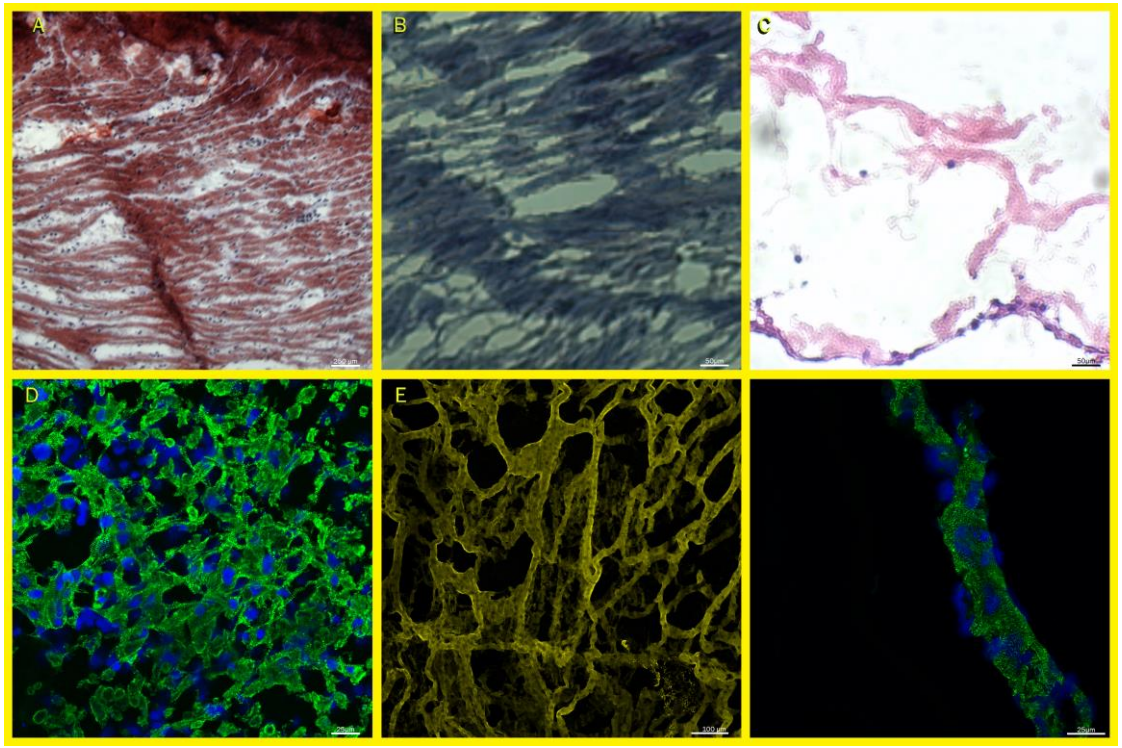

Figure 13: Histology of the BAH, **A**, Masson's trichrome of adult rat heart, **B**, Masson's of a decellularized heart, **C**, H&E of a BAH, **D**, IHC (α-actinin, DAPI) of BAH, **E**, IHC (collagen) of decelluarized heart, **F**, cross section IHC stain of a BAH.

Cross-sections stained with H&E were positive for nuclear stain around the acellular scaffold, indicating the presence of cardiac cells (Figure 11). The cell-rich AHM layer is visible around the perimeter of each image. The interior portion contains completely decellularized ECM. Masson's trichrome stained cross-section of a BAH were imaged and stitched to visualize an entire cross-section (Figure 12). The exterior layer contains red stained fibrin gel and black stained cell nuclei. The interior portion is completely decellularized ECM with no noticeable black spots.

3.3.6 Immunohistochemistry

Confocal images contained fluorescently labeled structures highlighting collagen type I, α-actinin and cell nuclei (Figure 13D and F). Confocal images of the decellularized scaffold showed a collagen rich network with many apparent empty spaces dispersed throughout the network (Figure

13A). A cell rich layer containing collagen (yellow) α-actinin (green) and DAPI (blue) was found around the perimeters of the stained sections (Figure 13B).

3.3.7 Biopotential measurements

Synchronous contractility was observed across 8 electrode channels in a waveform pattern consistent with native heart muscle (Figure 14). The sample measurement indicated a contractile rate of approximately 4.5 Hz with biopotential amplitudes in the range of 10-200 μV.

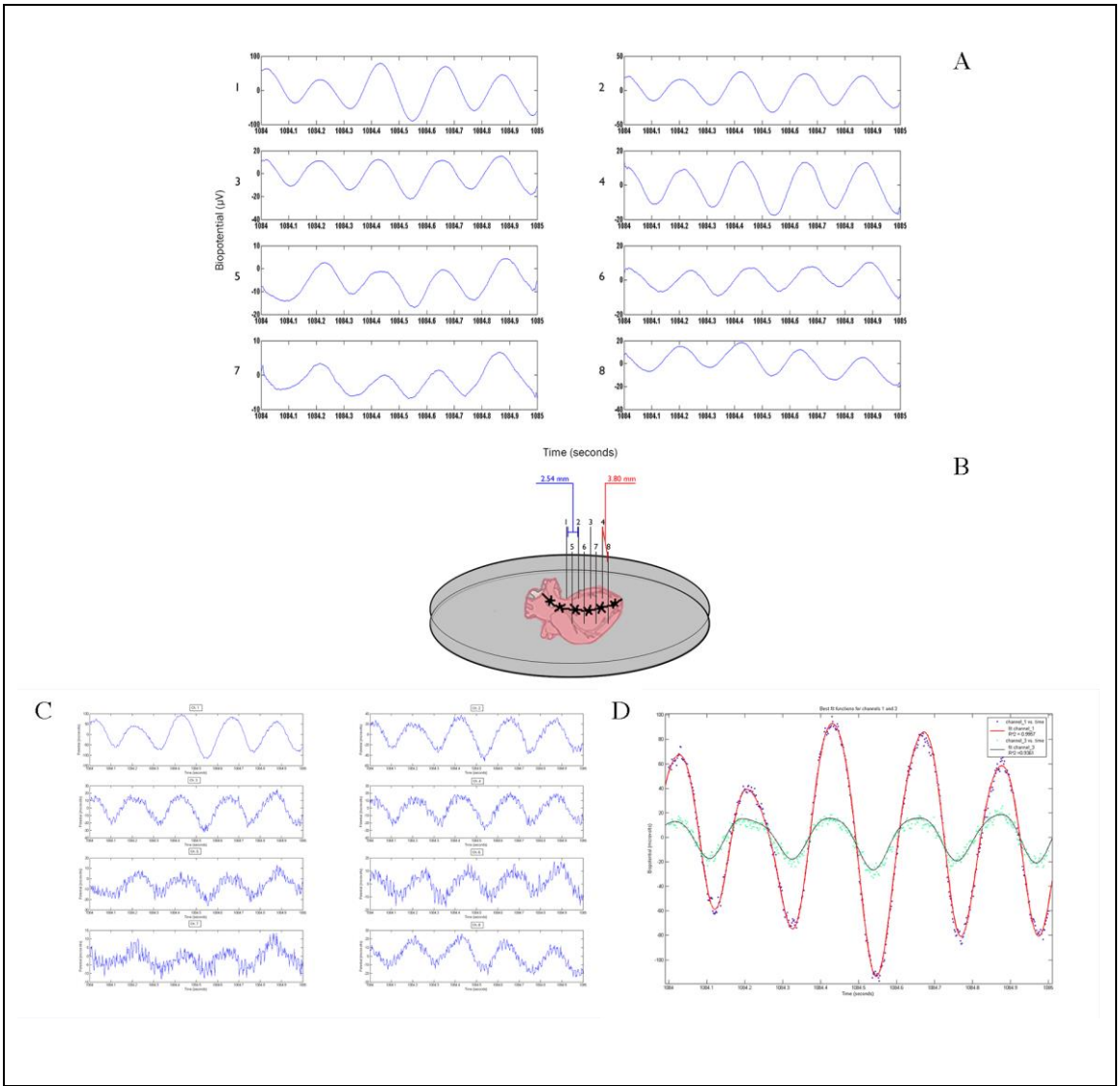

Figure 14: Biopotential measurements of a beating BAH, **A**, Biopotential measurements over time for 8 electrodes, **B**, Schematic of the approximate placement of each electrode throughout the BAH sample, **C**, Unfiltered readout, **D**, Smoothed signal fit

3.4 Discussion and Conclusion

The method used to generate patches in this study represents a novel tissue engineering protocol for the generation of AHM. Confocal analysis of the AHM indicates structural similarity to native heart muscle, (Figure 13B) and measured twitch forces represent a high degree of functionality. Fibrin gel was used as a scaffold as the two main components, fibrinogen and thrombin, can be isolated from human blood so patient specific scaffolds can be created. Use of minutein pins to control the geometry of the final patch gives us the ability to control AHM shape to fit a particular application. Throughout the course of this study, AHMs were generated in a variety of square sizes (2 - 3 cm^2) and in an octagonal geometry. Octagonal geometries afforded the most efficient means of coverage of the perimeter of decellularized rat hearts while requiring the fewest resources. High twitch forces along with a readily reproducible and bioactive scaffold render our AHM model an efficient mechanism for delivery of cells to a structurally sophisticated scaffold.

The decellularization process occurred over the course of 14 days (Figure 9). Decellularization solutions were not actively perfused through the hearts as in previous studies (Black et al., 2008). Simple submersion and agitation was used in order to increase the throughput of the method. After completion of the decellularization process, the remaining extracellular matrix structures appeared macroscopically intact. Vessels, ventricles and atriums are visible inside of the translucent structures. H&E and Masson's trichrome stains of the decellularized constructs show striated ECM networks with no cellular presence (Figure 11). Confocal images of the decellularized scaffold show a collagen rich network containing no cells. High-resolution images reveal empty spaces ~5-10 μm in diameter where cells were located prior to decellularization of the heart (Figure 13A). Effective decellularization of the hearts indicates the efficiency of the decellularization protocol.

There are two phases to the overall process for the formation of a BAH (Figure 10). AHM formation is the phase in which the functional components of the construct are created. The second phase of construct formation involves decellularization of the scaffold and subsequent attachment of the functional component. AHM represents an effective delivery vehicle for functional cardiomyocytes to the decellularized scaffold. Passive seeding of cells into a decellularized matrix, through coating or injection is an inefficient process, as most cells wash out of the matrix. (Black et al., 2008). The biologically active fibrin matrix contains functional sites at which cells can bind more readily. Physically combining the AHM with a structurally complex decellularized scaffold represents an alternative strategy for delivery of cells to a biologically similar matrix.

After the AHM is formed, it is inverted and a decellularized heart is placed on the surface. Cells aggregate on the upper surface of the fibrin gel in an AHM. Inverting the AHM exposes the cells to the outer surface thereby insuring more effective nutrient delivery from CM to the cells of the AHM. Initial studies performed without inversion of the AHM resulted in lower contraction of the construct. We hypothesize that this is due to limited nutrient delivery. After attachment of the AHM, BAHs were placed in static culture during which they experienced a period of latency of 1-2 days with no observable contraction. After culture for 4 days, slight pulling of the exterior AHM did not cause the fibrin layer to detach from the decellularized surface. This indicates some degree of interaction between the fibrin scaffold and ECM of the decellularized heart.

Noticeable contractility was observed around the entire perimeter of BAH constructs. While the contraction was typically microscopic, observable contraction indicates retention of basic myocardial function. Introduction of electrical pacing and perfusion may improve contraction rates and overall contractile force. Continually, only 4 million cells were used in order to produce the AHM tissue, while a typical adult rat heart is estimated to have approximately 100 million cells (Rakusan et al., 1984; Banerjee et al., 2007).

Confocal staining of cross-sections of the samples indicated 3 main components: a cell-rich layer, a fibrin scaffold and a decellularized matrix (Figure 13). Positive stains for α-actinin, a

protein found in Z-discs of cardiac muscle, confirm the presence of cardiomyocytes in the BAH constructs. Positive collagen stains indicate healthy cells in the cell-rich layer. Furthermore, the collagen network visualized in confocal images of the decellularized scaffold is structurally complex and contains no cells (Figure 13A).

The synchronicity of biopotential peaks in channels 1-8 indicates a degree of cell-cell interactivity (Figure 14). While channels 1-8 represent the biopotentials at 8 distinct locations across the construct, the peaks and troughs of the biopotential readings are relatively well matched. Variations in the biopotential amplitudes amongst electrodes may be due to minor variations in cell density at different locations around the BAH. Constructs were not paced prior to measurement, indicating the AHMs ability to self-pace. Furthermore, the spontaneous contractile frequency measured in Figure 14 is approximately 4.5 Hz, which is similar to the resting heart rate of a newborn rat.

The methods described for generation of BAH constructs characterize an original protocol for establishing the framework of a tissue-engineered heart. Advanced tissue engineered heart muscle with a bioactive scaffold and high twitch force represents a novel vehicle for cellular delivery. A decellularized and highly structured scaffold allows potential for future sophistication and adaptability of the concept. Combination of the two allows for the inception of contractile and pumping ability to a structurally complex, natural heart scaffold.

Static culture of tissue-engineered constructs is a limited technique and generally unsuitable for 3D tissue culture. True tissues *in vivo* are constantly subjected to a variety of stimuli, which direct the form and function of cells in the tissues. As such, it is essential to recreate some of the aspects of the in vivo environment in order to ensure enhanced performance and viability of tissue-engineered constructs (Chen and Hu 2006). Towards this end, we have begun work on several bioreactors for enhancing BAH function, including an electrical stimulation and a dual-purpose perfusion bioreactor with the ability to perfuse media and provide mechanical stimulation simultaneously. While inclusion of AHM to the outer surface of the constructs is an efficient means

of cellular delivery, there was little cellular penetration into the decellularized scaffold. Recellularization of the decllularized matrix must occur in order to produce a more innate structure. The current model is formed using only 4 million cells per heart. Consequently, in order to improve construct similarity to native tissue, more cells must be added. One potential seeding method involves ε-aminocaproic acid. The acid is added during culture of the AHM to reduce degradation of the fibrin gel. If the acid is not added after construct formation, degradation of the gel occurs resulting in the deposition of a thin layer of cells to the outer surface of the decellularized matrix. If this process is repeated to embed multiple layers of AHM, it could represent an effective means of delivering a high number of cells to the construct. Another method for deposition of cells to the decellularized matrix involves direct injection. Unfortunately, direct injection is a relatively inefficient method with the majority of the cells washing out in culture. Pretreatment of cardiac myocytes with linker molecules or integrin stabilizers such as Manganese Chloride ($MnCl_2$) may increase the efficiency of attachment of directly injected cells (Shimaoka, Takagi, and Springer 2002; Grinnell 1984; McGinn et al., 2011).

In this study, we describe a method establishing the framework for the formation of a bioartificial heart construct. Our use of sophisticated tissue engineered heart muscle along with a highly organized decellularized scaffold represents a promising advance towards the development of a true total bioartificial heart.

Chapter 4: Magnets and 3D Cultures

Magnetic Cell Labeling and Levitation to Support the Rapid Assembly of Three-Dimensional Cardiac Cultures

Easily assembled organotypic co-cultures have long been sought in medical research. *In vitro* tissue constructs with faithful representation of *in vivo* tissue characteristics are highly desirable for screening and characteristic assessment of a variety of tissue types. Cardiac tissue analogs are particularly sought after due to the phenotypic degradation and difficulty of culture of primary cardiac myocytes. This study utilized magnetic nanoparticles and primary cardiac myocytes in order to levitate and culture multicellular cardiac aggregates (MCAs). Cells were isolated from 2 day old Sprague Dawley rat hearts and subsequently two groups were incubated with either C_1: 33 μL NanoShuttle/million cells or C_2: 50 μL NanoShuttle/million cells. Varying numbers of cells for each concentration were cultured in a magnetic field in a 24 well plate and observed over a period of 12 days. Constructs generally formed spherical structures. Constructs exhibited noticeable contraction after 4 days of culture and continued contracting past day 12 of culture. Phenotypic conservation of cardiac cells was ascertained using IHC staining by α-actinin, ki67, n-cadherin, cTnI and collagen. CD31 and fibrinogen were probed in order to confirm the presence of endothelial cells and levels of ECM production respectively. This study verifies a protocol for the use of magnetic levitation in order to rapidly assemble 3D cardiac cultures that preserve phenotypes and exhibit contractile activity.

4.1 Introduction

Three-dimensional (3D) cell culture systems represent an emerging and critical area of biomedical research. In recent years, the importance of a cost-effective, serviceable 3D culture system has become increasingly apparent (Zhang 2004; Haycock 2010; Griffith and Swartz 2006; Cukierman et al., 2001; Abbott 2003; Atala 2007; Pedersen and Swartz 2005). While two-

dimensional (2D) cell culture experiments compose the primary mode of discovery since the inception of cell research, there are innate limits to flat culture. The gaps in complexity and fidelity between 2D cultures and native tissues, limit potential of research in 2D in vitro experiments. De-differentiation, lack of multi-dimensional cell-cell connectivity, and structural simplicity contribute to the fundamental shortfalls of traditional culture models (Pampaloni, Reynaud, and Stelzer 2007).

Organotypic culture systems, thus, have been a central area of concern in biomedical research for decades. Development of efficacious high throughput screening (HTS) methods for tissue-mimetic models represents a holy grail in the field (H. Zimmermann, Shirley, and Zimmermann 2007; Mueller-Klieser 1997; Mehta et al., 2012; Kwapiszewska et al., 2014; Takayama et al., 2013). Organotypic culture systems must meet several criteria in order to achieve prevalence. Simplified, cost-effective and consistent models retain greater potential for ubiquity than coordinately complex systems. A simple and effective model for 3D culture, which provides useful information on tissue response to chemical and physical environmental changes, is highly desirable. While pre-made scaffolds can be designed to mimic *in vivo* microenvironments, the extent to which this is possible is limited. Most scaffolds tend to limit the amount of cell-cell connectivity possible. This is particularly important when considering models involving cells like cardiac myocytes, which contain gap junctions that are essential to propagate action potentials. Scaffold free, spheroids have been found to have many desirable properties for drug screening purposes, and have compared favorably against more simplistic 2D screening models (Mehta et al., 2012; Kwapiszewska et al., 2014; Takayama et al., 2013).

Many forms of 3D tissue culture have been researched up to this point. Microfluidics based systems enjoy the advantages of a potential control of the microenvironment of systems along with a potential for improved sterility (Kwapiszewska et al., 2014; Wu, Huang, and Lee 2010). Unfortunately, procedural complexity and extensive equipment limit use of microfluidics HTS models in research. Rotational cell culture systems (RCCS) have the ability to spontaneously generate cell-dense 3D structures utilizing microgravity; however size and logistics are limiting

factors for HTS (Terai et al., 2002; Buckley, Thorpe, and Kelly 2009). Rapid generation of large numbers of individual 3D cultures can be logistically very difficult in rotating bioreactor systems. Further, altering the chemical characteristics of a large number of individual cultures simultaneously using RCCS presents a significant challenge. The limits of microgravitic forces on the surface of the Earth place a practical boundary on the size of tissue cultures generated using traditional rotating bioreactor culture methods. Scaffold based systems also have the ability to generate 3D architecture; however they are limited by material type/complexity and ability to truly mimic in vivo conditions (Asthana and Kisaalita 2013). Dr. Souza's group have developed magnetic NanoShuttle which can be used to magnetically label and levitate cells in order to form a 3D multicellular cardiac aggregate (MCA) (Haisler et al., 2013). A self-assembling model, requiring cells, one reagent and a magnetic source is not only a streamlined and simple model for the rapid generation of 3D organotypic tissues, it has also proven to be an effective model for preserving phenotype, functionality and viability of cells as well (Daquinag, Souza, and Kolonin 2012; Tseng et al., 2013). Cardiac tissue analogs are particularly sought after due to the phenotypic degradation of primary cardiac myocytes in culture (Spahr et al., 1984; Coulombe et al., 2014; Hirt, Hansen, and Eschenhagen 2014). Cardiovascular drug development is one of the most important areas of pharmaceutical research with roughly 6 million people affected by heart disease in the United States (Go et al., 2013). The large market combined with the difficulty of culture of cardiac myocytes in a 2D environment make a 3D cardiac tissue culture model highly desirable.

In vitro tissue constructs with faithful representation of *in vivo* tissue characteristics are highly desirable for screening and characteristic assessment of a variety of tissue types. This study established a method for the generation of 3D cardiac cultures through cellular coupling with and manipulation of ferromagnetic nanoparticles.

4.2 Materials and methods:

All materials were purchased from Sigma-Aldrich (St. Louis, MO) unless otherwise specified.

4.2.1 Ethics Statement

All studies were performed in accordance with protocols approved by The Institutional Animal Care and Use Committee (IACUC) at the University of Houston (Protocol 11-040). Research was performed in compliance with the NIH Guide for Care and Use of Laboratory Animals.

4.2.2 Isolation of primary cardiac cells

Cardiac cells were isolated from the hearts of 2-3 day old neonatal Sprague-Dawley rats using an established method (L Khait and Birla 2007). Tissues were minced into 1 mm^3 pieces and transferred to a dissociation solution (DS) consisting of filtered 0.32 mg/ml collagenase type 2 (Worthington Biochemical Corporation, Lakewood, NJ) and 0.6 mg/ml pancreatin in phosphate buffer. A 50 mL conical tube containing 15 mL of DS and the minced tissues was placed in an orbital shaker and maintained at 37°C for 30 minutes at 60 rpm. At the end of the digestion process, the supernatant was collected in 3 ml of horse serum to neutralize the enzyme and centrifuged at 1,000 rpm for 5 minutes at 4°C. The cell pellet was re-suspended in 5 ml horse serum and kept in an incubator at 37°C supplied with 5% CO_2. Fresh DS was added to the partially digested tissue and the digestion process was repeated an additional 2-3 times. Cells from all the digests were pooled, centrifuged and suspended in culture medium (CM) consisting of M199 (Life Technologies, Grand Island, NY), with 20% F12k (Life Technologies), 10% fetal bovine serum, 5% horse serum, 1% antibiotic-antimycotic, 40 ng/ml hydrocortisone and 100 ng/ml insulin. Cell concentration and viability was assessed by Trypan blue (4%) staining according to the manufacturer's protocol.

4.2.3 Magnetic Levitation

Cells were converted to 3D cultures using the Bio-Assembler Kit (Nano3D Biosciences, Houston, TX). Two 50 mm tissue culture plates were coated with 3 ml of SYLGARD (PDMS, type 184 silicone elastomer) (Dow Chemical Corporation, Midland, MI). The plates were air dried for 2 weeks and sterilized with 80% ethanol before use. Magnetic levitation occurs through magnetic labeling with a nanoparticle assembly consisting of poly-L-lysine (PLL), magnetic iron oxide (MIO; Fe_3O_4, magnetite), and gold nanoparticles that self-assemble into networks based on electrostatic interactions (NanoShuttle; Nano3D Biosciences) (Hajitou et al., 2006; Arap, Pasqualini, and Ruoslahti 1998; Souza et al., 2006; Souza et al., 2008; Souza et al., 2010). Cells suspended in CM were plated on each petri dish and the nanoparticle assembly was added at concentrations of C_1: 33 μL/10^6 cells or C_2: 50 μL/10^6 cells. Cellular uptake of the biocompatible nanoparticles renders the cell magnetic, allowing for magnetic manipulation of cells; in particular, cells in a culture dish can be levitated to the air–liquid interface with the application of a low-magnitude magnetic field (50–300G). The cell and nanoparticle suspensions were then incubated at 37^{o}C for 30 minutes at 80 RPM. Nanoparticle loaded cell suspensions were subsequently centrifuged at 1000 rpm for 1 minute and the pellets were re-suspended to a concentration of 2.5x10^6 cells/mL in CM. Nanoparticle treated cell suspensions were distributed in ultra lo-bind 24 well culture plates (Corning Inc., Tewksbury, MA) at cell densities of 600,000, 300,000, 150,000 and 75,000 cells with 400 μL of CM per well. Neodymium magnets with field strengths of 50 Gauss were immediately placed over each of the 24 wells of the culture plate to levitate the cells to the air-liquid interface (Figure 15).

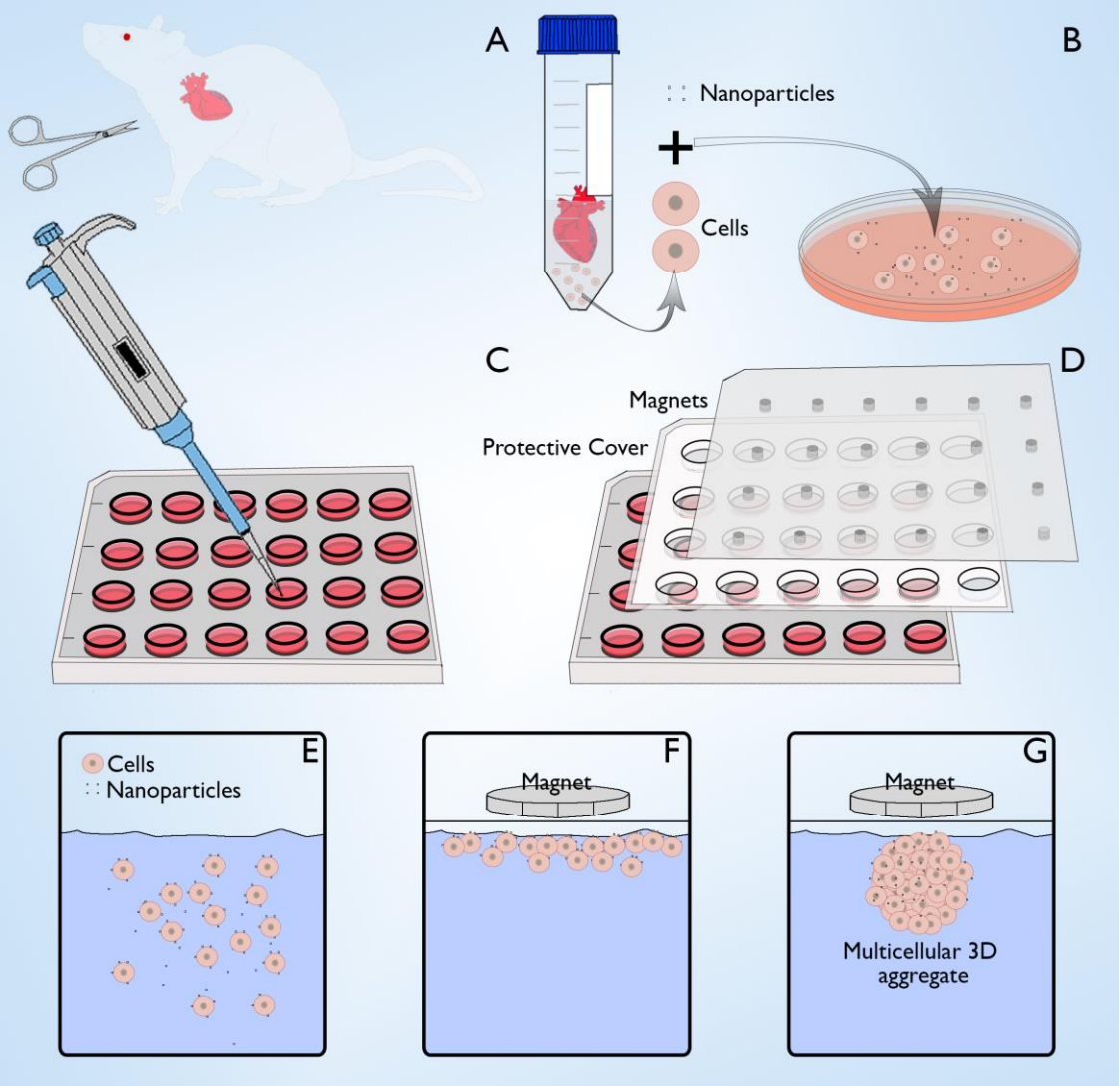

Figure 15: Schematic of magnetic levitation in a 24-well plate, **A**, Cells are isolated, **B**, **E**, magnetically labeled with NanoShuttle, **C**, distributed within a 24-well plate , **D**, **F**, a magnet is applied, **G**, The levitated cells compact and form a cell dense MCA.

4.2.4 3D Culture Formation and Activity

Levitated 3D cultures were examined daily to examine contractile action and gross morphology using an inverted phase-contrast microscope (Nikon Instruments Inc., Melville, NY). Still photographs and videos were captured daily and examined using NIS elements software (Nikon Instruments Inc., Melville, NY) (Figure 16). MCAs were picked up and placed as necessary

during culture using a Teflon coated magnetic pen. MCAs were held along the bottom of the 24 well plates with a magnet during media changes. Fresh media was added every other day.

4.2.5 Histology and Immunohistochemistry

For whole mount immunohistochemistry (IHC), each sample was lifted from the 24 well culture plate and placed in a 96-well plate using a Teflon coated magnetic pen. A magnet was applied to the bottom surface of the 96-well plate to hold the samples in place. Samples were rinsed with PBS, fixed in 10% NBF for 10 minutes, rinsed again, permeabilized with 0.5% Triton X-100 in PBS followed by a final wash in PBS. Cross-sections were obtained by freezing samples in OCT and sectioning them with a cryotome (Thermo Fisher Scientific, Waltham, MA). Cross-sections were fixed in ice-cold acetone for 10 minutes. Depth-specific cross-sections of entire particles were obtained at regular intervals for several samples. Nonspecific epitope antigens were blocked with 10% goat serum at room temperature for 1 hour for cross-sections and whole mount samples. Samples were incubated with some combination of mouse anti-α-actinin monoclonal antibody (Sigma, A7811) 1:200 with polyclonal rabbit anti-collagen type I (Abcam, ab34710) 1:100, polyclonal rabbit anti-CD31 (Abbiotec, 250590) 1:100, polyclonal rabbit anti-fibronectin (Abbiotec, 252234) 1:80, polyclonal rabbit anti cTnI (Abcam, ab47003) 1:100, polyclonal rabbit anti-ki67 (Abcam, ab15580) 1:100 or polyclonal rabbit anti-n-Cadherin (Abcam, ab12221) at room temperature for 1 hour. α-actinin presence was attributed to cardiac myocytes. CD31 was assessed in order to ascertain the localization and abundance of endothelial cells. Fibronectin was similarly observed for ECM robustness (Figure 17). Cardiac troponin I is a cardiac specific marker associated actin and tropomyosin and is part of a complex which confers calcium sensitivity to striated muscle. Further, ki67, a protein associated with cell division and n-cadherin, a transmembrane protein associated with adherens junctions were similarly probed to visualize associated structures. Subsequently, samples were treated with goat anti-mouse and goat anti-rabbit secondary antibodies (Alexa Fluor 488 and Alexa Fluor 546, Life Technologies, Grand Island, NY) 1:400 at room temperature for 1 hour. Nuclei were counterstained with 4, 6-diamidino-2-phenylindole (DAPI)

(2.5 µg/ml) for 5 min at room temperature. Fluorescent images were obtained with a Nikon C2+ confocal laser-scanning microscope (Nikon Instruments Inc., Melville, NY). Z-stack images were taken in order to examine 3D structures of the samples. Masson's trichrome stains were performed on interval sections of an MCA and observed under a light microscope.

4.3 Results

4.3.1 Formation

Formation of the MCAs was reproducible for all cell densities used throughout our trials. The process was repeated n=10 times for a total of 240 MCAs formed with a variety of cell concentrations. Addition of the particles tended to cause clumping during the incubation phase. Simple agitation was sufficient to disrupt these transient interactions and re-disperse the cells in the medium. Upon application of the magnet, the cells moved to the air-liquid interface. By day 2, a centralized aggregate began to form. Within 4 days most cells were incorporated into the central aggregate with few remaining satellite structures (Figure 16). There was little difference between the size and structure of 3D constructs generated using either C_1 or C_2 concentrations of NanoShuttle. Constructs were generally stable in geometry and mostly remained intact through 12 days of culture. Satellite

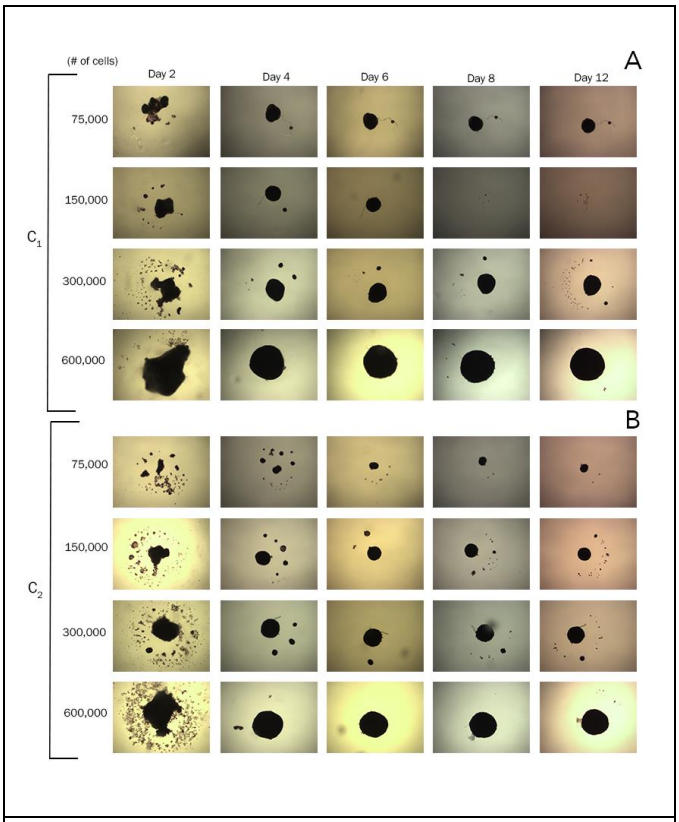

Figure 16: MCA aggregate formations over time, **A**, C_1: 33 µL particle/million cells, **B**, C_2: 50 µL particle/million cells.

structures tended to merge with larger structures and compact slightly over time. MCAs were easily moved and manipulated using the Teflon-coated magnetic pen.

4.3.2 Activity

MCA contractions were observable beginning at day 3 or 4 and were visible by spontaneous deformation, rotation, and translation. Contraction was clearly observable in 75% (n=24) of MCAs. Higher cell densities may correlate to a higher degree of observable contraction given that in one study MCAs with a density of 300,000 cells per well contracted observably 83.3% (n=12) of the time while those with a density of 150,000 cells per well contracted observably 66.7% (n=12) of the time.

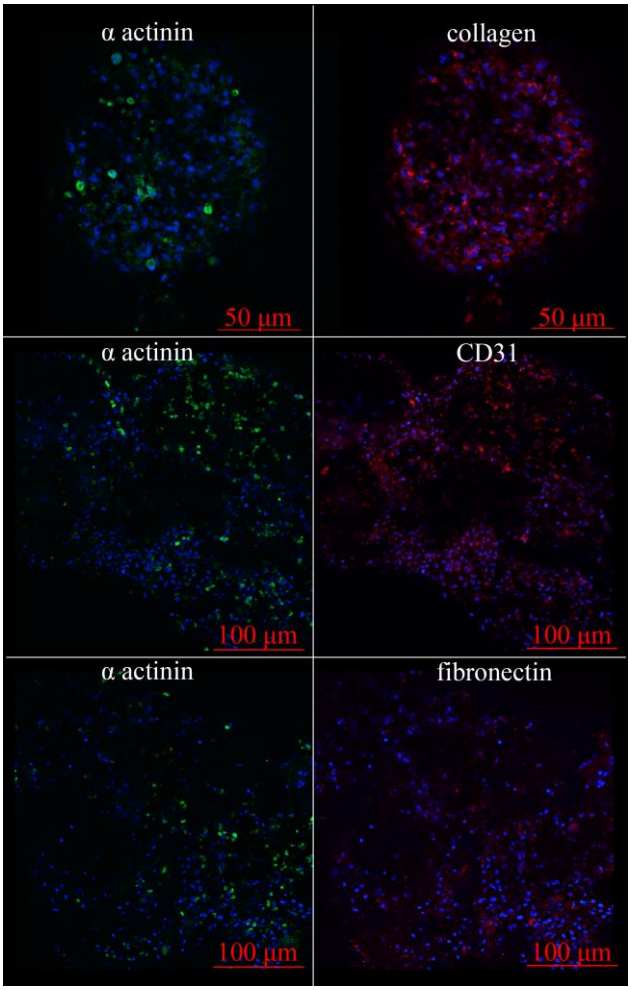

Figure 17: IHC images of whole-mount MCAs probed for α-actinin (green) and either collagen, CD31 or fibronectin (red).

4.3.3 Histology and immunohistochemistry

Immunohistological staining of whole-mount preparations confirmed a spherical architecture of the MCAs (Figure 18). Three-dimensional images of MCAs probed for α-actinin and collagen illuminate the periphery of the spherical constructs. Interior portions were not visible in deeper z-slices of the stained preparations. Sections of an MCA at regular 100 µm intervals revealed cell-dense structures with pronounced collagen networks (Figure 19). Interior portions

were positive for α-actinin and DAPI stains confirmed cell-presence throughout. Z-band α-actinin formations can be seen, however alignment and fiber lengths are lower than in native tissues (Figure 20B). MCAs probed for CD31 and Fibronectin illustrated protein presence under whole-mount preparations. MCAs probed for cTnI indicated troponin I presence along muscle fibers (Figure 20A, B). Probes for ki67 illustrate that MCAs were positive for cellular division, and n-cadherin probes indicate moderate expression of the proteins at 12 days (Figure 20C, D).

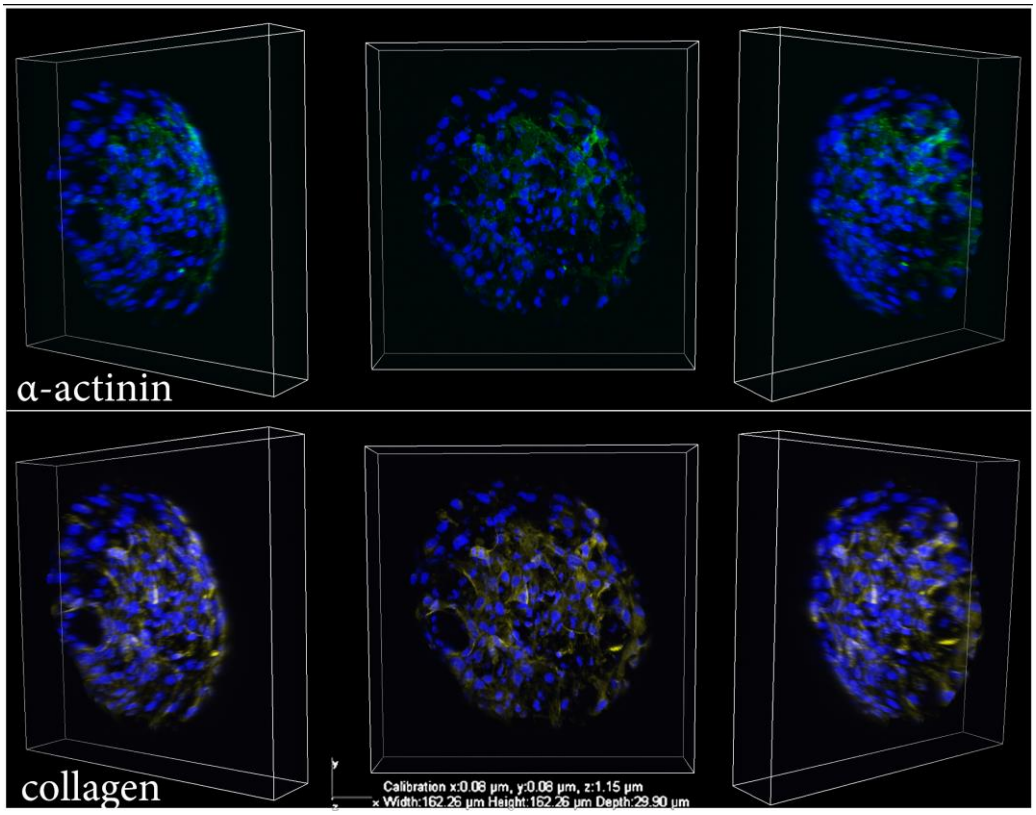

Figure 18: Z-stack 3D reconstruction of IHC images from whole-mount MCA, Probed for α-actinin (green) and collagen (yellow).

4.4 Discussion

The technique presented in this paper was used to successfully generate hundreds of MCAs with relative ease. The MCAs presented with similar geometry and formed with a 100% success rate. The ease with which this technique was applied to generate 3D cardiac structures using primary cardiac myocytes makes it an attractive multidimensional culture technique. MCA size

manifested in approximate proportion to the number of cells used up to 600,000 cells, indicating a rough ability to control MCA size in culture. The amounts of nanoparticle added to the cells prior to levitation (C_1 and C_2) were proscribed based on previously successful magnetic nanoparticle concentrations for levitation of other cell types and results of preliminary studies (Tseng et al., 2013). An estimated 1 μL per 10,000 cells had previously been used to successfully levitate other cell types, however it was apparent that less particle could be used when incubating cardiac cells with the protocol described herein. Given that there was no discernable difference between formation time and size of C_1 and C_2 treated MCAs, it is conceivable that even less magnetic nanoparticle could be used. All studies were performed using a 24 well culture plate, however the technology could conceivably be scaled up to a 96 well system in order to increase throughput.

Most MCAs were observed to contract visibly under the light microscope; however, it was difficult to visibly ascertain contractile frequency due to the small size of the particles and variability of the motion caused by contraction. The visible contractility serves as an obvious indicator of cardiac myocyte presence and phenotypic stability. It was observed that MCAs formed with higher concentrations of cells contracted more visibly under a light microscope. It may be that higher concentrations of cells allow for greater cardiac myocyte coordination and action; however the inherent uncertainty of qualitative assessment prohibits any conclusive analysis. Smaller MCA contraction may be present in proportionally similar amounts to those of larger MCAs. Given that there are less cells generating contractile action in smaller MCAs, the overall stabilizing force of the magnetic field and air-liquid interface may overcome the net contractile action of the cardiac myocytes. A more reliable and quantifiable method of functional detection is necessary for further analysis of MCA capabilities. Given the small size of the MCAs, functional extraction is not as straightforward as with larger tissue constructs. EKG, twitch force and calcium transient data extraction, remain non-trivial challenges which can be addressed to improve the significance of this model.

Whole mount confocal assessment of the MCAs revealed α-actinin, collagen, CD31, fibronectin, ki67, cTnI and n-cadherin presence (Figures 17-20). Three-dimensional images of whole mount sections revealed interconnected collagen networks around the perimeter of the MCAs (Figure 18). Interior portions of the MCAs were not visible using this method due to light scattering. In order to confirm cellular presence and activity of interior portions, interval cross-sections of an MCA were probed for collagen and α-actinin (Figure 19).

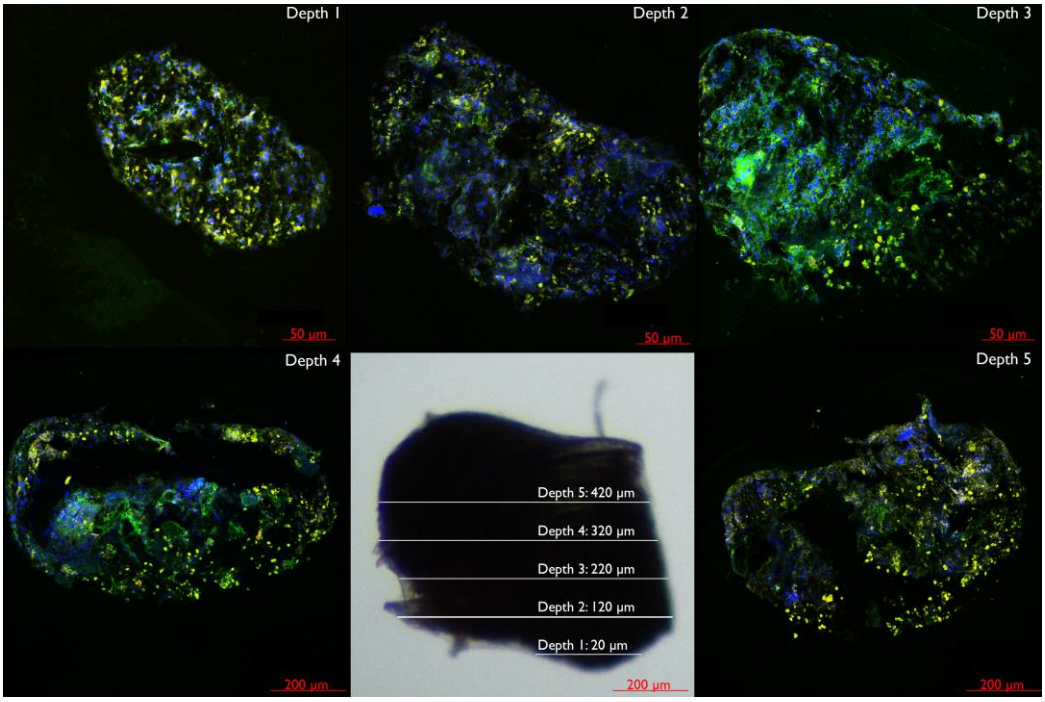

Figure 19: Cell dense structures, IHC images of cross sections of MCA sectioned at discrete depths probed for α-actinin (green) and collagen (yellow) and the corresponding bright-field image of the MCA prior to sectioning.

Interior sections revealed cellular presence and were positive for both collagen and α-actinin throughout the interior of the MCAs. Furthermore, given that the confocal analysis was performed after 12 days of culture, positive stains for fibronectin and collagen, CD31, and α-actinin indicate the relative phenotypic stability of fibroblasts, endothelial cells and SM cardiac myocytes and a similarity of cellular composition of the MCAs to cardiac smooth muscle after a moderate period of culture. Given that cardiac myocytes tend to de-differentiate immediately in 2D culture,

phenotypic stability is invaluable for *in vitro* testing (Spahr et al., 1984). The presence of ki67 suggests maintenance of active cell division within levitated MCAs (Figure 20C). Z-band striations indicate some degree of phenotypic preservation of muscle fiber structure (Figure 20B). However, the lack of alignment and reduced length of muscle fibers visualized by distinct z-bands indicates a limit to the structural similarity of MCAs to heart muscle tissue. Further, while n-cadherin presence is indicative of adherens junctions, the organization does not indicate tissue level organization of the structures (Figure 20D). Still, three dimensional geometry allows for an increased n-cadherin presence through interlayer connectivity between cells in MCAs when compared to monolayers. Moreover, cellular organization strategies, electrical stimulation, perfusion and magnetic mechanical stimulus can all potentially be incorporated into the system in order to improve structural and phenotypic resemblance of MCAs to native tissues.

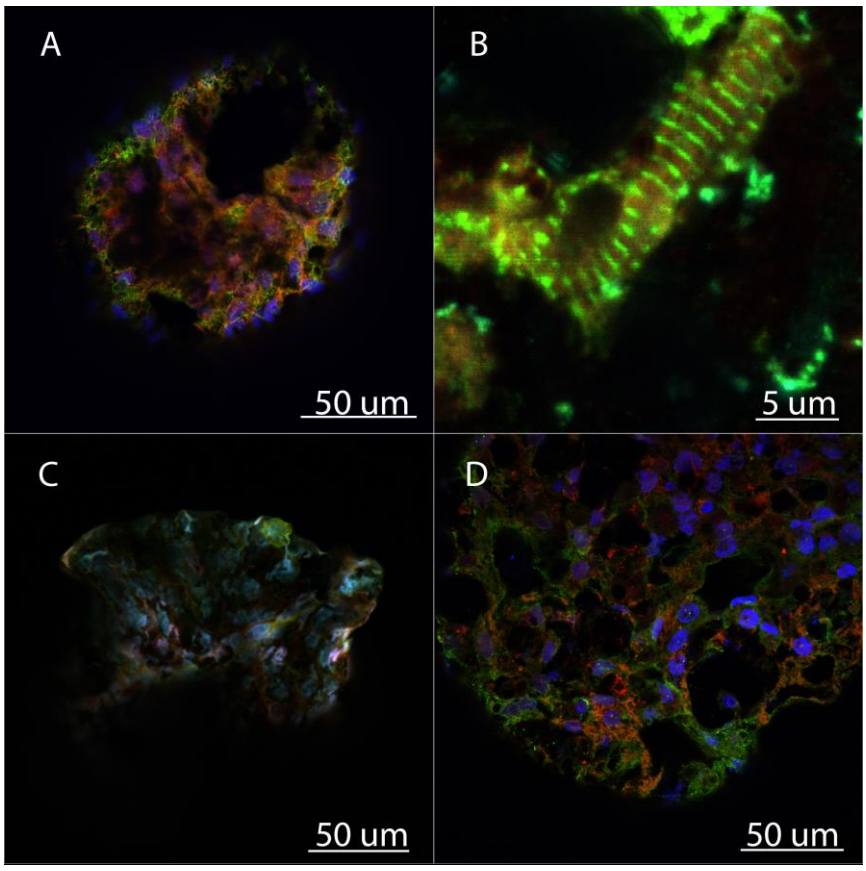

Figure 20: Structural Preservation, MCAs were probed for α-actinin (green) and DAPI (blue). MCAs were secondarily probed for (red), **A**, **B**, cardiac troponin 1, **C**, ki67 and, **D**, n-cadherin.

Each experiment was performed using a 24 well plate. Individual wells in the plate can be prepared with a different chemical or physical stimulus allowing for an increased throughput when compared to rotational bioreactor systems. What is more, the form factor of the equipment is reduced when compared to RCCS strategies. The entire 24 well system measures 5" L x 3.3" W x 1.1" H. Furthermore, scalability is a simple matter as 96 well plates can easily be prepared to implement the same formation strategy.

4.5 Summary

MCAs generated using the methods described above clearly generated 3D cell dense aggregates. The inter-dimensional cell-cell activity conferred not only a degree of phenotypic stability, but also allowed for continued functionality of the active cell types in cardiac muscle. Given the ease with which MCAs were generated and the similarity to heart muscle, the described technology presents an intriguing potential for high-throughput screening of cardiac muscle analogs.

Section 2: Bioreactors for Conditioning of Cardiovascular Tissue Models

Chapter 5: Magnetic Stretch Conditioning

Field Manipulation for Non-Contact Magnetic Stretch Conditioning of Cardiovascular Tissue Models

Bioreactor systems have become an integral component of tissue engineering methods. Cardiovascular stretch conditioning systems have a wide array of beneficial effects for maintenance and enhancements of *in vitro* tissue engineered cardiac muscle systems; however a high degree of axial control, enclosed environments to enhance sterility and diffused loading are difficult to achieve in a contact based system. We endeavored to apply magnetically induced stretch conditioning through application of an oscillating magnetic field to a ferromagnetic heart muscle model. Fibrin scaffolds were loaded with magnetic particles prior to tissue model formation. Oscillating magnetic fields were applied by a novel bioreactor system through displacement of a neodymium magnet. Addition of Iron (III) Oxide (Fe_2O_3) in sufficient quantities to allow for physiologically relevant stretch (15% axial displacement) caused toxic effects after 4 days of culture. Loading scaffolds with magnetite (Fe_3O_4) nanoparticles in tight size distributions increased the field strength of magnetized fibrin 10 fold over Fe_2O_3 with disperse distributions. Loading with Fe_3O_4 allowed for relevant stretch and negligible toxicity within 8 days of culture.

5.1 Introduction

5.1.1 Motivation

Heart failure is a leading cause of death worldwide and there remains an unprecedented need to develop novel treatment strategies. Tissue engineering is an investigational strategy being developed to support lost myocardial function, focused on fabrication of artificial tissue that can be used as a therapeutic strategy for myocardial infarction. The principle of heart muscle tissue engineering is to culture isolated cells within complex 3D matrices, resulting in fabrication of 3D artificial heart muscle (3D-AHM). Subsequently, 3D-AHM is conditioned using stretch bioreactors

to support alignment of cells. Stretch is an important modulator of heart muscle function and several groups, including work from the PI's lab, have demonstrated a positive correlation between stretch and 3D-AHM function. However, all stretch bioreactors are contact-based and lead to physical tissue damage and limit functional benefit. In order to address this, we propose to engineer a novel non-contact magnetic stretch bioreactor (MSB) to support functional improvement of 3D-AHM.

5.1.2 Viable Tissue Engineered Heart Muscle

Heart disease is one of the most important medical concerns in this country and is the leading cause of death in the United States. Over 3 million people live with heart disease in the United States. Managing these patients accrues costs of nearly 25 billion per year. Given that cardiac muscle tissue has very limited regenerative capabilities, a viable tissue engineered muscle replacement/supplement to augment contractile function may serve as a bridge or even alternative treatment to heart transplant. Furthermore, successful generation of a physiologically relevant tissue engineered heart muscle will be an important first step in the creation of a true tissue engineered whole heart. Three-dimensional tissues also hold relevance in the field of drug screening and tissue response in *vitro*.

5.1.3 Current Models

Tissue engineering strategies are focused on the fabrication of artificial tissue constructs in a controlled laboratory environment. (Atala 2004; Luda Khait et al. 2008) The definition of tissue engineering was provided by Dr. Robert Langer in one of his seminal papers, where he states that "*Tissue engineering is an interdisciplinary field that applies the principles of engineering and the life sciences toward the development of biological substitutes that restore, maintain, or improve tissue function"* (Langer and Vacanti 1993). This seminal publication has been influential in the field and has resulted in an exponential increase in research participation. Advances in tissue and organ fabrication technology have led to clinical implantation of bioengineered tracheas and bladders and organ model have been developed for artificial hearts, lungs and kidneys.

The most common strategy to fabricate 3D-AHM has been to culture neonatal cardiac myocytes within a suitable 3D scaffold, resulting in artificial tissue that replicates a partial subset of mammalian heart muscle function. Three pillars of heart muscle tissue engineering have evolved: cells, biomaterials and bioreactors (Chiu et al., 2011; Hecker and Birla 2007; Eschenhagen et al., 1997).

- *Cells* – cells provide the functional component of 3D artificial tissue and most models of artificial heart muscle have been developed using neonatal cardiac myocytes. While artificial tissue fabricated using neonatal cells cannot be used clinically, these models provide valuable insight into 3D organization and development.
- *Biomaterials* – many biomaterials have been tested to support artificial heart muscle, including fibrin, collagen, alginate, chitosan and polyglycolic acid (Williams et al., 2014; H.-J. Wei et al., 2006; H. Zimmermann, Shirley, and Zimmermann 2007; Feng et al., 2008; Pok et al., 2014). These materials have demonstrated varying degrees of success and replicated partial functionality of artificial heart muscle.
- *Bioreactors* – bioreactors are used to replicate *in vivo* conditions during controlled *in vitro* culture; specific signals include mechanical stretch, electrical stimulation and fluid stress (Maidhof et al., 2008; Boonen et al., 2010; Gwak et al., 2008; Au et al., 2009). These signals are important in guiding the formation and function.

5.1.4 Effects of Stretch Conditioning

There have been several studies describing the fabrication of artificial heart muscle, including publications from our lab (Luda Khait and Birla 2008; Hogan et al., 2014; Y.-C. Huang, Khait, and Birla 2007). These studies have often been coupled with studies designed to evaluate the role of physiological stimulation (mechanical stretch, electrical stimulation, and perfusion) to guide 3D tissue formation/function. Our group has developed several models of 3D heart muscle, and one of the models developed by our group, the 3D-AHM, is based on the spontaneous

delamination of a monolayer of primary neonatal cardiac cells that are distributed within a fibrin gel network (described in the preliminary data). Cardiac cells are plated on a tissue culture surface that has been coated with a layer of fibrin gel. Spontaneous contractions of the cell monolayer lead to compaction of the fibrin gel, resulting in formation of functional 3D artificial heart muscle. 3D-AHM can be electrically stimulated to generate twitch forces of over 4 mM and can also be electrically paced at frequencies of 1-7 Hz without fatigue.

Under normal physiological conditions, the heart responds to changes in hemodynamic loads by increases in extracellular matrix components in addition to hypertrophic and hyperplasic growth of the cardiac cells. Under normal physiological conditions, pressure overload in the heart leads to an increase in the rate of proliferation of cardiac fibroblasts associated with an increase in expression of collagen type I. Changes in hemodynamic loading resulting from volume overload are also associated with cardiac myocyte hypertrophy, in addition to increases in collagen deposition. A significant amount of information has been obtained about the changes in phenotype of cardiac myocytes and fibroblasts in response to mechanical stretch using *in vitro* models. In addition to validating the increase in collagen production and rate of proliferation of cardiac fibroblasts, there is growing evidence to suggest that several growth factors (TGF-β, PDGF, b-FGF, IGF-1, AngII, ET-1) may play a pivotal role in mediating the response of cardiac fibroblasts to mechanical stretch. The current data suggest that hemodynamic overload initiates a cellular response, which is further modulated by changes in growth factor environment through an autocrine loop. Myocardial stretch promotes a release of Ang II that induces the release/formation of endothelin (ET) through the activation of the AT_1 receptors, which in turn, and acting in an autocrine/paracrine fashion, activates the cardiac Na^+/H^+ exchanger (NHE-1). The increase in intracellular Na^+ concentration ($[Na^+]_i$), mediated by this NHE-1 activation, but not the change in pH_i, drives the Na^+/Ca^{2+} exchanger (NCX) in reverse mode, increasing Ca^{2+} transient ($Ca^{2+}T$) and contractility.

5.1.5 Bioreactors: Current State of the Art

There have been several studies which describe a positive correlation between stretch and heart muscle function (Ku et al., 2006; Balachandran Philippe Jo, Hanjoong Yoganathan, Ajit P. 2009; Aida Salameh, Wustmann, et al., 2010; Riehl and Park 2012; Boonen et al., 2010). Fink et al utilized a mechanical stretch regime to study changes in 3-dimensional cardiac muscle that was engineered by culturing neonatal cardiac cells within a collagen gel (Fink et al., 2000). The constructs were subjected to a 20% stretch protocol at a frequency of 1.5 Hz for a period of 6 days; this resulted in doubling of the twitch force. In addition, mechanical stretch resulted in an increase in calcium sensitivity and an increase in the β-adrenergic response (Aida Salameh, Karl, et al., 2010). Akyhari utilized a model of 3-dimensional heart muscle by culturing cells obtained from human hearts and culturing the cells in a gelatin sponge. The constructs were subjected to a protocol of 20% stretch at a frequency of 1.33 Hz for a period of 14 days. Although the contractile properties were not evaluated, stretch did result in an increase in cell proliferation (Akhyari et al., 2002).

5.1.6 Novel Stretch Bioreactors

In the previous section, we looked at a few examples of stretch bioreactors and the effect of controlled stretch on artificial heart muscle function. In all cases, stretch bioreactors have been custom fabricated by the lab; all stretch bioreactors till date require physical contact with artificial heart muscle. We believe that physical contact with tissue results in physical damage and loss of function. The current study is designed to address this limitation and fabricate a non-contact MSB. We believe that non-contact stretch bioreactors will lead to greater degree of functional improvement, when compared with stretch bioreactors.

During preliminary studies, we used magnetic fields for controlled stretch of 3D-AHM. In order to achieve this objective, we first developed a novel method to engineer 3D-AHM using iron(III) oxide particles; this resulted in magnetized 3D-AHM, termed m3D-AHM. Our second objective was to use controlled magnetic fields for stretch conditioning of m3D-AHM. During

preliminary studies, we successfully fabricated two generations of non-contact MSBs. *To the best of our knowledge, this work was the first demonstration of magnetic fields used non-contact stretch of 3D heart muscle.* The purpose of this study is to build upon this foundation and develop a new generation of MSBs, optimize culture conditions to support fabrication of m3D-AHM and couple these two technologies and guide m3D-AHM development using non-contact MSBs. We propose to build a new MSB to condition m3D-AHMs that have been fabricated using optimized culture conditions; we hypothesize that non-contact MSBs will provide significant functional enhancement, greater that obtained using contact based stretch bioreactors.

This work will provide technology for controlled non-contact mechanical stretch to condition 3D-AHM; this work can also be extended to other tissue systems. Successful completion of the proposed study will lead to the development of novel non-contact based technology for tissue engineering bioreactors; this will be a significant advancement based on current state of the art in the field.

5.2 Materials and Methods

All animal protocols were approved by the Institutional Animal Care and Use Committee (IACUC) at the University of Houston, in accordance with the *Guide for the Care and Use of Laboratory Animals* (NIH Publication No. 86–23, 1996). All materials were purchased from Sigma-Aldrich (St. Louis, MO, USA) unless otherwise specified. The chemicals used in the syntheses and characterization were of analytical grade and were used as received from the supplier without further purification. Millipore water (resistivity of >18 MΩ-cm) from a Milli-Q water system and filtered through a 0.22 μm filter membrane was used in the synthesis and washing steps. All glassware and equipment were cleaned in an aqua regia solution and rinsed with Milli-Q water prior to use.

5.2.1 Isolation of primary cardiac cells

Cardiac cells were isolated from the hearts of 2–3 day-old neonatal Sprague–Dawley rat pups, using an established method. (Y.-C. Huang, Khait, and Birla 2007) Each heart was cut into three or four pieces in an ice-cold phosphate buffer consisting of 116 mM NaCl, 20 mM HEPES, 1 mM Na_2HPO_4, 5.5 mM glucose, 5.4 mM KCl and 0.8 mM $MgSO_4$. After the blood cells had been rinsed out, the heart pieces were transferred to a dissociation solution consisting of 0.32 mg/ml collagenase type 2-filtered (Worthington Biochemical Corporation, Lakewood, NJ, USA) and 0.6 mg/ml pancreatin in phosphate buffer. The hearts were cut into 1 mm^3 pieces and then transferred to an orbital shaker and maintained at 37°C for 30 min at 60 rpm. At the end of the digestion process, the supernatant was collected in 3 ml horse serum to neutralize the enzyme and centrifuged at 1000 rpm for 5 min at 4°C. The cell pellet was re-suspended in 5 ml horse serum and kept in an incubator at 37°C, supplied with 5% CO_2. Fresh dissociation solution was added to the partially digested tissue and the digestion process was repeated a further two or three times. Cells from all the digests were pooled, centrifuged and suspended in culture medium (CM) consisting of M199 (Life Technologies, Grand Island, NY, USA) with 20% F12k (Life Technologies), 10% fetal bovine serum, 5% horse serum, 1% antibiotic–antimycotic, 40 ng/ml hydrocortisone and 100 ng/ml insulin. Cell viability was analyzed by Trypan blue (4%) staining, according to the manufacturer's protocol.

5.2.2 Fabrication of artificial cardiac patch

A 35 mm tissue culture plate was coated with 2 ml SYLGARD (PDMS, type 184 silicone elastomer; Dow Chemical, Midland, MI, USA). The plate was air- dried for 2 weeks and sterilized with 80% ethanol before use. Four minutien pins (Fine Science Tools, Foster City, CA, USA), 0.1 mm diameter, were placed in the culture plate to form a 2×2 cm square. The fibrin gel was made by plating 1 ml CM containing 10 U/ml thrombin,

adding 500 μl saline containing 20 mg/ml fibrinogen and mixing well to promote gel formation within 10 min. Primary cardiac cells were diluted in CM at a pre-set density, and 2 ml of the cell suspension was transferred to the culture plate. Aminocaproic acid (2 mg/ml) was added to the culture plate to inhibit fibrinolysis by endogenous proteases. The cells were cultured in an incubator at 37°C and 5% CO_2 with CM changes every other day.

5.2.3 Magnetized fibrin gel

Magnetized fibrin scaffolds were formed and seeded the same way as their un-magnetized counterparts. Fe_20_3 particles (Sigma Aldrich) with diameters <5 μm were added to the fibrinogen in saline and thrombin in CM mixture immediately after combination of the CM and saline in a PDMS coated petri dish. Fe_20_3 was added by weight % in increments of 2 wt% with groups of 1, 3, 5, 7, 9, 11 and 13 wt% corresponding to 15, 45, 75, 105, 120 and 135 mg respectively. Cells were added to the magnetized fibrin gel in the same manner as with un-magnetized matrices. Magnetized fibrin gels were also formed using well characterized magnetite (Fe_3O_4) nanoparticles of 100nm and 300 nm diameters. Particles were sonicated in CM and mixed with fibrinogen in saline and thrombin in CM.

5.2.4 Patch formation and contraction rate

Sixteen hours after cell plating, spontaneously beating cardiomyocytes were counted manually from five ×200 fields (center and top, right, left and bottom-most from the center of the patch) under an inverted phase-contrast microscope (Olympus, Centre Valley, PA, USA). The contraction of cultured cardiac constructs and fibrin gel detachment from culture plates were observed from day 1 to day 6; the patch growth progress was captured in still photographs and videos, using a camera (Lumenera, Ottawa, ON) mounted on an inverted phase-contrast microscope. The videos were replayed slowly and the contraction rates manually counted.

5.2.5 Contractile twitch force and electrocardiogram (ECG)

From the first day of patch formation, spontaneous and electrical paced twitch force (10 V, 0.1 s) were measured within a thermostatic (37°C) water bath using a high-sensitivity isometric force transducer (MLT0202, ADInstruments, Colorado Springs, CO, USA) connected to a quad bridge amplifier (FE224, ADInstruments). ECG signal was measured using Octal Bio Amp (ML138, ADInstruments). Data were acquired through a 16-channel PowerLab system (PL3516/P, ADInstruments). The contractile twitch force was measured by attaching the force transducer arm to one free-corner of the square patch, while the other three ends of the square patch were held fixed by pins. In order to obtain the Frank– Starling relationship for the measured twitch force, pretension was adjusted using a micro-manipulator (Radnoti LLC, Monrovia, CA, USA) and measurements of spontaneous contraction were recorded. We defined a spontaneous con- traction rate of > 120 bpm as high-rate contraction and a spontaneous contraction rate of < 20 bpm as low-rate con- traction. The ECG of the patch was measured by inserting a needle cathode (MLA1213, ADInstruments) into the centrer of the patch and a needle anode in one of the four patch corners. The medium immersing the patch was used as ground. LabChart (ADInstruments) was used for data analysis. The peak analysis module was used to calculate the maximal twitch force and baseline force (pre-tension). The ECG analysis module was used to calculate the R-wave amplitude. Electrical pacing was performed by attaching the stimulating electrodes (MLA0320, ADInstruments) on the edge of the patch tissue at frequencies of 0.25, 0.5 and 1–8 Hz (in 1 unit increments) at 2, 4 and 6 days after patch formation.

5.2.6 Morphology

Seven days after plating, the formed patches were cut diagonally. The diagonal edge of the triangular block was aligned with the edge of a slide. The cross-section and surface of the triangular block were photographed and the images were traced using

ImageJ 1.47d (Wayne Rashand, National Institutes of Health, USA) to obtain the area of the cross-section, the thickness and the height of the triangular block, and then this triangular block was weighed. From the central part of the patch, two 0.5 × 0.5 cm blocks were taken, placed in a peel-away disposable embedding mold (VWR International, Radnor, PA, USA), frozen in liquid N2 and then immediately immersed in Tissue Tek OCT compound (VWR International, Radnor, PA, USA) and placed in a -80°C freezer. Once the OCT compound solidified, each sample was sliced using a cryostat (Thermo Fisher Scientific, Waltham, MA, USA). Tissue cross-sections and planar sections were cut at a thick- ness of 10 or 6 μm. The sections were placed on VWR® Microslides for preparation of morphological and immunofluorescence examinations. Images from cross-sections of 6 μm thickness were taken directly under a phase-contrast light microscope (Olympus, Centre Valley, PA, USA). For measurement of the 'real cardiac layer' (a layer of cells and naturally produced extracellular matrix forming on top of the fibrin gel scaffold) thickness, 10 μm thick cross-sections were stained with Masson's trichrome, according to the manufacturer's protocol, and images were taken under a light microscope. The distinct tissue layers were traced and thicknesses calculated using ImageJ.

5.2.7 Immunofluorescence

For observation of endothelial cell growth, nuclear division and collagen type I distribution in the patch, fresh tissue patches were directly fixed in ice-cold acetone for 10 min; 1.0 × 1.0 cm tissue patch blocks from the center were trimmed, non-specific epitope antigens were blocked and the cell membranes permeated with 10% goat serum/ 0.5% Triton X-100 at room temperature for 45 min. Tissue patch blocks were then incubated in mouse anti-α-actinin antibody (1:200; Sigma, A7811), rabbit anti-collagen type I (1:100; Abcam, ab34710), rabbit anti-von Willebrand factor (vWF; 1:750; Abcam, ab6994), rabbit anti-ki 67 (1:100; Abcam, ab66155) or rabbit anti-connexin 43 (Cx43; 1:100) at room temperature

for 2 h. Subsequently, tissue blocks were treated with goat anti-mouse and goat anti-rabbit secondary antibodies (1:400; AlexaFluor 488, 546 and 633, Life Technologies) at room temperature for 1 h. Nuclei were counterstained with 4,6-diamidino- 2-phenylindole (DAPI; 2.5 μg/ml) for 5 min at room temperature. Fluorescent images were obtained using a Nikon $C2^{+}$ confocal laser-scanning microscope (Nikon Instruments, Melville, NY, USA). For measurement of the volume indices of gap junctions, collagen fibers and myofibrils, signal volumes of Cx43, collagen type I and α-actinin expressions were examined within 6 μm cross- sections. Two Z-stack scans from each sample were acquired, with a signal depth of 8 μm over 33 frames. After determining specific thresholds for Cx43, collagen type I and α-actinin, signal volumes for each sample were measured.

5.2.8 Statistics

Results are presented as mean ± standard deviation (SD). χ^2 analysis was used to test frequency variables. Comparisons among groups were made with a one-way analysis of variance (ANOVA) followed by the Bonferroni *post hoc* comparison test. In all tests, differences were considered statistically significant at $p < 0.05$.

5.2.9 Magnetic conditioning

Magnetized AHM was placed on a stage and held in place using metal clamps. A neodymium magnet was physically displaced relative to the m-AHM using a stepper motor driven ball-screw. The rate, distance and ramp speed of the oscillation was controlled through a custom user interface using a C2000 microcontroller (Texas Instruments, Austin, TX, USA) to drive the stepper motor. Code Composer Studios (CCS) was used to develop the UI, encode the microcontroller and display real-time feedback.

5.2.10 Synthesis of Fe_3O_4 Magnetic Nanoparticles (MNPs)

The Fe_3O_4 MNPs were synthesized by a modification of a procedure reported by Deng *et al* (Deng et al., 2005). In this modified procedure, a 150ml round-bottomed flask pressure vessel

was charged with $FeCl_3 \cdot 6H_2O$ (4.2 g) in 30 mL of ethylene glycol followed by the addition of sodium acetate (3.08 g). The latter addition leads to a rapid change in the color of the solution from orange to brown. The solution was then stirred for 30 min followed by the addition of polyethylene glycol (0.50 g) with 20 mL of ethylene glycol. The flask was sealed by a Teflon cap and heated at 188°C for 21 hours. The black precipitate obtained was separated using a strong bar magnet and washed with three cycles each of ethanol and water and then dispersed in ethanol. The synthesized particles formed a powder upon drying at 40 °C and were set aside for future use. The concentration of starting materials and diethylene glycol was varied to obtain MNPs with varying sizes (Xuan et al., 2009).

5.2.11 Characterization of MNPs

The MNPs were characterized by scanning electron microscopy (SEM; LEO-1525 operating at 15 kV) and vibrating sample magnetometry (VSM; LakeShore VSM 7300 Series with LakeShore 735 Controller and LakeShore 450 Gaussmeter Software Version 3.8.0). To obtain high resolution SEM images, all samples were deposited on a silicon wafer. The magnetic properties (saturation magnetization and coercivity) were measured by VSM with known mass.

5.2.12 SEM Sample Preparation for MNPs in Fibrin Gel

The MNP-scaffold samples were imaged using SEM (LEO-1525 operating at 15 kV). Prior to imaging, we prepared our samples based on the procedure of fixation, dehydration and drying methods (Khantamat et al., 2015). The fibrin scaffolds with MNPs were fixed with 2.5% (v/w) glutaraldehyde for 20 h in 0.1M PBS buffer at $4^{O}C$. The fibrin samples dehydrated in a gradient ethanol series (50%, 70%, 85%, 95%, and 100%) for 10 min each. The dehydrated samples were immersed and frozen in 100% t-butanol and followed by freeze-drying using a Scanvac CoolSafe 110-4 (LaboGene). The freeze-dried samples were then sputter-coated (Hummer 6.2 Sputter System; Anatech USA) with a resultant thickness of about 10 nm platinum and then examined under SEM.

5.3 Results

5.3.1 Concept

Initial analysis of magnetic scaffolds was performed on fibrin gels containing uncharacterized Fe_2O_3. The process for magnetization and deformation of fibrin gels can be seen in Figure 21. Upon loading with Fe_2O_3, the fibrin gels became sensitive to magnetic fields. Higher initial loads of Fe_2O_3 resulted in effluent particles, which were not retained in the fibrin gel. The excess particle indicates that there is a threshold for loading of Fe_2O_3 in fibrin gel. The unloaded Fe_2O_3 became significant when attempting to form higher than 13 wt% Fe_2O_3 magnetized fibrin scaffolds placing an upper limit on efficient magnetic particle loading. Stretch was found to positively correlate with magnetic field strength, which is inversely related to neodymium magnet distance from the culture chamber.

5.3.2 Bioreactor Design

Ideally, the system would be able to rapidly adjust magnetic field strengths so as to reproduce native contraction speeds and to allow for the greatest degree in variability of control. Ultimately we would like the translation distance to be completely variable to allow for the control of magnetic forces on a construct via distance. Precision is also paramount. Given the cubic ratio of magnetic force to distance, a small change in distance would result in a compounded effect on applied force. Exactly precise movements are required.

Fixed electromagnetic manipulation represents an interesting potential control mechanism for the manipulation of ferromagnetic particles. By controlling current through a magnetic plate system, an electromagnetic field can be generated which can manipulate the magnetic particles in the construct without any moving parts. No moving parts means reduced vibration, wear and tear, and more compact overall design. Direct control of current through a plate is a relatively simple control mechanism and the geometries can be adapted to fit a variety of tissue types.

Electromagnets are powerful, however they require a large amount of power to achieve magnetic fields on the order of simple neodymium magnets. Passing large amounts of current generates heat, which can disrupt the environment inside an incubation chamber. Passing large currents through a plate is dangerous and considerations for safety would be paramount. Larger electromagnetic noise and disruption field may disrupt other control/measurement systems nearby. Electroplating/deposition becomes an issue, especially in a humid environment such as an incubator.

Motor controlled manipulation of a neodymium magnet involves translation of a magnet via a physical motor driven system. By controlling the total distance of a magnet of a fixed strength from a magnetized tissue construct, we can control the magnetic forces on the tissue construct. The action of all described types of motor control would produce the same effect, which is to manipulate the motion of a magnet in space relative to a magnetized construct. Speed of translation, frequency of repetition and strength of the magnet are all variable parameters. This method should limit heat generation. Magnetic fields are cube of distance so modeling magnetic forces will be possible. Further, manipulation of a rare earth magnet is relatively safe. Electromagnetic noise and disruption is less of a concern with fixed strength magnets compared to electromagnetic systems, and electroplating/deposition is not an issue.

There are design issues with a mechanical system. Moving parts introduces an element of wear and tear. Translation will introduce vibration, which could disrupt measurement systems and inhibit cell function. Compacting the design will be a key concern due to the necessity of inclusion of a motor and slide/translation system. Motors will need to be waterproof and corrosion resistant for use in an incubator.

There are many types of motor systems capable of translating a permanent magnet. An air-controlled system can be compact and strong with minimal vibration and high-speed translation. Air controlled systems require advanced control systems. The stroke distance of an actuator is limited and controlling traversing speed represents a non-trivial challenge. A hydraulic system can

be strong with minimal vibration and high-speed translation. Hydraulic controlled systems require advanced control systems. The stroke distance of an actuator is limited and controlling traversing speed represents a non-trivial challenge. Motor control of hydraulic fluids is non-trivial and requires significant design work. An electronic linear actuating system can be very strong and compact with minimal vibration. Controlling speed of translation is relatively easy and the control systems for electronic linear actuators don't require air pressure generation or liquid reservoirs and pumps. Also, electronic linear actuators are fairly ubiquitous so obtaining parts would be easy. Electronic linear actuators are typically slow if their speed is variable. Also they have limited stroke distances and it can be difficult to program discrete distance control. Controlling exact distances of travel without the actuator extending or contracting a full stroke distance is very difficult and can result in a low degree of precision. Motor control is fairly easy and can be converted to linear motion using a variety of methods. With a ball screw and slide mechanism, stepper/servo motors are very precise. Translation can occur relatively rapidly using the ball screw and slide method. With a rigid chain/belt system, speed can be improved, however accuracy and vibration aspects suffer. Ball screw and slide methods are used for precision machining and suit our purposes very well. Servo/Stepper motors are even more ubiquitous than electronic linear actuators. There are thousands of control systems available and motors can be configured for almost any design consideration. There is no stroke limit on the ultimate positioning system and servo/stepper motors can be configured to translate an object to any distance. Systems can be bulkier than other options due to the size of the motors. They can also be noisy and generate some vibration.

We concluded that based on design requirements and existing technologies a stepper motor driven ball-screw slide mechanism translating a fixed strength neodymium magnet is the ideal solution for a magnetic stretch bioreactor. Our proposed design solution is presented in Figure 22. As a part of this study, we fabricated and tested our design with m3D-AHM.

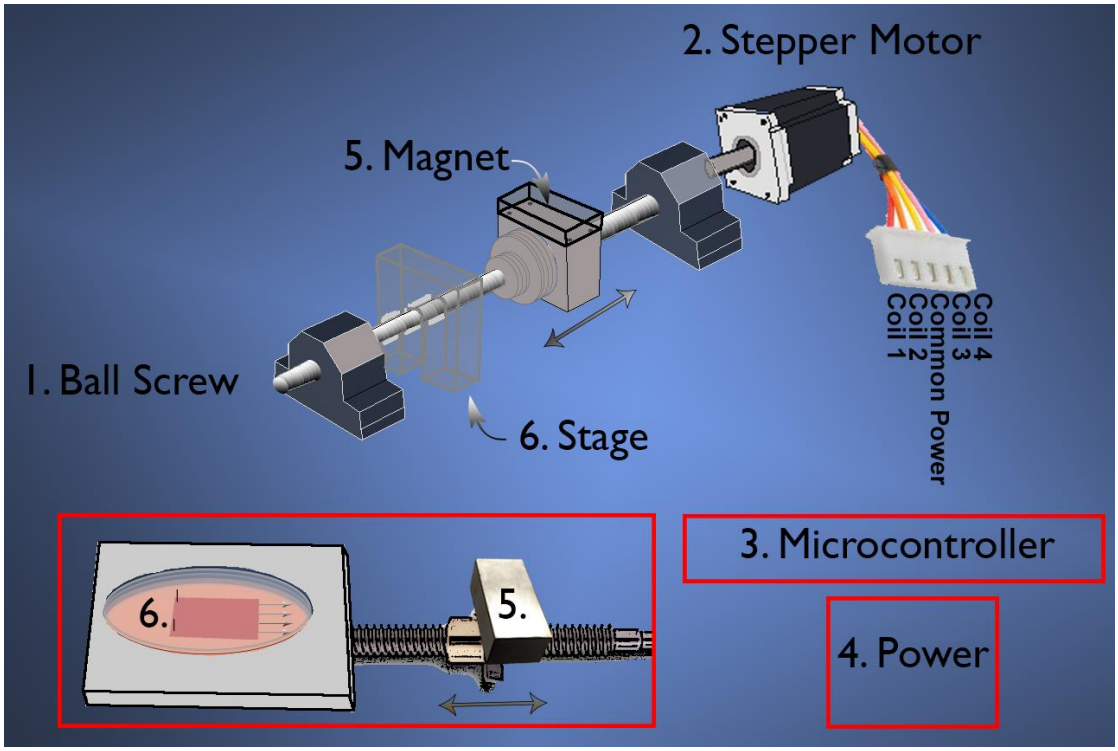

Figure 22: Design concept of magnetic stretch bioreactor

5.3.3 Microcontroller and UI

We chose the C2000 launchpad as the controller for our system. The C2000 LaunchPad Microcontroller (μC) is ideally suited for developmental/evaluation purposes. It contains a C2000 chipset with 60MHz, 64 kb Flash, 12KB RAM, 9 PWM, and 4 HR PWM, 1 Capture, 22 GPIOs, 12-bit 4.6MSPS ADC with 13 ch., SCI/UART, SPI, I2C. An h-bridge configuration was used to amplify the GPIO signals (which output 3.3v control signals) to higher power signals capable of driving a magnetic stepper motor. The TI C2000 chipset was designed for real-time control purposes and is frequently used in motor control applications. The LaunchPad configuration allows for accessible transfer of commands and real-time control via a USB-UART connection. There remains untapped potential for incorporation of real-time readout and control feedback systems to the μC unit. The μC allows for connection of LCD displays, capacitive touch systems, distance feedback systems, temperature sensors and potentially pH sensors for more complex bioreactor

control and sample analysis. Force and EKG probes could also be incorporated, however μC systems with more powerful processing units, which are designed to handle high rate analog inputs, would be preferable. C2000 LaunchPad μCs utilize analog-to-digital converters (ADCs) which quantize continuous signals into digital outputs. This inherently results in some small error and is not ideally suited for real-time analysis of complex analog waveforms. The MSP family of TI microcontrollers are better suited for such purposes, however more research on suitable μC systems would undoubtedly reveal stronger applicants. The versatility and favorable cost of the C2000 μC system, however makes it a suitable choice for our current endeavors. All control code was written in C. It was found that each stepper motor step accounted for 0.012654 mm of axial translation. A UI was developed in order to allow for direct control of the system through a graphical interface (Figure 23).

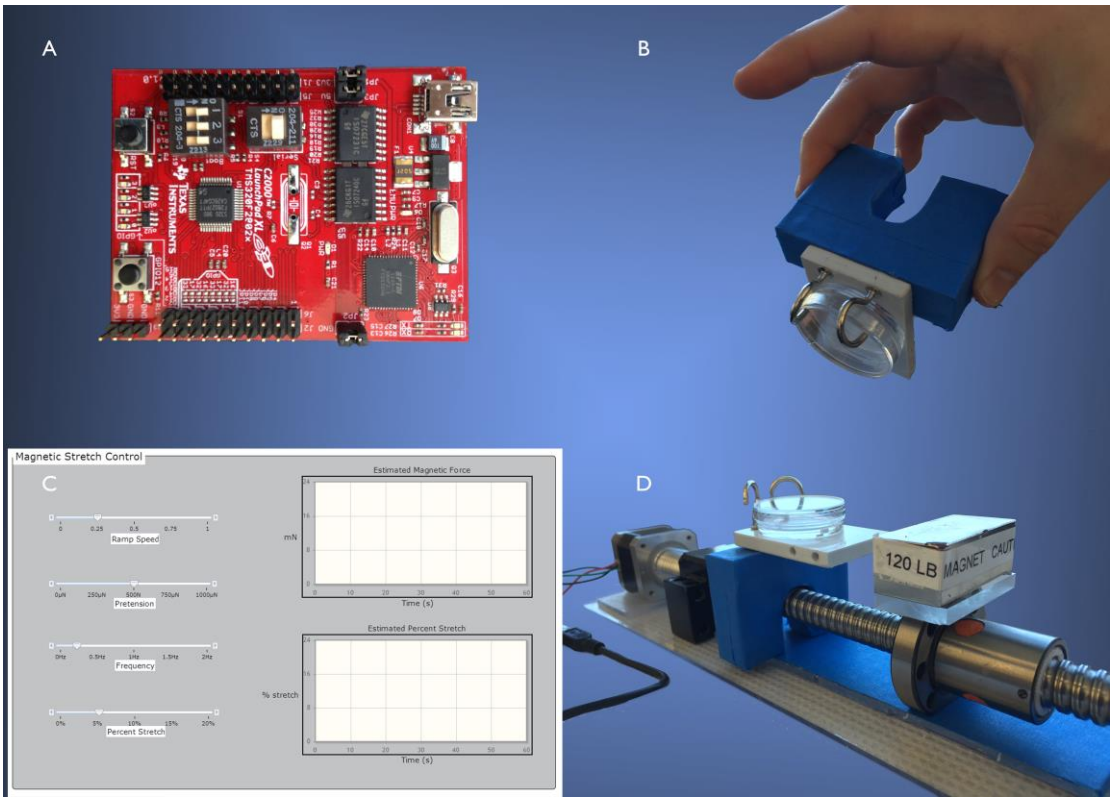

Figure 23: Prototype of a magnetic stretch bioreactor, **A**, μC, **B**, Stage mount, **C**, User interface, **D**, Bioreactor system.

5.3.3 Magnetic forces and efficacy of Fe_2O_3

Fibrin samples prepared with varying concentrations of Fe_2O_3 became darker and slightly stiffer with increasing iron content (Figure 24A). Upon application of a magnetic field, axial displacement was observed. The patches remained intact and underwent smooth deformation under magnetic load. A force curve was calibrated in order to determine the active forces on samples of fibrin containing different amounts of iron. It was determined that increasing Fe_2O_3 loading led to a direct increase in the forces generated at a discrete distance. Further, controlling the maximum distance of the magnet from the leading edge of a patch allowed for a baseline force to be present (Figure 24C). Maximal deformation was assessed when the magnet was 10 mm from the leading edge. Higher iron content was observed to produce larger axial distortions at each discrete distance (Figure 24D). Maximal stretch with 3 and 7 wt% Fe_2O_3 loads were 5 and 10% stretch respectively.

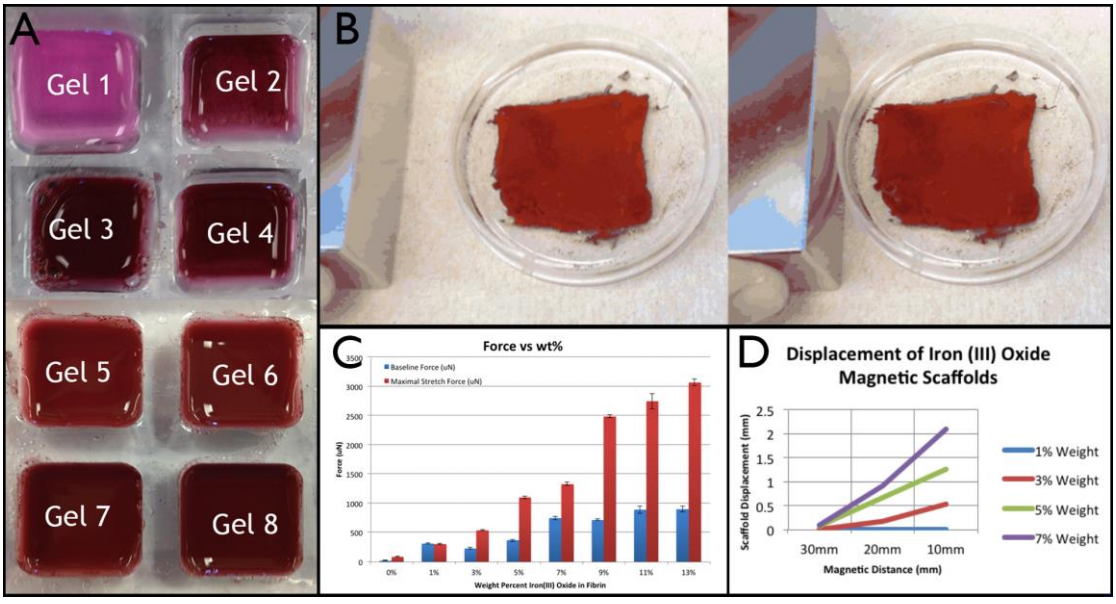

Figure 24: Magnetic stretch forces, **A**, Fibrin gels with 8 different concentrations of Fe2O3, **B**, Magnetically induced deformation, **C**, Magnetic forces with changing concentrations, **D**, Deformation correlated with concentrations.

5.3.4 Toxicity of Fe_2O_3

Effects of Fe_2O_3 content on AHM formation and function were assessed with regards to twitch force, appearance and immunohistological properties (Figure 25). At day 4 after formation, the control, 3 wt% and 7 wt% magnetic seeded patches exhibited the same contractile activity. At day 7 after formation, there was a significant drop in functional activity of iron containing heart muscle. There did not appear to be any difference in the severity of the force drop off from day 4 to day 7 between groups containing 3 and 7 wt% iron oxide. Fe_2O_3 containing patches exhibited a reduced definition around the edges of the patches (Figure 25B, C and D) and significantly less well defined α-actinin expression when compared with control heart muscle (Figure 25E, F and G). Collagen expression appeared to be unaffected, however no numerical assessments were applied.

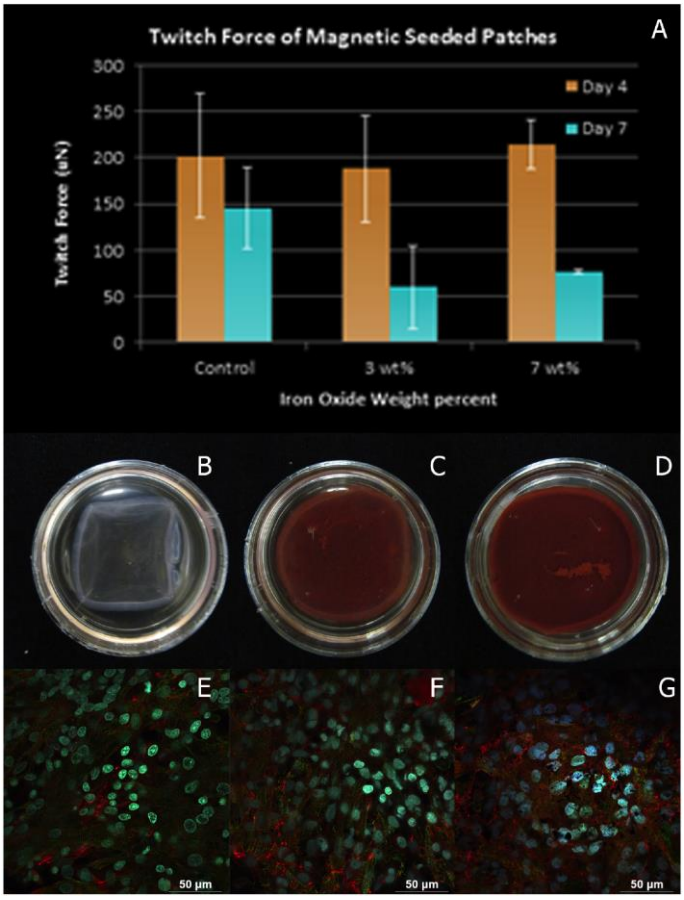

Figure 25: Toxicity effects of Iron Oxide (Fe_2O_3), **A**, Effects of Fe_2O_3 on twitch force, **B, C, D,** Images of 0, 3 and 7 wt% heart tissue patches, **E, F, G**, IHC probing for DAPI (blue), α-actinin (green) and collagen (red) for each respective concentration.

5.3.5 Magnetic forces, loading and toxicity of Fe_3O_4

The magnetic properties of the as-bought α-Fe_2O_3 and our synthesized Fe_3O_4 MNPs were investigated using a vibrating sample magnetometer (VSM) at 300K. For 100 nm and 300 nm MNPs, the saturation magnetization (Ms) values are 79 and 82 emu/g and coercivity values are 43 and 37 Oe respectively. The bulk α-Fe_2O_3 used for the preliminary experiments has an Ms of ~5 emu/g. Loading with Fe_3O_4 produced a 10 fold increase in sensitivity to magnetic fields. As such, we were able to achieve viable stretch activity (10-15% stretch) with less than 1 wt% Fe_3O_4. Toxicity effects of 1 wt% Fe_3O_4 loads were negligible. There was no visible reduction in definition around the edges of the patches when comparing loaded and unloaded controls. Fe_3O_4 particles were found to be homogenous in size and shape (Figure 26). Loading occurred well in the fibrin gel matrix, however some microscopic clumping was observed upon loading fibrin gel with Fe_3O_4 under SEM.

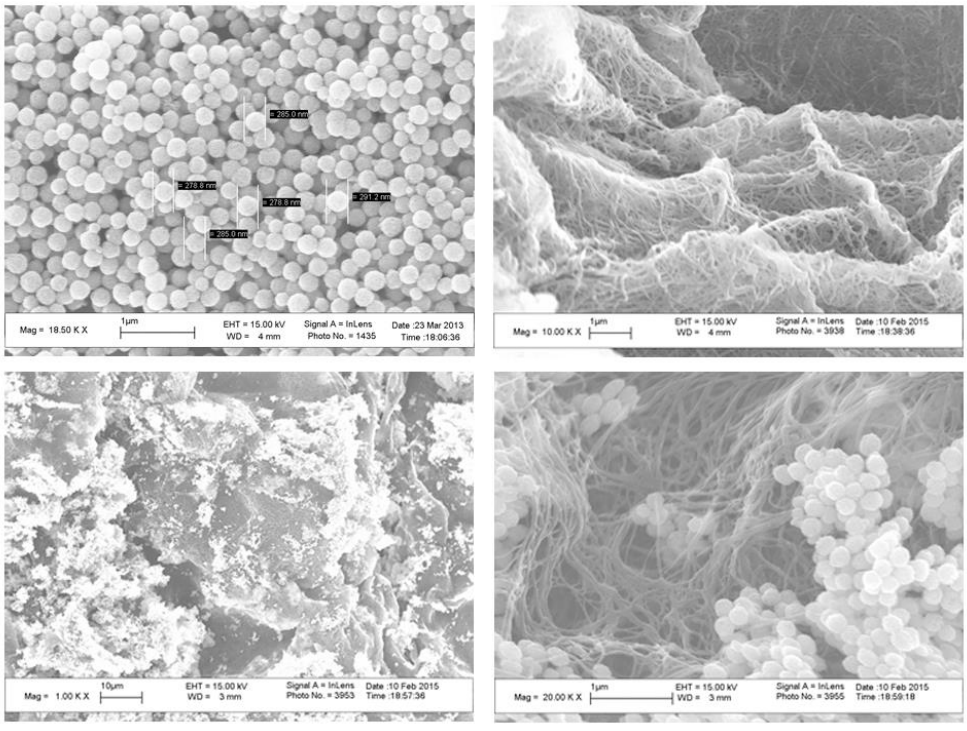

Figure 26: SEM of characterized Fe_3O_4 particles and fibrin gel.

5.4 Discussion

Typical mechanical stretch bioreactors inherently place stress on fragile scaffolds. In our experience with contact-based stretch bioreactor systems, prolonged stretch regimens primarily led to deformation and even tearing under the gentlest stretch cycles. Further, direct contact bioreactor systems necessitate some degree direct physical of interaction between the bioreactor system and the cultured tissue. Our heart muscle tissues are cultured in disposable vessels and nothing is re-used. Re-using culture materials is generally considered bad practice as it can add a potential source for contamination. In best case scenarios for contact based systems, a custom chamber must be built for each culture cycle. Expediency often necessitates re-using these custom built chambers after a rigorous decontamination procedure, however such procedures are not full-proof and add complexity and uncertainty to an already difficult process. Many bioreactors use open air chambers in order to bypass these issues. In our experience, open air culture chambers are at a much higher risk for contamination. Non-contact stretch bioreactors should not need custom culture chambers. In our case, we did not have to modify the culture chambers in any way and were able to use rigorous sterile technique.

A traditional stretch bioreactor relies on physical attachment to the scaffold at several anchor points. The arm holding the edge of the scaffold is then translated axially in an oscillating pattern. This method provides a single degree of axial control, applies discrete points of stress, and relies on the scaffold to distribute forces along the axis of deformation. Physical distortion of a scaffold can cause deformation and break at the points of contact due to a lack of force distribution. Further, this mechanism of stretch has little physical resemblance to the forces involved in the heart under rhythmic contractile stretch. More advanced bioreactors which attempt to mimic physiological conditions apply a deformation force to a pliable surface underneath the culture dish. A piston-like component moves tangentially to the surface of a culture plane and pushes the pliable-PDMS surface vertically. This distends the cultured tissue in a manner more closely related to the

mechanics of heart muscle *in vivo*. Unfortunately, discrete control can be more difficult under these circumstances. Further, such systems necessitate custom built chambers and exhibit little geometric control. We attempted to bypass these issues by developing a non-contact stretch bioreactor system which uses magnetic forces in order to induce the deformation forces.

In our preliminary studies, we used Fe_2O_3 as the ferromagnetic component of our scaffold. The powder which we purchased was fairly uncharacterized (<5 μm diameter) and was not in any way functionalized to make it less toxic. Adding higher weight percentages of Fe_2O_3 made the scaffolds stiffer and darker in color. After a certain load, Fe_2O_3 precipitated out of the scaffold. We found that 11 wt% was the highest load at which the fibrin gel could encapsulate the powder without protocol modification. Physical stretch regimens typically involve an axial deformation of 5-15%. We were able to achieve deformations in this range using loads upwards of 5 wt%. At 7 wt%, a deformation of 12% stretch was possible. Using uncharacterized iron (III) oxide, we were able to magnetize our scaffold and induce physiologically relevant levels of stretch without saturating the scaffold (Figure 24).

Iron oxide is considered slightly toxic in the body, and as such we expected a negative effect when loading with unmodified iron powder. After 4 days of culture, there was no difference in activity between AHM formed using Fe_2O_3 loaded scaffolds and controls (Figure 25). After 7 days of culture, there was a significant drop in contractile activity between AHM formed on both 3wt% and 7wt% Fe_2O_3 fibrin scaffolds and controls. As such, a delayed toxic effect was observed. We confirmed a change in cellular expression with IHC microscopy. Controls exhibited higher levels of α-actinin and better overall organization than 3 and 7 wt % AHM constructs.

Such effects were expected, however the above study was intended as a proof of concept for the base principles involved. In order to reduce toxicity and improve the versatility of the system, we set out to synthesize a new magnetic component for our scaffolds. In coordination with Dr. Randy Lee's lab, we developed well characterized Fe_3O_4 nanoparticles (Figure 26). The particles exhibited a 10-fold increase in magnetic sensitivity over the Fe_2O_3 particles used

previously. Further the uniform structure of the particles allows for more uniform application of magnetic forces within the scaffold. We were able to achieve 15% axial stretch using only 1 wt% of the 300 nm Fe_3O_4 nanoparticle. At such levels, toxic effects were negligible at 7 days, however higher loads of particle produced negative effects within 8 days of culture. Toxicity can be reduced via functionalization of the nanoparticles. Common techniques involve silicating the surface of the nanoparticles or functionalizing the magnetic core with polymer chains. Should toxicity of the particles become a concern, Dr. Randy Lee's group is very familiar with the necessary synthesis techniques to combat such issues.

Constructs were stretched using magnetic fields and the highly characterized 300 nm Fe_3O_4 nanoparticles. The stretch protocols were highly tunable via parameters sent to the user-interface. Starting distance, frequency (magnet speed), ending distance and ramp speed were all parameters which could be adjusted in order to develop the best stretch protocol.

5.5 Summary

We developed a novel, non-contact, stretch based bioreactor to induce mechanical stimulation of tissue engineered cardiac muscle. The system is capable of delivering axial stretch via application of an oscillating magnetic field to a magnetized AHM construct. We began with bulk, uncharacterized iron oxide as the magnetic component. We then synthesized highly magnetic, low toxicity Fe_3O_4 magnetic nanoparticles. The system is capable of delivering physiologically relevant stretch without issuing undue stress on the constructs.

References:

Abbott, Alison. 2003. “Cell Culture: Biology’s New Dimension.” *Nature* 424 (June): 870+. http://go.galegroup.com/ps/i.do?id=GALE|A187749303&v=2.1&u=txshracd2588&it=r&p=HRCA&sw=w.

Ahmed, Tamer A E, Emma V Dare, and Max Hincke. 2008. “Fibrin: A Versatile Scaffold for Tissue Engineering Applications.” *Tissue Engineering Part B: Reviews* 14 (2). Mary Ann Liebert, Inc. 140 Huguenot Street, 3rd Floor New Rochelle, NY 10801 USA: 199–215.

Akhyari, Payam, Paul W M Fedak, Richard D Weisel, Tsu-Yee Joseph Lee, Subodh Verma, Donald A G Mickle, and Ren-Ke Li. 2002. “Mechanical Stretch Regimen Enhances the Formation of Bioengineered Autologous Cardiac Muscle Grafts.” *Circulation* 106 (12 suppl 1). Am Heart Assoc: I – 137.

Akins, R E, R A Boyce, M L Madonna, N A Schroedl, S R Gonda, T A McLaughlin, and C R Hartzell. 1999. “Cardiac Organogenesis in Vitro: Reestablishment of Three-Dimensional Tissue Architecture by Dissociated Neonatal Rat Ventricular Cells.” *Tissue Engineering* 5 (2). Mary Ann Liebert, Inc. 2 Madison Avenue Larchmont, NY 10538 USA: 103–18.

Amado, Luciano C, Anastasios P Saliaris, Karl H Schuleri, Marcus St. John, Jin-Sheng Xie, Stephen Cattaneo, Daniel J Durand, et al. 2005. “Cardiac Repair with Intramyocardial Injection of Allogeneic Mesenchymal Stem Cells after Myocardial Infarction.” *Proceedings of the National Academy of Sciences of the United States of America* 102 (32): 11474–79. doi:10.1073/pnas.0504388102.

Annabi, Nasim, Kelly Tsang, Suzanne M Mithieux, Mehdi Nikkhah, Afshin Ameri, Ali Khademhosseini, and Anthony S Weiss. 2013. "Highly Elastic Micropatterned Hydrogel for Engineering Functional Cardiac Tissue." *Advanced Functional Materials* 23 (39). Wiley Online Library: 4950–59.

Anversa, Piero, Jan Kajstura, Marcello Rota, and Annarosa Leri. 2013. "Regenerating New Heart with Stem Cells." *The Journal of Clinical Investigation* 123 (1). Am Soc Clin Investig: 62–70.

Arap, Wadih, Renata Pasqualini, and Erkki Ruoslahti. 1998. "Cancer Treatment by Targeted Drug Delivery to Tumor Vasculature in a Mouse Model." *Science* 279 (5349). American Association for the Advancement of Science: 377–80.

Archundia, Abel, José Luis Aceves, Manuel López-Hernández, Martha Alvarado, Emma Rodriguez, Guillermo Díaz Quiroz, Araceli Páez, Felipe Masso Rojas, and Luis Felipe Montaño. 2005. "Direct Cardiac Injection of G-CSF Mobilized Bone-Marrow Stem-Cells Improves Ventricular Function in Old Myocardial Infarction." *Life Sciences* 78 (3): 279–83. doi:http://dx.doi.org/10.1016/j.lfs.2005.04.080.

Asthana, Amish, and William S Kisaalita. 2013. "Biophysical Microenvironment and 3D Culture Physiological Relevance." *Drug Discovery Today* 18 (11–12): 533–40. doi:http://dx.doi.org/10.1016/j.drudis.2012.12.005.

Atala, Anthony. 2004. "Tissue Engineering and Regenerative Medicine: Concepts for Clinical Application." *Rejuvenation Research* 7 (1). Mary Ann Liebert, Inc.: 15–31.

Atala, Anthony. 2007. "Engineering Tissues, Organs and Cells." *Journal of Tissue Engineering and Regenerative Medicine* 1 (2). John Wiley & Sons, Ltd.: 83–96. doi:10.1002/term.18.

Au, Hoi Ting Heidi, Christopher Cannizzaro, Pen-Hsiu Grace Chao, Robert Maidhof, Anna Marsano, Milica Radisic, Nina Tandon, and Gordana Vunjak-Novakovic. 2009. "Electrical Stimulation Systems for Cardiac Tissue Engineering." *Nature Protocols* 4 (April): 155+. http://go.galegroup.com/ps/i.do?id=GALE|A193793161&v=2.1&u=txshracd2588&it=r&p=HRCA&sw=w.

Baar, Keith, Ravi Birla, Marvin O Boluyt, Gregory H Borschel, Ellen M Arruda, and Robert G Dennis. 2004. "Self-Organization of Rat Cardiac Cells into Contractile 3-D Cardiac Tissue." *The FASEB Journal*, December. doi:10.1096/fj.04-2034fje.

Baheiraei, Nafiseh, Hamid Yeganeh, Jafar Ai, Reza Gharibi, Mahmoud Azami, and Faezeh Faghihi. 2014. "Synthesis, Characterization and Antioxidant Activity of a Novel Electroactive and Biodegradable Polyurethane for Cardiac Tissue Engineering Application." *Materials Science and Engineering: C* 44. Elsevier: 24–37.

Balachandran Philippe Jo, Hanjoong Yoganathan, Ajit P., Kartik Sucosky. 2009. "Elevated Cyclic Stretch Alters Matrix Remodeling in Aortic Valve Cusps: Implications for Degenerative Aortic Valve Disease." *American Journal of Physiology - Heart and Circulatory Physiology* 296 (3): H756–64. http://ajpheart.physiology.org/content/296/3/H756.abstract.

Banerjee, Indroneal, John W Fuseler, Robert L Price, Thomas K Borg, and Troy A Baudino. 2007. "Determination of Cell Types and Numbers during Cardiac Development in the Neonatal and Adult Rat and Mouse" 293 (3): H1883–91. http://ajpheart.physiology.org/highwire/citation/25602/mendeley.

Barsotti, Maria Chiara, Francesca Felice, Alberto Balbarini, and Rossella Di Stefano. 2011. "Fibrin as a Scaffold for Cardiac Tissue Engineering." *Biotechnology and Applied Biochemistry* 58 (5). Wiley Online Library: 301–10.

Bhaarathy, V, J Venugopal, C Gandhimathi, N Ponpandian, D Mangalaraj, and S Ramakrishna. 2014. "Biologically Improved Nanofibrous Scaffolds for Cardiac Tissue Engineering." *Materials Science and Engineering: C* 44. Elsevier: 268–77.

Birla, Ravi K, Scott J Hollister, and Francesco B T - Regenerative Medicine Migneco. 2008. "Tissue-Engineered Heart Valve Prostheses: 'State of the Heart'" 3 (3): 399+. http://go.galegroup.com/ps/i.do?id=GALE|A225282563&v=2.1&u=txshracd2588&it=r&p=HRCA&sw=w LA - English.

Black, Lauren D, Saik-Kia Goh, Stefan M Kren, Thomas S Matthiesen, Theoden I Netoff, Harald C Ott, and Doris A Taylor. 2008. "Perfusion-Decellularized Matrix: Using Nature's Platform to Engineer a Bioartificial Heart." *Nature Medicine* 14 (January): 213+. http://go.galegroup.com/ps/i.do?id=GALE|A198547575&v=2.1&u=txshracd2588&it=r&p=HRCA&sw=w LA - English.

Blan, Nicole R, and Ravi K Birla. 2008a. "Design and Fabrication of Heart Muscle Using Scaffold-based Tissue Engineering." *Journal of Biomedical Materials Research Part A* 86 (1). Wiley Online Library: 195–208.

Blombäck, B, K Carlsson, B Hessel, A Liljeborg, R Procyk, and N Åslund. 1989. "Native Fibrin Gel Networks Observed by 3D Microscopy, Permeation and Turbidity." *Biochimica et Biophysica Acta (BBA)-Protein Structure and Molecular Enzymology* 997 (1). Elsevier: 96–110.

Boengler, Kerstin, Rainer Schulz, and Gerd Heusch. 2006. “Connexin 43 Signalling and Cardioprotection.” *Heart* 92 (12). BMJ Publishing Group Ltd and British Cardiovascular Society: 1724–27.

Bond, A Elaine, Karl Nelson, Cara Lynn Germany, and Angie N Smart. 2003. “CE Credit: The Left Ventricular Assist Device.” *The American Journal of Nursing* 103 (1). Lippincott Williams & Wilkins: 32–41 CR – Copyright © 2003 Wolters Kluwer He. doi:10.2307/29744914.

Boonen, Kristel J M, Marloes L P Langelaan, Roderick B Polak, Daisy W J van der Schaft, Frank P T Baaijens, and Mark J Post. 2010. “Effects of a Combined Mechanical Stimulation Protocol: Value for Skeletal Muscle Tissue Engineering.” *Journal of Biomechanics* 43 (8): 1514–21. doi:http://dx.doi.org/10.1016/j.jbiomech.2010.01.039.

Buckley, Conor T, Stephen D Thorpe, and Daniel J Kelly. 2009. “Engineering of Large Cartilaginous Tissues through the Use of Microchanneled Hydrogels and Rotational Culture.” *Tissue Engineering Part A* 15 (11). Mary Ann Liebert, Inc. 140 Huguenot Street, 3rd Floor New Rochelle, NY 10801 USA: 3213–20.

Bursac, N, M Papadaki, R J Cohen, F J Schoen, S R Eisenberg, R Carrier, G Vunjak-Novakovic, and L E Freed. 1999. “Cardiac Muscle Tissue Engineering: Toward an in Vitro Model for Electrophysiological Studies .” *American Journal of Physiology - Heart and Circulatory Physiology* 277 (2): H433–44. http://ajpheart.physiology.org/content/277/2/H433.abstract.

Caspi, Oren, Ayelet Lesman, Yaara Basevitch, Amira Gepstein, Gil Arbel, Irit Huber Manhal Habib, Lior Gepstein, and Shulamit Levenberg. 2007. “Tissue Engineering of Vascularized Cardiac Muscle from Human Embryonic Stem Cells.” *Circulation Research* 100 (2). Am Heart Assoc: 263–72.

Chen, Huang-Chi, and Yu-Chen Hu. 2006. "Bioreactors for Tissue Engineering." *Biotechnology Letters* 28 (18). Springer Netherlands: 1415–23. doi:10.1007/s10529-006-9111-x.

Chiu, L L, Rohin K Iyer, Lewis A Reis, Sara S Nunes, and Milica Radisic. 2011. "Cardiac Tissue Engineering: Current State and Perspectives." *Frontiers in Bioscience (Landmark Edition)* 17: 1533–50.

Copeland, Jack G, Richard G Smith, Francisco A Arabia, Paul E Nolan, Gulshan K Sethi, Pei H Tsau, Douglas McClellan, and Marvin J Slepian. 2004. "Cardiac Replacement with a Total Artificial Heart as a Bridge to Transplantation." *New England Journal of Medicine* 351 (9). Massachusetts Medical Society: 859–67. doi:10.1056/NEJMoa040186.

Coulombe, Kareen L K, Vivek K Bajpai, Stelios T Andreadis, and Charles E Murry. 2014. "Heart Regeneration with Engineered Myocardial Tissue." *Annual Review of Biomedical Engineering* 16 (1). Annual Reviews: 1–28. doi:10.1146/annurev-bioeng-071812-152344.

Cui, Haitao, Yadong Liu, Yilong Cheng, Zhe Zhang, Peibiao Zhang, Xuesi Chen, and Yen Wei. 2014. "In Vitro Study of Electroactive Tetraaniline-Containing Thermosensitive Hydrogels for Cardiac Tissue Engineering." *Biomacromolecules* 15 (4). ACS Publications: 1115–23.

Cukierman, Edna, Roumen Pankov, Daron R Stevens, and Kenneth M Yamada. 2001. "Taking Cell-Matrix Adhesions to the Third Dimension." *Science*, New Series, 294 (5547). American Association for the Advancement of Science: 1708–12. doi:10.2307/3085299.

Curtis, Matthew W, and Brenda Russell. 2009. "Cardiac Tissue Engineering." *The Journal of Cardiovascular Nursing* 24 (2). NIH Public Access: 87.

Daquinag, Alexes C, Glauco R Souza, and Mikhail G Kolonin. 2012. "Adipose Tissue Engineering in Three-Dimensional Levitation Tissue Culture System Based on Magnetic

Nanoparticles." *Tissue Engineering Part C: Methods* 19 (5). Mary Ann Liebert, Inc. 140 Huguenot Street, 3rd Floor New Rochelle, NY 10801 USA: 336–44.

Dar, Ayelet, Michal Shachar, Jonathan Leor, and Smadar Cohen. 2002. "Optimization of Cardiac Cell Seeding and Distribution in 3D Porous Alginate Scaffolds." *Biotechnology and Bioengineering* 80 (3). Wiley Online Library: 305–12.

Deng, Hong, Xiaolin Li, Qing Peng, Xun Wang, Jinping Chen, and Yadong Li. 2005. "Monodisperse Magnetic Single-Crystal Ferrite Microspheres." *Angewandte Chemie* 117 (18). Wiley Online Library: 2842–45.

Dhingra, Sanjiv, Richard D Weisel, and Ren-Ke Li. 2014. "Synthesis of Aliphatic Polyester Hydrogel for Cardiac Tissue Engineering." In *Cardiac Tissue Engineering*, 51–59. Springer.

Ehler, Elisabeth, and Suwan N Jayasinghe. 2014. "Cell Electrospinning Cardiac Patches for Tissue Engineering the Heart." *Analyst* 139 (18). Royal Society of Chemistry: 4449–52.

Endl, Elmar, and Johannes Gerdes. 2000. "The Ki-67 Protein: Fascinating Forms and an Unknown Function." *Experimental Cell Research* 257 (2). Elsevier: 231–37.

Eschenhagen, T, C Fink, U Remmers, H Scholz, J Wattchow, J Weil, W Zimmermann, H H Dohmen, H Schäfer, and N Bishopric. 1997. "Three-Dimensional Reconstitution of Embryonic Cardiomyocytes in a Collagen Matrix: A New Heart Muscle Model System." *The FASEB Journal* 11 (8). FASEB: 683–94.

Evers, Rebecca, Luda Khait, and Ravi K Birla. 2011. "Fabrication of Functional Cardiac, Skeletal, and Smooth Muscle Pumps In Vitro." *Artificial Organs*. Wiley-Blackwell. 10.1111/j.1525-1594.2010.01007.x.

Feng, Ting, Yuanwei Chen, Guoqi Shi, Xixun Yu, and Changxiu Wan. 2008. “A Collagen Based Vitro Model of Angiogenesis Designed for Tissue-Engineering Material.” *Applied Surface Science* 255 (2): 312–14. doi:http://dx.doi.org/10.1016/j.apsusc.2008.06.091.

Finegold, Judith A, Perviz Asaria, and Darrel P Francis. 2013. “Mortality from Ischaemic Heart Disease by Country, Region, and Age: Statistics from World Health Organisation and United Nations.” *International Journal of Cardiology* 168 (2). Elsevier: 934–45.

Fink, Christine, Suleman Ergun, Dirk Kralisch, U T E Remmers, Joachim Weil, and Thomas Eschenhagen. 2000. “Chronic Stretch of Engineered Heart Tissue Induces Hypertrophy and Functional Improvement.” *The FASEB Journal* 14 (5). FASEB: 669–79.

Fisher, Matthew B, and Robert L Mauck. 2013. “Tissue Engineering and Regenerative Medicine: Recent Innovations and the Transition to Translation.” *Tissue Engineering Part B: Reviews* 19 (1). Mary Ann Liebert, Inc. 140 Huguenot Street, 3rd Floor New Rochelle, NY 10801 USA: 1–13.

Fleischer, Sharon, Ron Feiner, Assaf Shapira, Jing Ji, Xiaomeng Sui, H Daniel Wagner, and Tal Dvir. 2013. “Spring-like Fibers for Cardiac Tissue Engineering.” *Biomaterials* 34 (34). Elsevier: 8599–8606.

Foy, D. 2007. “Clinical Updates. Heart Failure.” Edited by D Twedell. *Journal of Continuing Education in Nursing* 38 (5): 198–99. http://ezproxy.lib.uh.edu/login?url=http://search.ebscohost.com/login.aspx?direct=true&db=rzh&AN=2009677705&site=ehost-live.

Fujimoto, Kazuro L, Kelly C Clause, Li J Liu, Joseph P Tinney, Shivam Verma, William R Wagner, Bradley B Keller, and Kimimasa Tobita. 2010. “Engineered Fetal Cardiac Graft

Preserves Its Cardiomyocyte Proliferation within Postinfarcted Myocardium and Sustains Cardiac Function." *Tissue Engineering Part A* 17 (5-6). Mary Ann Liebert, Inc. 140 Huguenot Street, 3rd Floor New Rochelle, NY 10801 USA: 585–96.

Gálvez-Montón, Carolina, Cristina Prat-Vidal, Santiago Roura, Carolina Soler-Botija, and Antoni Bayes-Genis. 2013. "Cardiac Tissue Engineering and the Bioartificial Heart." *Revista Española de Cardiología (English Edition)* 66 (5). Elsevier: 391–99.

Gilbert, Thomas W, Tiffany L Sellaro, and Stephen F Badylak. 2006. "Decellularization of Tissues and Organs." *Biomaterials* 27 (19): 3675–83. doi:http://dx.doi.org/10.1016/j.biomaterials.2006.02.014.

Go, Alan S, Dariush Mozaffarian, Véronique L Roger, Emelia J Benjamin, Jarett D Berry, Michael J Blaha, Shifan Dai, Earl S Ford, Caroline S Fox, and Sheila Franco. 2014. "Heart Disease and Stroke Statistics--2014 Update: A Report from the American Heart Association." *Circulation* 129 (3): e28.

Go, Alan S, Dariush Mozaffarian, Véronique L Roger, Emelia J Benjamin, Jarett D Berry, William B Borden, Dawn M Bravata, Shifan Dai, Earl S Ford, and Caroline S Fox. 2013. "Heart Disease and Stroke Statistics--2013 Update: A Report from the American Heart Association." *Circulation* 127 (1): e6.

Griffith, Linda G, and Melody A Swartz. 2006. "Capturing Complex 3D Tissue Physiology in Vitro." *Nature Reviews Molecular Cell Biology* 7 (3). Nature Publishing Group: 211–24. 10.1038/nrm1858.

Grinnell, F. 1984. "Manganese-Dependent Cell-Substratum Adhesion." *Journal of Cell Science* 65 (1): 61–72. http://jcs.biologists.org/content/65/1/61.abstract.

Guo, Xi-Min, Yun-Shan Zhao, Hai-Xia Chang, Chang-Yong Wang, E Ling-Ling, Xiao-Ai Zhang, Cui-Mi Duan, Ling-Zhi Dong, Hong Jiang, and Jing Li. 2006. "Creation of Engineered Cardiac Tissue in Vitro from Mouse Embryonic Stem Cells." *Circulation* 113 (18). Am Heart Assoc: 2229–37.

Gutierrez, Jose, Gilbert Ramirez, Tatjana Rundek, and Ralph L Sacco. 2012. "Statin Therapy in the Prevention of Recurrent Cardiovascular Events: A Sex-Based Meta-Analysis." *Archives of Internal Medicine* 172 (12). American Medical Association: 909–19.

Guyette, Jacques P, Michael Fakharzadeh, Evans J Burford, Ze-Wei Tao, George D Pins, Marsha W Rolle, and Glenn R Gaudette. 2013. "A Novel Suture-based Method for Efficient Transplantation of Stem Cells." *Journal of Biomedical Materials Research Part A* 101 (3). Wiley Online Library: 809–18.

Gwak, So-Jung, Suk Ho Bhang, Il-Kwon Kim, Sang-Soo Kim, Seung-Woo Cho, Oju Jeon, Kyung Jong Yoo, Andrew J Putnam, and Byung-Soo Kim. 2008. "The Effect of Cyclic Strain on Embryonic Stem Cell-Derived Cardiomyocytes." *Biomaterials* 29 (7): 844–56. doi:http://dx.doi.org/10.1016/j.biomaterials.2007.10.050.

Haisler, William L, David M Timm, Jacob A Gage, Hubert Tseng, T C Killian, and Glauco R Souza. 2013. "Three-Dimensional Cell Culturing by Magnetic Levitation." *Nat. Protocols* 8 (10). Nature Publishing Group, a division of Macmillan Publishers Limited. All Rights Reserved.: 1940–49. http://dx.doi.org/10.1038/nprot.2013.125.

Hajitou, Amin, Martin Trepel, Caroline E Lilley, Suren Soghomonyan, Mian M Alauddin, Frank C Marini III, Bradley H Restel, et al. 2006. "A Hybrid Vector for Ligand-Directed Tumor Targeting and Molecular Imaging." *Cell* 125 (2): 385–98. doi:http://dx.doi.org/10.1016/j.cell.2006.02.042.

Hayashi, Chikako, Urara Hasegawa, Yoshitomo Saita, Hiroaki Hemmi, Tadayoshi Hayata, Kazuhisa Nakashima, Yoichi Ezura, Teruo Amagasa, Kazunari Akiyoshi, and Masaki Noda. 2009. "Osteoblastic Bone Formation Is Induced by Using Nanogel-Crosslinking Hydrogel as Novel Scaffold for Bone Growth Factor." *Journal of Cellular Physiology* 220 (1). Wiley Subscription Services, Inc., A Wiley Company: 1–7. doi:10.1002/jcp.21760.

Haycock, J W. 2010. *3D Cell Culture: Methods and Protocols*. Methods in Molecular Biology. Humana Press. http://books.google.com/books?id=s15MbwAACAAJ.

Hecker, Louise, and Ravi K Birla. 2007. "Engineering the Heart Piece by Piece: State of the Art in Cardiac Tissue Engineering." Future Medicine.

Hennekens, Charles H, Mark L Dyken, and Valentin Fuster. 1997. "Aspirin as a Therapeutic Agent in Cardiovascular Disease A Statement for Healthcare Professionals From the American Heart Association." *Circulation* 96 (8). Am Heart Assoc: 2751–53.

Hirt, Marc N, Arne Hansen, and Thomas Eschenhagen. 2014. "Cardiac Tissue Engineering State of the Art." *Circulation Research* 114 (2). Am Heart Assoc: 354–67.

Hogan, Matthew, Mohamed Mohamed, Ze-Wei Tao, Laura Gutierrez, and Ravi Birla. 2014. "Establishing the Framework to Support Bioartificial Heart Fabrication Using Fibrin-Based Three-Dimensional Artificial Heart Muscle." *Artificial Organs*. Wiley Online Library.

Huang, Yen-Chih, Luda Khait, and Ravi K Birla. 2007. "Contractile Three-Dimensional Bioengineered Heart Muscle for Myocardial Regeneration." *Journal of Biomedical Materials Research Part A* 80A (3). Wiley Subscription Services, Inc., A Wiley Company: 719–31. doi:10.1002/jbm.a.31090.

Huang, Yen-Chih, Luda Khait, and Ravi K Birla. 2007. “Contractile Three-dimensional Bioengineered Heart Muscle for Myocardial Regeneration.” *Journal of Biomedical Materials Research Part A* 80 (3). Wiley Online Library: 719–31.

Kantrowitz, Adrian, Steinar Tjønneland, Paul S Freed, Steven J Phillips, Alfred N Butner, and Jacques L Sherman. 1968. “Initial Clinical Experience with Intraaortic Balloon Pumping in Cardiogenic Shock.” *Jama* 203 (2). American Medical Association: 113–18.

Kawamura, Masashi, Shigeru Miyagawa, Satsuki Fukushima, Atsuhiro Saito, Kenji Miki, Emiko Ito, Nagako Sougawa, Takuji Kawamura, Takashi Daimon, and Tatsuya Shimizu. 2013. “Enhanced Survival of Transplanted Human Induced Pluripotent Stem Cell–Derived Cardiomyocytes by the Combination of Cell Sheets With the Pedicled Omental Flap Technique in a Porcine Heart.” *Circulation* 128 (11 suppl 1). Am Heart Assoc: S87–94.

Kelly, B B, C.P.G.E.C.D.M.C.D. Countries, V Fuster, B G Health, and I Medicine. 2010. *Promoting Cardiovascular Health in the Developing World:: A Critical Challenge to Achieve Global Health*. National Academies Press. https://books.google.com/books?id=uNEoYaJ_NWwC.

Kensah, George, Ina Gruh, Jörg Viering, Henning Schumann, Julia Dahlmann, Heiko Meyer, David Skvorc, Antonia Bär, Payam Akhyari, and Alexander Heisterkamp. 2011. “A Novel Miniaturized Multimodal Bioreactor for Continuous in Situ Assessment of Bioartificial Cardiac Tissue during Stimulation and Maturation.” *Tissue Engineering Part C: Methods* 17 (4). Mary Ann Liebert, Inc. 140 Huguenot Street, 3rd Floor New Rochelle, NY 10801 USA: 463–73.

Ketchedjian, Ara, Alyce Linthurst Jones, Paula Krueger, Elliot Robinson, Katrina Crouch, Lloyd Wolfinbarger, and Richard Hopkins. 2005. “Recellularization of Decellularized Allograft

Scaffolds in Ovine Great Vessel Reconstructions." *The Annals of Thoracic Surgery* 79 (3): 888–96. doi:10.1016/j.athoracsur.2004.09.033.

Khait, L, and RK Birla. 2007. "Cell-Based Cardiac Pumps and Tissue-Engineered Ventricles." *Regenerative Medicine*. http://www.futuremedicine.com/doi/abs/10.2217/17460751.2.4.391.

Khait, Luda, and Ravi K Birla. 2008. "Effect of Thyroid Hormone on the Contractility of Self-Organized Heart Muscle." *In Vitro Cellular & Developmental Biology. Animal* 44 (7). Society for In Vitro Biology: 204–13. doi:10.2307/40205874.

Khait, Luda, Louise Hecker, Nicole R Blan, Garrett Coyan, Francesco Migneco, Yen-Chih Huang, and Ravi K Birla. 2008. "Getting to the Heart of Tissue Engineering." *Journal of Cardiovascular Translational Research* 1 (1). Springer: 71–84.

Khantamat, Orawan, Chien-Hung Li, Fei Yu, Andrew C Jamison, Wei-Chuan Shih, Chengzhi Cai, and T Randall Lee. 2015. "Gold Nanoshell-Decorated Silicone Surfaces for the NIR Photothermal Destruction of the Pathogenic Bacterium E. Faecalis." *ACS Applied Materials & Interfaces*. ACS Publications.

Ku, Ching-Hsin, Philip H Johnson, Puspa Batten, Padmini Sarathchandra, Rachel C Chambers, Patricia M Taylor, Magdi H Yacoub, and Adrian H Chester. 2006. "Collagen Synthesis by Mesenchymal Stem Cells and Aortic Valve Interstitial Cells in Response to Mechanical Stretch." *Cardiovascular Research* 71 (3): 548–56. http://cardiovascres.oxfordjournals.org/content/71/3/548.abstract.

Kwapiszewska, K, A Michalczuk, M Rybka, R Kwapiszewski, and Z Brzozka. 2014. "A Microfluidic-Based Platform for Tumour Spheroid Culture, Monitoring and Drug

Screening." *Lab on a Chip* 14 (12). The Royal Society of Chemistry: 2096–2104. doi:10.1039/C4LC00291A.

Langer, Robert, and P Joseph. 1993. "Vacanti. Tissue Engineering." *Science, L* 993: 26O.

Langer, Robert, and Joseph P Vacanti. 1993. "Tissue Engineering." *Science*, New Series, 260 (5110). American Association for the Advancement of Science: 920–26. http://www.jstor.org/stable/2885618.

Leor, Jonathan, Sharon Aboulafia-Etzion, Ayelet Dar, Lilia Shapiro, Israel M Barbash, Alexander Battler, Yosef Granot, and Smadar Cohen. 2000. "Bioengineered Cardiac Grafts a New Approach to Repair the Infarcted Myocardium?" *Circulation* 102 (suppl 3). Am Heart Assoc: Iii – 56.

Li, Ren-Ke, Zhi-Qiang Jia, Richard D Weisel, Donald A G Mickle, Angel Choi, and Terrence M Yau. 1999. "Survival and Function of Bioengineered Cardiac Grafts." *Circulation* 100 (suppl 2). Am Heart Assoc: II – 63.

Li, Ren-Ke, Terrence M Yau, Richard D Weisel, Donald A G Mickle, Tetsuro Sakai, Angel Choi, and Zhi-Qiang Jia. 2000. "Construction of a Bioengineered Cardiac Graft." *The Journal of Thoracic and Cardiovascular Surgery* 119 (2). Elsevier: 368–75.

Liau, Brian, Nicolas Christoforou, Kam W Leong, and Nenad Bursac. 2011. "Pluripotent Stem Cell-Derived Cardiac Tissue Patch with Advanced Structure and Function." *Biomaterials* 32 (35). Elsevier: 9180–87.

Maidhof, Robert, Anna Marsano, Milica Radisic, Gordana Vunjak-Novakovic, and Yadong Wang. 2008. "Cardiac Tissue Engineering Using Perfusion Bioreactor Systems." *Nature Protocols* 3 (January): 719+.

http://go.galegroup.com/ps/i.do?id=GALE|A186854637&v=2.1&u=txshracd2588&it=r&p=HRCA&sw=w LA - English.

Maton, A, and inc Prentice-Hall. 1994. *Human Biology and Health*. Human Biology and Health. Prentice Hall. https://books.google.com/books?id=ImHLSQAACAAJ.

Matsuura, Katsuhisa, Shinako Masuda, and Tatsuya Shimizu. 2014. "Cell Sheet-Based Cardiac Tissue Engineering." *The Anatomical Record* 297 (1). Wiley Online Library: 65–72.

McCarthy, Patrick M, Satoshi Nakatani, Rita Vargo, Kandice Kottke-Marchant, Hiroaki Harasaki, Karen B James, Robert M Savage, and James D Thomas. 1995. "Structural and Left Ventricular Histologic Changes after Implantable LVAD Insertion." *The Annals of Thoracic Surgery* 59 (3). Elsevier: 609–13.

McGinn, Owen J, William R English, Stephanie Roberts, Ann Ager, Peter Newham, and Gillian Murphy. 2011. "Modulation of Integrin α4β1 by ADAM28 Promotes Lymphocyte Adhesion and Transendothelial Migration." *Cell Biology International* 35 (10): 1043–53. http://www.cellbiolint.org.ezproxy.lib.uh.edu/cbi/035/cbi0351043.htm.

Mehta, Geeta, Amy Y Hsiao, Marylou Ingram, Gary D Luker, and Shuichi Takayama. 2012. "Opportunities and Challenges for Use of Tumor Spheroids as Models to Test Drug Delivery and Efficacy." *Journal of Controlled Release* 164 (2): 192–204. doi:http://dx.doi.org/10.1016/j.jconrel.2012.04.045.

Members, Writing Group, Véronique L Roger, Alan S Go, Donald M Lloyd-Jones, Emelia J Benjamin, Jarett D Berry, William B Borden, et al. 2012. "Heart Disease and Stroke Statistics—2012 Update." *Circulation* 125 (1): e2–220. doi:10.1161/CIR.0b013e31823ac046.

Mendis, S, P Puska, B Norrving, World Health Organization, World Heart Federation, and World Stroke Organization. 2011. *Global Atlas on Cardiovascular Disease Prevention and Control*. Nonserial Publications Series. World Health Organization in collaboration with the World Heart Federation and the World Stroke Organization. https://books.google.com/books?id=ZRbKygAACAAJ.

Mueller-Klieser, Wolfgang. 1997. "Three-Dimensional Cell Cultures: From Molecular Mechanisms to Clinical Applications." *American Journal of Physiology - Cell Physiology* 273 (4): C1109–23. http://ajpcell.physiology.org/content/273/4/C1109.abstract.

Nerem, Robert M. 2006. "Tissue Engineering: The Hope, the Hype, and the Future." *Tissue Engineering* 12 (5). Mary Ann Liebert, Inc. 2 Madison Avenue Larchmont, NY 10538 USA: 1143–50.

Pampaloni, Francesco, Emmanuel G Reynaud, and Ernst H K Stelzer. 2007. "The Third Dimension Bridges the Gap between Cell Culture and Live Tissue." *Nature Reviews Molecular Cell Biology* 8 (10). Nature Publishing Group: 839–45. 10.1038/nrm2236.

Papadaki, M, N Bursac, R Langer, J Merok, G Vunjak-Novakovic, and L E Freed. 2001. "Tissue Engineering of Functional Cardiac Muscle: Molecular, Structural, and Electrophysiological Studies." *American Journal of Physiology-Heart and Circulatory Physiology* 280 (1). Am Physiological Soc: H168–78.

Pedersen, JohnA., and MelodyA. Swartz. 2005. "Mechanobiology in the Third Dimension." *Annals of Biomedical Engineering* 33 (11). Kluwer Academic Publishers-Plenum Publishers: 1469–90. doi:10.1007/s10439-005-8159-4.

Platis, A, and D F Larson. 2009. “CardioWest Temporary Total Artificial Heart.” *Perfusion* 24 (5). Circulatory Sciences Graduate Perfusion Program, College of Medicine, University of Arizona, Tucson, AZ, USA: 341–46. doi:http://dx.doi.org/10.1177/0267659109351330.

Pok, Seokwon, Omar M Benavides, Patrick Hallal, and Jeffrey G Jacot. 2014. “Use of Myocardial Matrix in a Chitosan-Based Full-Thickness Heart Patch.” *Tissue Engineering Part A*. Mary Ann Liebert, Inc. 140 Huguenot Street, 3rd Floor New Rochelle, NY 10801 USA.

Porrello, Enzo R, Ahmed I Mahmoud, Emma Simpson, Joseph A Hill, James A Richardson, Eric N Olson, and Hesham A Sadek. 2011. “Transient Regenerative Potential of the Neonatal Mouse Heart.” *Science* 331 (6020). American Association for the Advancement of Science: 1078–80.

Prabhakaran, Molamma P, Dan Kai, Laleh Ghasemi-Mobarakeh, and Seeram Ramakrishna. 2011. “Electrospun Biocomposite Nanofibrous Patch for Cardiac Tissue Engineering.” *Biomedical Materials* 6 (5). IOP Publishing: 55001.

Prabhakaran, Molamma P, A Sreekumaran Nair, Dan Kai, and Seeram Ramakrishna. 2012. “Electrospun Composite Scaffolds Containing Poly (octanediol-co-citrate) for Cardiac Tissue Engineering.” *Biopolymers* 97 (7). Wiley Online Library: 529–38.

Procurement, Organ, and Transplantation Network. 2011. “And Scientific Registry of Transplant Recipients (SRTR).” *OPTN/SRTR 2010 Annual Data Report. Rockville, MD: Department of Health and Human Services, Health Resources and Services Administration, Healthcare Systems Bureau, Division of Transplantation* 12 (Suppl 1): 1–156.

Qazi, Taimoor H, Ranjana Rai, Dirk Dippold, Judith E Roether, Dirk W Schubert, Elisabetta Rosellini, Niccoletta Barbani, and Aldo R Boccaccini. 2014. “Development and Characterization of Novel Electrically Conductive PANI–PGS Composites for Cardiac Tissue Engineering Applications.” *Acta Biomaterialia* 10 (6). Elsevier: 2434–45.

Rakusan, K, P W Hrdina, Z Turek, E G Lakatta, H A Spurgeon, and G D Wolford. 1984. “Cell Size and Capillary Supply of the Hypertensive Rat Heart: Quantitative Study.” *Basic Research in Cardiology* 79 (4). Steinkopff-Verlag: 389–95. doi:10.1007/BF01908138.

Ravichandran, Rajeswari, Jayarama Reddy Venugopal, Subramanian Sundarrajan, Shayanti Mukherjee, Radhakrishnan Sridhar, and Seeram Ramakrishna. 2013. “Expression of Cardiac Proteins in Neonatal Cardiomyocytes on PGS/fibrinogen Core/shell Substrate for Cardiac Tissue Engineering.” *International Journal of Cardiology* 167 (4). Elsevier: 1461–68.

Riehl, BD, and JH Park. 2012. “Mechanical Stretching for Tissue Engineering: Two-Dimensional and Three-Dimensional Constructs.” *Tissue Engineering Part B: …*. http://online.liebertpub.com/doi/abs/10.1089/ten.TEB.2011.0465.

Ruggeri, Zaverio M. 1999. “Structure and Function of von Willebrand Factor.” *THROMBOSIS AND HAEMOSTASIS-STUTTGART*- 82. FK SCHATTAUER VERLAGSGESELLSCHAFT MBH: 576–84.

Rustad, Kristine C, Michael Sorkin, Benjamin Levi, Michael T Longaker, and Geoffrey C Gurtner. 2010. “Strategies for Organ Level Tissue Engineering.” *Organogenesis* 6 (3). Taylor & Francis: 151–57.

Salameh, A, S Krautblatter, S Karl, K Blanke, D Rojas Gomez, S Dhein, D Pfeiffer, and J Janousek. 2009. “The Signal Transduction Cascade Regulating the Expression of the Gap

Junction Protein connexin43 by B-adrenoceptors." *British Journal of Pharmacology* 158 (1). Wiley Online Library: 198–208.

Salameh, Aida, Sebastian Karl, Hjalmar Djilali, Stefan Dhein, Jan Janousek, and Ingo Daehnert. 2010. "Opposing and Synergistic Effects of Cyclic Mechanical Stretch and A-or B-Adrenergic Stimulation on the Cardiac Gap Junction Protein Cx43." *Pharmacological Research* 62 (6). Elsevier: 506–13.

Salameh, Aida, Anne Wustmann, Sebastian Karl, Katja Blanke, Daniel Apel, Diana Rojas-Gomez, Heike Franke, Friedrich W Mohr, Jan Janousek, and Stefan Dhein. 2010. "Cyclic Mechanical Stretch Induces Cardiomyocyte Orientation and Polarization of the Gap Junction Protein connexin43." *Circulation Research* 106 (10): 1592–1602. doi:10.1161/CIRCRESAHA.109.214429.

Scheidt, Stephen, Michael Collins, Jonathan Goldstein, and Jeffrey Fisher. 1982. "Mechanical Ciculatory Assistance with the Intraaortic Balloon Pump and Other Counterpulsation Devices." *Progress in Cardiovascular Diseases* 25 (1). Elsevier: 55–76.

Sekine, Hidekazu, Tatsuya Shimizu, Izumi Dobashi, Katsuhisa Matsuura, Nobuhisa Hagiwara, Masafumi Takahashi, Eiji Kobayashi, Masayuki Yamato, and Teruo Okano. 2011. "Cardiac Cell Sheet Transplantation Improves Damaged Heart Function via Superior Cell Survival in Comparison with Dissociated Cell Injection." *Tissue Engineering Part A* 17 (23-24). Mary Ann Liebert, Inc. 140 Huguenot Street, 3rd Floor New Rochelle, NY 10801 USA: 2973–80.

Severs, Nicholas J, Alexandra F Bruce, Emmanuel Dupont, and Stephen Rothery. 2008. "Remodelling of Gap Junctions and Connexin Expression in Diseased Myocardium." *Cardiovascular Research* 80 (1). Oxford University Press: 9–19.

Shachar, Michal, Nessi Benishti, and Smadar Cohen. 2012. “Effects of Mechanical Stimulation Induced by Compression and Medium Perfusion on Cardiac Tissue Engineering.” *Biotechnology Progress* 28 (6). Wiley Subscription Services, Inc., A Wiley Company: 1551–59. doi:10.1002/btpr.1633.

Shevach, Michal, Sharon Fleischer, Assaf Shapira, and Tal Dvir. 2014. “Gold Nanoparticle-Decellularized Matrix Hybrids for Cardiac Tissue Engineering.” *Nano Letters* 14 (10). ACS Publications: 5792–96.

Shimaoka, Motomu, Junichi Takagi, and Timothy A Springer. 2002. “Conformational Regulation of Integrin Structure and Function.” *Annual Review of Biophysics and Biomolecular Structure* 31 (1). Annual Reviews: 485–516. doi:10.1146/annurev.biophys.31.101101.140922.

Shimizu, Tatsuya, Masayuki Yamato, Takumitsu Akutsu, Takahiko Shibata, Yuki Isoi, Akihiko Kikuchi, Mitsuo Umezu, and Teruo Okano. 2002. “Electrically Communicating Three-dimensional Cardiac Tissue Mimic Fabricated by Layered Cultured Cardiomyocyte Sheets.” *Journal of Biomedical Materials Research* 60 (1). Wiley Online Library: 110–17.

Shimizu, Tatsuya, Masayuki Yamato, Yuki Isoi, Takumitsu Akutsu, Takeshi Setomaru, Kazuhiko Abe, Akihiko Kikuchi, Mitsuo Umezu, and Teruo Okano. 2002. “Fabrication of Pulsatile Cardiac Tissue Grafts Using a Novel 3-Dimensional Cell Sheet Manipulation Technique and Temperature-Responsive Cell Culture Surfaces.” *Circulation Research* 90 (3). Am Heart Assoc: e40–48.

Shimizu, Tatsuya, Masayuki Yamato, Akihiko Kikuchi, and Teruo Okano. 2001. “Two-Dimensional Manipulation of Cardiac Myocyte Sheets Utilizing Temperature-Responsive

Culture Dishes Augments the Pulsatile Amplitude." *Tissue Engineering* 7 (2). Mary Ann Liebert, Inc.: 141–51.

Singh, Inder M, Mehdi H Shishehbor, and Benjamin J Ansell. 2007. "High-Density Lipoprotein as a Therapeutic Target: A Systematic Review." *Jama* 298 (7). American Medical Association: 786–98.

Sipe, Jean D. 2002. "Tissue Engineering and Reparative Medicine." *Annals of the New York Academy of Sciences* 961 (1). Wiley Online Library: 1–9.

Souza, Glauco R, Dawn R Christianson, Fernanda I Staquicini, Michael G Ozawa, Evan Y Snyder, Richard L Sidman, J Houston Miller, Wadih Arap, and Renata Pasqualini. 2006. "Networks of Gold Nanoparticles and Bacteriophage as Biological Sensors and Cell-Targeting Agents." *Proceedings of the National Academy of Sciences of the United States of America* 103 (5): 1215–20. doi:10.1073/pnas.0509739103.

Souza, Glauco R, Jennifer R Molina, Robert M Raphael, Michael G Ozawa, Daniel J Stark, Carly S Levin, Lawrence F Bronk, et al. 2010. "Three-Dimensional Tissue Culture Based on Magnetic Cell Levitation." *Nat Nano* 5 (4). Nature Publishing Group: 291–96. http://dx.doi.org/10.1038/nnano.2010.23.

Souza, Glauco R, Esra Yonel-Gumruk, Davin Fan, Jeffrey Easley, Roberto Rangel, Liliana Guzman-Rojas, J Houston Miller, Wadih Arap, and Renata Pasqualini. 2008. "Bottom-up Assembly of Hydrogels from Bacteriophage and Au Nanoparticles: The Effect of Cis- and Trans-Acting Factors." Edited by Jianren Lu. *PloS One* 3 (5). Public Library of Science: e2242. doi:10.1371/journal.pone.0002242.

Spahr, R, H M Piper, P Schwartz, I Probst, and P G Spieckermann. 1984. “Morphological Dedifferentiation of Adult Cardiac Myocytes in Coculture with Hepatocytes.” In *Adult Heart Muscle Cells SE - 16*, edited by H M Piper and P G Spieckermann, 83–86. Steinkopff. doi:10.1007/978-3-662-11041-6_16.

Srinivasa Reddy, Chaganti, Jayarama Reddy Venugopal, Seeram Ramakrishna, and Eyal Zussman. 2014. “Polycaprolactone/oligomer Compound Scaffolds for Cardiac Tissue Engineering.” *Journal of Biomedical Materials Research Part A* 102 (10). Wiley Online Library: 3713–25.

Swartz, Daniel D, James A Russell, and Stelios T Andreadis. 2005. “Engineering of Fibrin-Based Functional and Implantable Small-Diameter Blood Vessels.” *American Journal of Physiology-Heart and Circulatory Physiology* 288 (3). Am Physiological Soc: H1451–60.

Takahashi, Kazutoshi, and Shinya Yamanaka. 2006. “Induction of Pluripotent Stem Cells from Mouse Embryonic and Adult Fibroblast Cultures by Defined Factors.” *Cell* 126 (4). Elsevier: 663–76.

Takayama, Kazuo, Kenji Kawabata, Yasuhito Nagamoto, Keisuke Kishimoto, Katsuhisa Tashiro, Fuminori Sakurai, Masashi Tachibana, Katsuhiro Kanda, Takao Hayakawa, Miho K Furue, Hiroyuki Mizuguchi. “3D Spheroid Culture of hESC/hiPSC-Derived Hepatocyte-like Cells for Drug Toxicity Testing.” *Biomaterials* 34 (7): 1781–89. doi:http://dx.doi.org/10.1016/j.biomaterials.2012.11.029.

Tallawi, Marwa, D Zebrowski, Ranjana Rai, Judith Roether, Dirk Schubert, Mirka El Fray, Felix Engel, Katerina Aifantis, and Aldo Roberto Boccaccini. 2014. “Poly (glycerol Sebacate)/poly (butylene Succinate-dilinoleate)(PGS/PBS-DLA) Fibrous Scaffolds for Cardiac Tissue Engineering.” *Tissue Engineering*, no. ja.

Terai, Hidetomi, Didier Hannouche, Erin Ochoa, Yoshiki Yamano, and Joseph P Vacanti. 2002. "In Vitro Engineering of Bone Using a Rotational Oxygen-Permeable Bioreactor System." *Materials Science and Engineering: C* 20 (1–2): 3–8. doi:http://dx.doi.org/10.1016/S0928-4931(02)00006-1.

Tseng, Hubert, Jacob A Gage, Robert M Raphael, Robert H Moore, Thomas C Killian, K Jane Grande-Allen, and Glauco R Souza. 2013. "Assembly of a Three-Dimensional Multitype Bronchiole Coculture Model Using Magnetic Levitation." *Tissue Engineering Part C: Methods* 19 (9). Mary Ann Liebert, Inc. 140 Huguenot Street, 3rd Floor New Rochelle, NY 10801 USA: 665–75.

Tulloch, Nathaniel L, Veronica Muskheli, Maria V Razumova, F Steven Korte, Michael Regnier, Kip D Hauch, Lil Pabon, Hans Reinecke, and Charles E Murry. 2011. "Growth of Engineered Human Myocardium with Mechanical Loading and Vascular Coculture." *Circulation Research* 109 (1). Am Heart Assoc: 47–59.

Wei, Hao-Ji, Chun-Hung Chen, Wen-Yu Lee, Iwen Chiu, Shiaw-Min Hwang, Wei-Wen Lin, Chieh-Cheng Huang, Yi-Chun Yeh, Yen Chang, and Hsing-Wen Sung. 2008. "Bioengineered Cardiac Patch Constructed from Multilayered Mesenchymal Stem Cells for Myocardial Repair." *Biomaterials* 29 (26). Elsevier: 3547–56.

Wei, Hao-Ji, Sung-Ching Chen, Yen Chang, Shiaw-Min Hwang, Wei-Wen Lin, Po-Hong Lai, Huihua Kenny Chiang, Lee-Feng Hsu, Hang-Hsing Yang, and Hsing-Wen Sung. 2006. "Porous Acellular Bovine Pericardia Seeded with Mesenchymal Stem Cells as a Patch to Repair a Myocardial Defect in a Syngeneic Rat Model." *Biomaterials* 27 (31). Elsevier: 5409–19.

Wei, J, K K Cheng, D Y Tung, C-Y Chang, W-M Wan, and Y-C Chuang. 1998. “Successful Use of Phoenix-7 Total Artificial Heart.” In *Transplantation Proceedings*, 30:3403–4. Elsevier.

Williams, Corin, Erica Budina, Whitney L Stoppel, Kelly E Sullivan, Sirisha Emani, Sitaram M Emani, and Lauren D Black III. “Cardiac Extracellular Matrix–fibrin Hybrid Scaffolds with Tunable Properties for Cardiovascular Tissue Engineering.” *Acta Biomaterialia*, no. 0. doi:http://dx.doi.org/10.1016/j.actbio.2014.11.035.

Williams, Corin, Erica Budina, Whitney L Stoppel, Kelly E Sullivan, Sirisha Emani, Sitaram M Emani, and Lauren D Black. 2014. “Cardiac Extracellular Matrix–fibrin Hybrid Scaffolds with Tunable Properties for Cardiovascular Tissue Engineering.” *Acta Biomaterialia*. Elsevier.

Wollert, Kai C, and Helmut Drexler. 2010. “Cell Therapy for the Treatment of Coronary Heart Disease: A Critical Appraisal.” *Nature Reviews Cardiology* 7 (4). Nature Publishing Group: 204–15.

Wu, Min-Hsien, Song-Bin Huang, and Gwo-Bin Lee. 2010. “Microfluidic Cell Culture Systems for Drug Research.” *Lab on a Chip* 10 (8). The Royal Society of Chemistry: 939–56. doi:10.1039/B921695B.

Xuan, Shouhu, Yi-Xiang J Wang, Jimmy C Yu, and Ken Cham-Fai Leung. 2009. “Tuning the Grain Size and Particle Size of Superparamagnetic Fe3O4 Microparticles.” *Chemistry of Materials* 21 (21). ACS Publications: 5079–87.

Ye, Kathy Yuan, Kelly Elizabeth Sullivan, and Lauren Deems Black. 2011. “Encapsulation of Cardiomyocytes in a Fibrin Hydrogel for Cardiac Tissue Engineering.” *Journal of Visualized Experiments: JoVE*, no. 55. MyJoVE Corporation.

Yu, Jiashing, An-Rei Lee, Wei-Han Lin, Che-Wei Lin, Yuan-Kun Wu, and Wei-Bor Tsai. 2014. "Electrospun PLGA Fibers Incorporated with Functionalized Biomolecules for Cardiac Tissue Engineering." *Tissue Engineering Part A* 20 (13-14). Mary Ann Liebert, Inc. 140 Huguenot Street, 3rd Floor New Rochelle, NY 10801 USA: 1896–1907.

Zhang, Shuguang. 2004. "Beyond the Petri Dish." *Nature Biotechnology* 22 (2). Nature Publishing Group: 151–52. 10.1038/nbt0204-151.

Zhou, Xiaoming, and Todd R Graham. 2009. "Reconstitution of Phospholipid Translocase Activity with Purified Drs2p, a Type-IV P-Type ATPase from Budding Yeast." *Proceedings of the National Academy of Sciences* 106 (39). National Acad Sciences: 16586–91.

Zimmermann, Heiko, StephenG. Shirley, and Ulrich Zimmermann. 2007. "Alginate-Based Encapsulation of Cells: Past, Present, and Future." *Current Diabetes Reports* 7 (4). Current Science Inc.: 314–20. doi:10.1007/s11892-007-0051-1.

Zimmermann, Wolfram H, Christine Fink, Dirk Kralisch, Ute Remmers, Joachim Weil, and Thomas Eschenhagen. 2000. "Three-Dimensional Engineered Heart Tissue from Neonatal Rat Cardiac Myocytes." *Biotechnology and Bioengineering* 68 (1). New York, Wiley [etc.]: 106–14.

Zimmermann, Wolfram-Hubertus, Ivan Melnychenko, and Thomas Eschenhagen. 2004. "Engineered Heart Tissue for Regeneration of Diseased Hearts." *Biomaterials* 25 (9). Elsevier: 1639–47.

Zimmermann, Wolfram-Hubertus, Ivan Melnychenko, Gerald Wasmeier, Michael Didié, Hiroshi Naito, Uwe Nixdorff, Andreas Hess, Lubos Budinsky, Kay Brune, and Bjela Michaelis.

2006. “Engineered Heart Tissue Grafts Improve Systolic and Diastolic Function in Infarcted Rat Hearts.” *Nature Medicine* 12 (4). Nature Publishing Group: 452–58.